

Numerical Simulation of Blunt Thoracic Trauma Followed by Aortic Rupture

Francisco Carrasco-Hernández, MSc, BEng

Impact Biomechanics

`Francisco.Carrasco-Hernández@nottingham.ac.uk`

Thesis submitted to

The University of Nottingham

For the degree of

Doctor of Philosophy

30th November, 2016

Abstract

Blunt thoracic trauma followed by aortic rupture (BTAR), is a unique injury to the aorta (which is the main output of blood from the heart). BTAR could be explained as a compression of the rib cage, (produced by a trauma to the chest), which affects the internal organs and injure the aorta in a specific spot. This thesis work will analyze the mechanism of this injury.

A hypothesis has been developed to explain the mechanism of BTAR, if the mechanism is known an external device could be designed to prevent it. In this thesis, numerical simulations will be performed as a way to recreate BTAR and prove that the mechanism is not due to only one assumption, instead being a complex trauma, it triggers different mechanisms.

The study starts with an explanation of the trauma and a rough rationale for the mechanisms proposed in this work. Literature has been reviewed marking the starting point for this research. This first chapter concludes with the methodology that will take place and how will be studied throughout the chapters.

A validation of the mechanical properties and material model is performed on the first simulation of the second chapter. Once the mechanical properties and material model have been validated, a simulation to prove the first mechanism proposed is performed.

A scar at the inner aspect of the aortic isthmus will generate a concentration of stress, if the tissue is subjected to an increment of pressure. A simulation of a bubble inflation test with the insertion of a patch, which varies in diameter and stiffness is performed on this second chapter, finding an intensity factor of 1.53, 1.43 and 1.66 in diameters of 1 *mm*, 2 *mm* and 3 *mm* respectively, these values represents a concentration of stress and strain at the border of the patch and the aorta. This is shown in the second chapter which validates the mechanism that a scar at the aortic isthmus, due to the closure of the Ductus Arteriosus, will weaken the aortic wall.

The third chapter compares two ways of geometry generation. With an increment of internal pressure first in a high pressure range having the highest error before 150 *kPa*, hence a normal physiological pressure range was simulated and a dramatic increase of errors started at 18.7 *kPa*, the outermost layer of the aorta shows the highest values. To achieve these a 10 *mm* specimen from the descending aorta was generated by two methods; a geometric approximated model designed with a Computational Assisted Design software, and a segmented model, which was designed by segmenting 3D medical images.

The simulation of the third chapter demonstrates that the aorta changes its cross section when it is subjected to hypertension values, therefore the fourth chapter tests the architecture of the thoracic aorta when is subjected to a pressure range which includes the different levels of hypertension.

For this analysis the aorta is divided into four different sections, ascending aorta, descending aorta, external aortic isthmus and internal aortic isthmus. The internal part of the aortic isthmus, at the innermost layer, shows higher stress values with less displacement. On the displacement analysis, the descending aorta shows a value at 18.7 *kPa* of 0.6×10^{-3} *m* and the internal part of the aortic isthmus of 0.2×10^{-3} *m*, for the stress values the descending aorta shows a value of 0.4 *MPa* and the internal part of the aortic isthmus of 0.35 *MPa*.

The last chapter employs the finite element method with a fluid solid interaction, and a smooth particle hydrodynamics formulation for the blood. This simulation uses a geometric approximation of the chest including the sternum and spine, heart and a three layered aorta. This model is subjected to different values of speed, introduced at the sternum, which will compress the heart recreating a blunt thoracic trauma. For this analysis the aorta is also divided into the same zones as in the fourth chapter.

It is shown that at a velocity of $20 \text{ m} \cdot \text{s}^{-1}$ values of pressure higher than 270 kPa (rupture pressure validated on the second chapter) and stress values higher than 1819.2 kPa experimental minimum ultimate stress [Pearson et al., 2008] (tested and validated on the second chapter) are located at the inner aspect of the aortic isthmus of the intima layer.

When the four results chapters are analysed together, it can be seen that the architecture of the aorta changes during hypertension values, and the concentration of stress and strain changes from the adventitia layer to the Intima layer, due to the change of the cross section geometry.

This thesis concludes that a mechanism of a BTAR is too complex to explained only by one mechanism, therefore a conjunction of numerical simulations test and validate a multivariate hypothesis proposed. The limitations of this thesis are also explored in the final chapter, with a proposal of a future work, to keep track with the research, and could design an external devise to prevent people from dying in car crashes due to BTAR.

Acknowledgements

Throughout this research project many people has been involved, showing support and interest, being this really helpful to the ending of this project.

I would like to thank first to my supervising team: Prof. Dr. Donal McNally, for his invaluable constructive criticism and friendly advice, during this project; Dr. Richard Brooks, who provided insight and expertise that greatly assisted this research; Dr. David Richens, for his support, guidance and medical knowledge, giving to this project the link between mechanical and medical fields. I would also like to thank to Mr. Mark Parry, for his support, friendship and chats about music and basses.

This research project would not have been possible without the unconditional love and support of my family: To my Mother Teté, I love you and it will never come a day, when I stop been grateful for all that you did, you do and you will do for me, Thank you very much momy; To my Father To, Thank you for all your support friendship and mechanical vibrations discussions, I love you dad; My brothers Toncho and Roncho, you two showed me the path to follow, give me the strength to continue and face every situation with a smile on my face, Love you hermanolos. To my friends in Mexico, thank you for still being in contact and showed me all your love at any time, Love you guys.

This four years would not have been amazing without the friendship of all the people that I met in this British town. I would like to show my gratitude, to my flatmates and my closest friends, who they know who they are, which gave a family taste and home warmth to this town. To the people from the Biomechanics lab and the Mexican Society for their support and friendship.

Finally I would like to thank to the sponsorship of this project: first to the Mexican government, to the Congreso Nacional de Ciencia y Tecnología and the Secretaría de Educación Pública, and to the University of Nottingham, for supporting this research.

Contents

Abstract	iii
Acknowledgements	vii
List of Figures	xvi
List of Tables	xvii
1 Introduction	1
1.1 Introduction	1
1.2 Aims and objectives	4
1.3 Car crashes	6
1.4 Anatomy	13
1.4.1 Thorax	13
1.4.2 Cardiovascular system	15
1.4.3 Great vessels	19
1.5 Mechanism of aortic rupture	27
1.5.1 Scar at the isthmus	28
1.5.2 Archimedes lever hypothesis	30
1.5.3 Water hammer hypothesis	31
1.5.4 Osseous pinch hypothesis	32
1.5.5 Multivariate hypothesis	34
1.6 Mechanical background	35
1.6.1 Material properties and material model	36
1.6.2 Hard tissue	39

1.6.3	Soft tissue	39
1.7	Simulation background	40
1.8	Literature review	46
1.8.1	Experimental test	46
1.8.2	Numerical methods	48
1.8.3	Blunt thoracic trauma followed by aortic rupture (BTAR)	49
1.9	Sequence of chapters	50
2	Biaxial comparison	53
2.1	Introduction	53
2.2	Rationale	54
2.3	Methods	55
2.4	Generation of the model	56
2.5	Constitutive behaviour of aortic tissue	57
2.6	Validation of the material model	59
2.6.1	Analytical comparison	59
2.6.2	Experimental comparison	60
2.6.3	Results	62
2.6.4	Conclusion	66
2.7	Patch FEM simulation	67
2.8	Results	68
2.9	Discussion	71
2.10	Conclusion	73
3	Architectural comparison	75
3.1	Introduction	75
3.2	Methods	76
3.3	Generation of specimens	79
3.4	FEM mesh analysis	81
3.5	Results	84
3.5.1	Comparison at high pressure range	85

<i>CONTENTS</i>	xi
3.5.2 Comparison normal physiological pressure range . . .	90
3.6 Discussion	95
3.7 Conclusion	97
4 Variation of pressure	99
4.1 Introduction	99
4.2 Rationale	100
4.3 Methods	102
4.4 Results	105
4.5 Discussion	112
4.6 Conclusion	114
5 Geometric impact chest model	115
5.1 Introduction	115
5.2 Rationale	116
5.3 Methods	117
5.3.1 Aorta properties, material and model	119
5.3.2 Blood properties, material and model	122
5.3.3 Heart properties, material and model	125
5.3.4 Bone properties, material and model	127
5.3.5 Specifications for the simulation	129
5.4 Results	130
5.5 Discussion	144
5.6 Conclusion	148
6 Conclusions and future work	149
6.1 General discussion	149
6.2 Limitations	155
6.3 Future work	157
6.4 General conclusion	160
Acronyms	163

Glossary

165

References

169

List of Figures

1.1	Fiat punto EuroNCAP 40 OBD frontal driver chest response [Payne, 2017]	3
1.2	Car occupant reaction in a car crash [Li et al., 2015]	8
1.3	Classification of traumatic aortic injury [Estreera et al., 2013]	13
1.4	Anatomy of the thorax	16
1.5	Circulatory system [cir, 2009]	17
1.6	Anatomy of the heart [Okubo, 2009]	18
1.7	Aortic valve: connection of the aorta to the heart [Resourse, 2014]	21
1.8	Aorta parts and location of the aortic isthmus [Okubo, 2009]	24
1.9	Vessel wall layers	27
1.10	Development of the aortic arch	29
1.11	Representation of the aorta as a lever [Okubo, 2009]	31
1.12	Aorta - water hammer [Okubo, 2009]	32
1.13	Osseous pinch	33
1.14	Range of strain rates found [Macaulay, 2012]	36
1.15	Hyperelastic - viscoelastic zones [Bower, 2009]	39
2.1	Dimensions of the specimen for the bubble inflation test	57
2.2	Material behaviour curves	58

2.3	Bubble inflation test. A - inflation orifice, B - clamping orifice, C - specimen sheet, P - pressure, t_0 - original thickness, a - initial radius, h - bubble height, t_t - thickness at bubble pole, d - diameter, r - radius of curvature, σ - engineering stress λ - stretch ratio [Johannknecht and Jerrams, 1999] . . .	61
2.4	Comparison of experimental VS FEM test of the isthmus zone. (a) Experimental from Pearson [Pearson et al., 2008], (b) equivalent FEM images.	62
2.5	Comparison using the rupture pressure	63
2.6	Comparison using the ultimate tensile stress	65
2.7	Comparison using Radial Extension	66
2.8	Location of the ductus arteriosus	67
2.9	Specimens showing the different diameter of patches from 7 mm down to 1 mm.	69
2.10	Intensity factor for stress and strain, varying dimensions and stiffness of a patch in a bubble inflation test.	70
3.1	Procedure to generate a complex FEM simulation using a geometric approximated and a segmented model	77
3.2	Geometric approximated model (GM) left, segmented model (SM) right	80
3.3	FEM mesh analysis, comparing element size of 0.200 mm, 0.250 mm, 0.300 mm, 0.325 mm, 0.350 mm, 0.375 mm, 0.400 mm, 0.500 mm, at a pressure of 18.7 kPa	82
3.4	Specific Sections for the acquisition of data	85
3.5	Comparison for percentage of error - Pressure for mechanical deformation, stress and strain for each layer for specific sections at rupture pressure (a)back (b)big branch (c)small branch; for intima (red), media (green) and adventitia (blue) layers	88

3.6	Comparison of shapes between (a) Geometric model, (b) Segmented model. Subjected to a rupture pressure range.	89
3.7	Comparison for percentage of error - Pressure for mechanical deformation, stress and strain for each layer for specific sections at normal physiological pressure. (a)Back zone, (b)big branch (c)small branch; for intima (red), media (green) and adventitia (blue) Layers	93
3.8	Comparison of shapes between (a)Geometric model, (b)Segmented model. Subjected to a normal physiological pressure for mechanical deformation, stress and strain for each layer for specific sections.	94
4.1	Selected zones of the aorta, for the data acquisition	105
4.2	Displacement ascending aorta, descending aorta, external and internal aortic isthmus; intima, media and adventitia layers; normal physiological pressure	107
4.3	Strain ascending aorta, descending aorta, external and internal aortic isthmus; intima, media and adventitia layers; normal physiological pressure	108
4.4	Stress ascending aorta, descending aorta, external and internal aortic isthmus; intima, media and adventitia layers; normal physiological pressure	109
4.5	Comparison of displacement, in meters, for a "U" tube Vs. thoracic aorta	111
5.1	Geometric approximated model of the human chest for numerical simulation	118
5.2	Geometric approximated model of the aorta for numerical simulation	121
5.3	Geometric approximated model of the blood for numerical simulation	124

5.4	Geometrically approximated model of the heart for numerical simulation	126
5.5	Geometric approximated model of the sternum and spine for numerical simulation	128
5.6	Displacement at intima layer, selected zones / velocity range 10 – 25 $m \cdot s^{-1}$	131
5.7	Displacement at media layer, selected zones / velocity range 10 – 25 $m \cdot s^{-1}$	132
5.8	Displacement at adventitia layer, selected zones / velocity range 10 – 25 $m \cdot s^{-1}$	133
5.9	Pressure intima, selected zones / velocity range 10 – 25 $m \cdot s^{-1}$	134
5.10	Pressure media, selected zones / velocity range 10 – 25 $m \cdot s^{-1}$	135
5.11	Pressure adventitia, selected zones / velocity range 10 – 25 $m \cdot s^{-1}$	135
5.12	Strain intima, selected zones / velocity range 10 – 25 $m \cdot s^{-1}$	136
5.13	Strain media, selected zones / velocity range 10 – 25 $m \cdot s^{-1}$	137
5.14	Strain adventitia, selected zones / velocity range 10 – 25 $m \cdot s^{-1}$	138
5.15	Comparison of ascending aorta, external isthmus and internal isthmus of displacement of the intima layer at 20 $m \cdot s^{-1}$	139
5.16	Comparison of ascending aorta, external isthmus and internal isthmus of pressure of the intima layer at 20 $m \cdot s^{-1}$. . .	141
5.17	Comparison of ascending aorta, external isthmus and internal isthmus of strain for the Intima layer at 20 $m \cdot s^{-1}$. . .	142
5.18	Comparison of ascending aorta, external isthmus and internal isthmus of stress for the Intima layer at 20 $m \cdot s^{-1}$. . .	143
5.19	Displacement vectors for the Intima layer of selected steps in a 20 $m \cdot s^{-1}$ chest impact simulation	145

List of Tables

1.1	Description and numbers of fatal thorax injuries for 287 car drivers, [Ndiaye et al., 2009] (n C - number of casualties).	8
1.2	Definition of the Abbreviated Injury Scale (AIS) [Haddadin et al., 2007]	11
1.3	Aorta and its branches in thorax	23
3.1	Input data for FEM simulation of aortic tissue	83
3.2	Range for High Pressure Range	86
3.3	Normal physiological pressure range	91
4.1	Range of pressure to be simulated	103
4.2	Input Data for FEM simulation of aortic tissue	104
5.1	Input data for FEM simulation of aortic tissue	120
5.2	Input data for FEM simulation of blood	125
5.3	Input data for FEM simulation of bone	127
5.4	Range of Impact Velocity	129

Chapter 1

Introduction

1.1 Introduction

A car crash occurs when a moving vehicle collides into something. A study to determine the types of crashes done by the Monash University, indicates that frontal impacts are the most prevalent with a 47%, followed by side impacts with a 25%, rear ends impacts with a 23% and the least prevalent of impacts are rollovers with a 5% [Fildes et al., 1991].

Injuries related to frontal impacts include, injuries to the abdomen, chest, upper and lower limbs. For the chest injuries can be included heart injuries, traumatic aortic injury, mediastinal haematoma, anterior rib fractures, sternal fracture, pulmonary contusion [Hammer et al., 2016; Yousef and Carr, 2014].

The leading cause of death in a car crash, is head injury. The second most common is a Blunt Thoracic Trauma followed by Aortic Rupture (BTAR) [Pavlidis et al., 2011; Kerut et al., 2005; Rastgar-Agah and Darvish, 2013; Richens et al., 2003]. As its name implies, this is an injury located

on the chest, known as thoracic trauma. Medically this kind of trauma includes injuries caused by penetrating or, as in the case of BTAR, an abrupt non-penetrating trauma, related by an impact or physical attack [Golden, 2000].

Considering these, this study will analyse a compression of the chest of a car occupant in an impact of a moving car which crashes with a perpendicular (90-degrees) barrier.

A thoracic trauma caused by penetrating laceration, occurs when an external object breaks into the human body, puncturing the skin and damaging tissues, leading to an open wound [Bronzino, 1999].

However, a thoracic trauma caused by a non-penetrating insult, or commonly known as blunt trauma, could lead to a compression of the chest. The skin does not show laceration, but depending on the strength of the forces, tissues housed inside the rib cage could be injured, damaging soft organs [Bronzino, 1999].

With the desire of evaluate, and the design of restrain devices in a moving vehicle, the tolerance of the human body to dynamic loads, was studied by Stapp in 1970 [Stapp, 1970], and Mertz and Gadd in 1968 [Gadd and Patrick, 1968], these studies develop a threshold for chest acceleration, which are applied to experimental crashes involving crash test dummies, which is a full-scale anthropomorphic test device, which simulates the human body.

Payne in 2017 made an experimental study in which the diagonal seat belt load, spine acceleration and the displacement of the chest compression were analysed [Payne, 2017], shown in Figure 1.1.

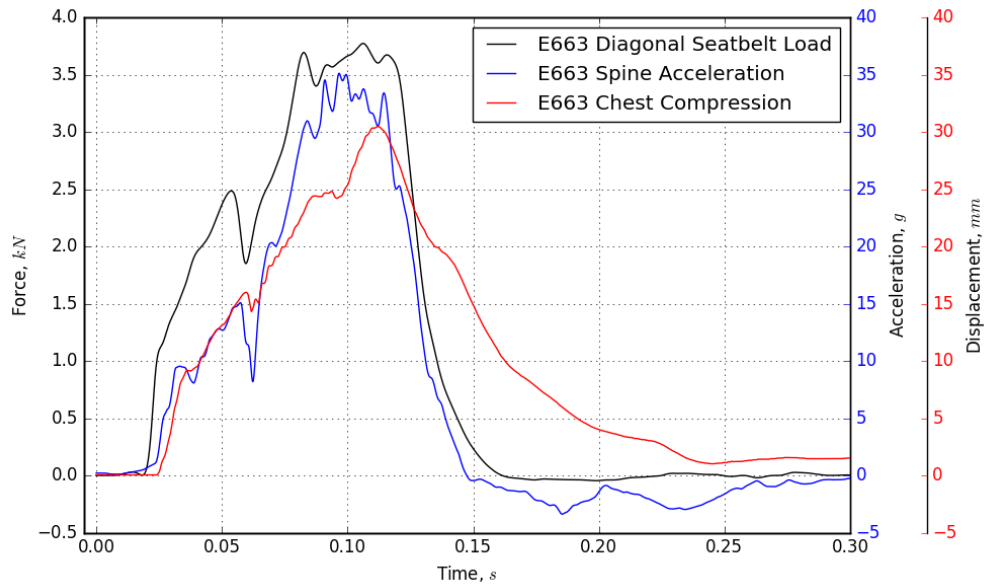


Figure 1.1: Fiat punto EuroNCAP 40 OBD frontal driver chest response [Payne, 2017]

BTAR was first documented in 1873 by Rindfleisch [Mohan and Melvin, 1982]. Greendyke in 1966 found that forty two deaths were caused by BTAR associated with accidents characterised by violent and sudden deceleration, his study includes 1,259 autopsies, and he also considered the possibility that survivors of these accidents, could have symptoms of BTAR [Cohen et al., 1992].

In 1997 Fabian et al. developed a study in United States of America and Canada, showing that each year around 7500 - 8000 occupants die in a car collision due to BTAR [Ismailov, 2006].

Recently, Richens et al. (2002) [Richens et al., 2002] published research on the true incidence and survivability of BTAR, between the years of 1992 - 1999, based on the United Kingdom. Richens included 7,067 accidents involving 14,435 passengers, showing 132 cases due to BTAR, and the 21% of car passenger's death in simple road traffic accidents are caused by BTAR.

The determining points of this research was: first that the use of the seatbelt or an air bag does not eliminate the risk of BTAR; and the second point is that BTAR can occur at low severity crashes, particularly in side impacts [Richens et al., 2004].

Researchers have found that BTAR shows a peculiarity; in 80% of the cases, rupture occurs at the proximal of the descending aorta, distal to the opening of the left subclavian artery, at the inner part of the aortic arch, in the inner aspect of a region commonly known as the aortic isthmus [Sevitt, 1977].

The mechanism of injury of BTAR has not been fully determined, even though that has been studied from different points of view, including biomechanical, medical and biological.

Therefore this PhD research will be focused on the understanding of the internal mechanism that leads a car collision to BTAR. Starting with the following section of aims and objectives.

1.2 Aims and objectives

The main aim of this research is to create a fully dynamic model of a geometric approximated model of the human aorta. As will be explained in detail later on this chapter the model of the aorta is formed from three different layers and includes: blood as a fluid, heart, sternum and spine.

This research will be using a numerical simulation of an impact load located on the chest, in order to understand the mechanical response of the aorta across different scenarios, to find a relation between chest compression and the declaration of BTAR to the car occupant.

To achieve the main aim, it is important to complete particular objectives including:

- Examine literature regarding causes, particular cases, medical reports, mechanism, among others in relation of BTAR. This will lead to the justification of the research
- Explore medical physiology of the human chest and the cardiovascular system, which should include the following components:
 - + AORTA - Built by three layers: intima, media and adventitia.
 - + BLOOD - Fluid part of the model.
 - + HEART - One solid piece of elastic material.
 - + BONES - Sternum and spine as solid shell elements.

These will establish the physiological boundary conditions that the model should heed.

- Material properties, material model, and mechanical behaviour of all the involved structures: soft tissue, hard tissue and blood.
- Understand the Finite Element Method (FEM) which is the base of this research work.
- Generate a finite element simulation for mechanical test, for the characterisation of materials to understand the way that the tissues behave under different loads. This will test out and validate the numerical model that it will be applied through the research.
- Develop a FEM simulation of a frontal impact models for the complete chest varying the range of velocities. In order to know the critical velocity.

In the following sections of this chapter these subjects should explain in particular the research:

1. Firstly an introduction of the automotive crashes will give a general idea of how the human body reacts when it is involved into a car collision.
2. This is followed by the explanation of the anatomy of the human chest and cardiovascular system.
3. Knowing the anatomy and the sequences of actions throughout the car collision, the presentation of the different hypotheses that explain an aortic rupture are mentioned.
4. A section of a mechanical background would explain the input data that it is needed for applying numerical methods to biological materials, including the different loads that can be applied.
5. An introduction to simulations and the FEM is important because this research will be based on this method, to determine the mechanism of injury of BTAR.
6. A review of the literature in these manners are explained establishing a starting point for this research, including research which related to experimental and numerical tests.
7. As a conclusion of this introduction, the disposition of the chapters that will structured the complete thesis is reviewed.

1.3 Car crashes

To understand how the human body reacts during a car crash, it is important to related with the laws of motion:

1. *A body will remain at rest or in a state of uniform motion in a straight line, unless it is acted upon by an external force, that changes its state of rest or motion* [Shigley, 1961].

2. *The rate of change of momentum of a body acted upon by an external force or forces is proportional to the resultant external force and in the direction of that force. If the mass is invariant, then the magnitude of the acceleration of the body is proportional to the force acting upon it and inversely proportional to the mass of the body. The direction of the acceleration is the same as the direction of the resultant external force [Shigley, 1961].*

3. *For every action of a force there is an equal and opposite reaction [Shigley, 1961].*

Following the first law of motion, also known as the law of inertia, if a vehicle is moving at a certain speed, the occupants are also travelling at the same speed, due to the movement of the vehicle. The mass, of the occupant and the vehicle possess energy, known as kinetic energy.

When an object interferes with the movement of the car, the motion of the car will stop quickly, and all the kinetic energy has to be dissipated, most of the energy is absorbed by the chassis of the vehicle and the restraint systems of the car (air bags and seat belt).

Since the occupant is still travelling at the same speed of the car, and the car stops the movement, the head and limbs of the occupant will continue moving, the seat belt will stop the movement of the chest of the occupant. The occupant will follow the movements shown in Figure 1.2.

Richens et al. states that the use of the contemporary designs of air bags and seat belts does not eliminate the risk of BTAR [Richens et al., 2004]. Being that the occupant is stopped by the seat belt, inside of the chest the spine will continue moving forward, leading to a compression of the chest.



Figure 1.2: Car occupant reaction in a car crash [Li et al., 2015]

The compression of the chest could be associated to a numerous of different injuries as: injuries to the central nervous system, brachial plexus injuries, pulmonary contusion, cardiac contusion, liver laceration and spleen laceration [Nano et al., 2011; Aidinian et al., 2006; Apostolakis et al., 2010], Table 1.1.

Table 1.1: Description and numbers of fatal thorax injuries for 287 car drivers, [Ndiaye et al., 2009] ($n|C$ - number of casualties).

Area of injury	$n C$	Severity	$n C$	Organ injured	$n C$	Nature of injury (n injuries)
Thorax	178	AIS 6	50	Whole area	44	Bilateral destruction
				Thoracic aorta	4	Major laceration with haemorrhage not confined to mediastinum
				Heart	2	Complex laceration or ventricular rupture

Table: 1.1 (continued)

Area of injury	$n C$ Severity	$n C$	Organ injured	$n C$	Nature of injury (n injuries)
	AIS 5	68	Thoracic	8	Major laceration, major laceration with valve involvement, major laceration with haemorrhage confined to mediastinum
			Aorta		
			Vena cava	1	Major laceration
			Heart	6	Interventricular or interatrial septum laceration, intracardiac valve laceration, ventricular or atrial perforation
			Trachea	1	Major fracture with laryngeal-tracheal separation
			Rib cage	60	Bilateral flail chest, fracture of more than three ribs on each of two sides, with haemothorax and/or pneumothorax
	AIS 4	60	Pulmonary artery	3	Major laceration
			Heart	2	Major myocardium contusion

Table: 1.1 (continued)

Area of injury	$n C$ Severity	$n C$ Organ inured	$n C$ Nature of injury (n injuries)
		Lung	23 Bilateral contusion, bilateral laceration, unilateral laceration with haemomediastinum, bilateral laceration with pneumomediastinum, laceration, not further specified as to laterally, with haemomediastinum
		Rib cage	44 Flail chest, not further specified as to laterally, flail chest with lung contusion, fracture of more than three ribs on the other side, with haemothorax/pneumothorax, fracture of more than three ribs on each of two sides

Table 1.1 uses an Abbreviated Injury Scale (AIS) which is a scale used by crash test dummies to define the severity of an injury. The ranges of AIS are shown in Table 1.2.

Table 1.2: Definition of the Abbreviated Injury Scale (AIS) [Haddadin et al., 2007]

AIS	Severity	Type of injury
0	None	None
1	Minor	Superficial injury
2	Moderate	Recoverable
3	Serious	Possible recoverable
4	Severe	Not fully recoverable without care
5	Critical	Not fully recoverable with care
6	Fatal	Unsurvivable

Aortic rupture is an injury associated with chest compression, induced by a non-penetrating thoracic trauma. This injury is positioned as the second most common cause of death in a car collision [Richens et al., 2004], this event is known as blunt thoracic trauma followed by aortic rupture.

In the event of BTAR, the compression of the chest, due to the quickly stop of the frontal chest by the seat belt, the spine will continue travelling, deforming the ribs until collapse of the rib cage, pushing inward the sternum.

The movement of the sternum to the inside of the chest, will compress the internal organs, affecting first the lungs followed by the heart. The heart will move backwards and injure the aortic valve which is the connection between the heart and the aorta [Moters et al., 1989].

At the moment when the heart moves backwards, the aorta gets compressed, the aortic arch also gets compressed and it will get a tear inside of the proximal descending aorta, distal to the opening of the left subclavian artery. At the aortic arch, in the inner zone of a place known as the Isthmus, the tear will be perpendicular to the aortic wall, starting at the inner wall [Kerut et al., 2005].

This injury could have four grades, shown in Figure 1.3:

1. **GRADE I: INTIMAL TEAR** The aorta is constructed by three layers, intima, media and adventitia (further in this chapter this will be explained in detail), this first grade is characterised by having a tear at the innermost layer of the aorta.
2. **GRADE II: INTRAMURAL HAEMATOMA** A collection of blood is situated between the innermost and outer layer of the aorta, at the media layer.
3. **GRADE III: PSEUDOANEURYSM** As in grade I, the tear starts at the Intima layer and the concentration of forces on the aortic wall, will break the media layer, the rupture of the intima and media layers will continue through all the perimeter of the aorta, leaving the adventitia layer to hold the blood.
4. **GRADE IV: RUPTURE** Is the yielding of the adventitia layer, starting as in grade I, the tear starts at the intima layer, following to grade III where the increase of forces will break the media layer through all the perimeter of the aorta, finally the internal pressure breaks the outermost layer.

More than 80% of the individual sustaining this injury die at the scene [Benjamin and Roberts, 2012]. For the reason that BTAR is only represented by internal symptoms, being hard to for the first aid team to identify at the scene of the accident.

The high mortality rate of BTAR has justified the research of potential risk factors, the use of new technologies as FEM, have been helpful performing crash simulations of real events. Thus this will contribute to understanding the forces involved in a crash and the effect to the human body.

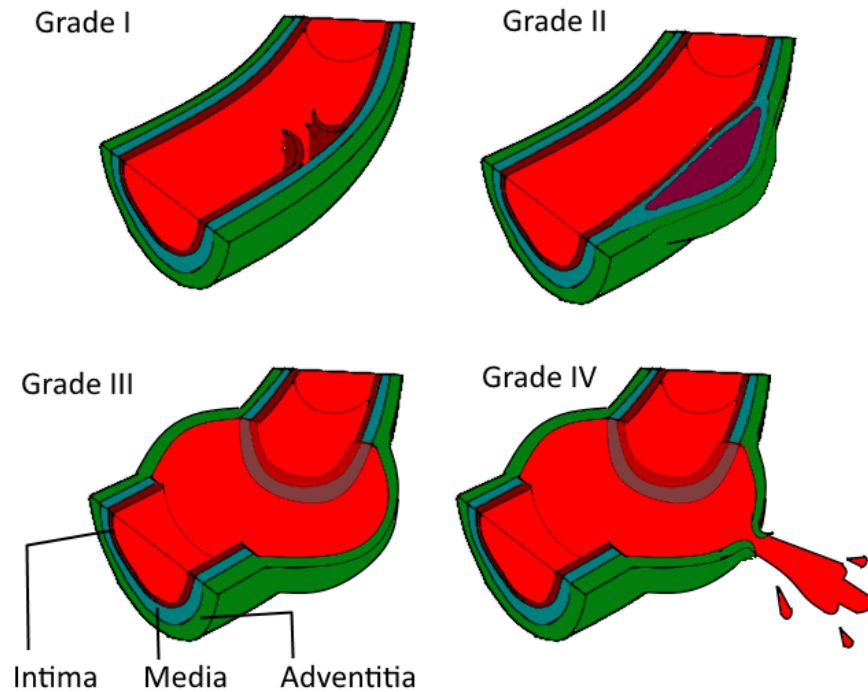


Figure 1.3: Classification of traumatic aortic injury [Estrera et al., 2013]

1.4 Anatomy

As the trauma that will be studied is situated on the chest, this section will present an overview of the anatomy of the thorax, as a way to know the architecture and disposition of the organs. It includes functions, structures and relationship to other regions, that are involved on a thoracic trauma.

This section will also include an overview of the cardiovascular system, including: parts of the system, functions, circulation of blood, blood vessel structure and classes of vessels.

1.4.1 Thorax

The shape of the thorax can be approximately described to an elliptic cone with round corners at the superior end which is open, connected directly with the base of the neck, known as Superior Thoracic Aperture situated at the top end is also the boundary with the upper limbs.

The cavity at the lower boundary is open in a bell shape, known as the inferior thoracic aperture. This aperture is closed by muscles which form the diaphragm, arranged in a dome shape for the chest.

Bounding this elliptical cone shape is a musculoskeletal wall, formed on the outside of:

- BONES Consisting of:
 - + Spine - Twelve Thoracic Vertebrae
 - + Ribs - Twelve curved bones
 - + Costal cartilage - The ribs are articulated with the vertebrae in one end, and on the other to a costal cartilage which articulate to the sternum, contributing to the mobility and elasticity of the wall.
 - + Sternum - Bone with an inverted trapezium shape on top, connected by a rectangle shape bone, connected to an inverted isosceles triangle shape bone.
- MUSCLES All the skeletal part is wrapped by muscles

In addition there are three components contained inside of the thoracic wall

- THE MEDIASTINUM A thick, flexible soft tissue partition oriented longitudinal in a median sagittal position, in this cavity the heart, oesophagus, trachea, major nerves and great blood vessels, are housed.
- PLEURAL CAVITIES Left and right cavities, each surrounding a lung and separated by the mediastium

Functions of the thorax

- BREATHING The thorax provides the system to allow the lungs to expand and contract to facilitate breathing.
- PROTECTION OF VITAL ORGANS The thorax is a shell that protects all the vital organs that are housed inside of it: lungs, heart, great vessels, stomach, spleen, kidneys.
- CONDUIT The mediastinum acts as a conduit for structures that pass completely through the thorax, from the neck to the stomach and vice versa.

1.4.2 Cardiovascular system

The cardiovascular system is principally constituted of the heart, blood and blood vessels [Fung, 2013].

Within the cavity of the thorax, at the centre of the mediastinum, it contains the pericardium, which is a sac that contains: the heart, origins of the great vessels, various nerves, and smaller vessels.

Functions of the cardiovascular system

There are three principal functions of the cardiovascular system, observed in Figure 1.5:

- TRANSPORT AND REMOVAL - One of the functions of the cardiovascular system is to transport nutrients and the removal of waste. Blood vessels which are known as arteries distribute oxygen, glucose, amino acids, fatty acids, vitamins, drugs and water to the tissues; blood vessels known as veins are assigned to washout metabolic waste products from tissues [Levick, 2013]

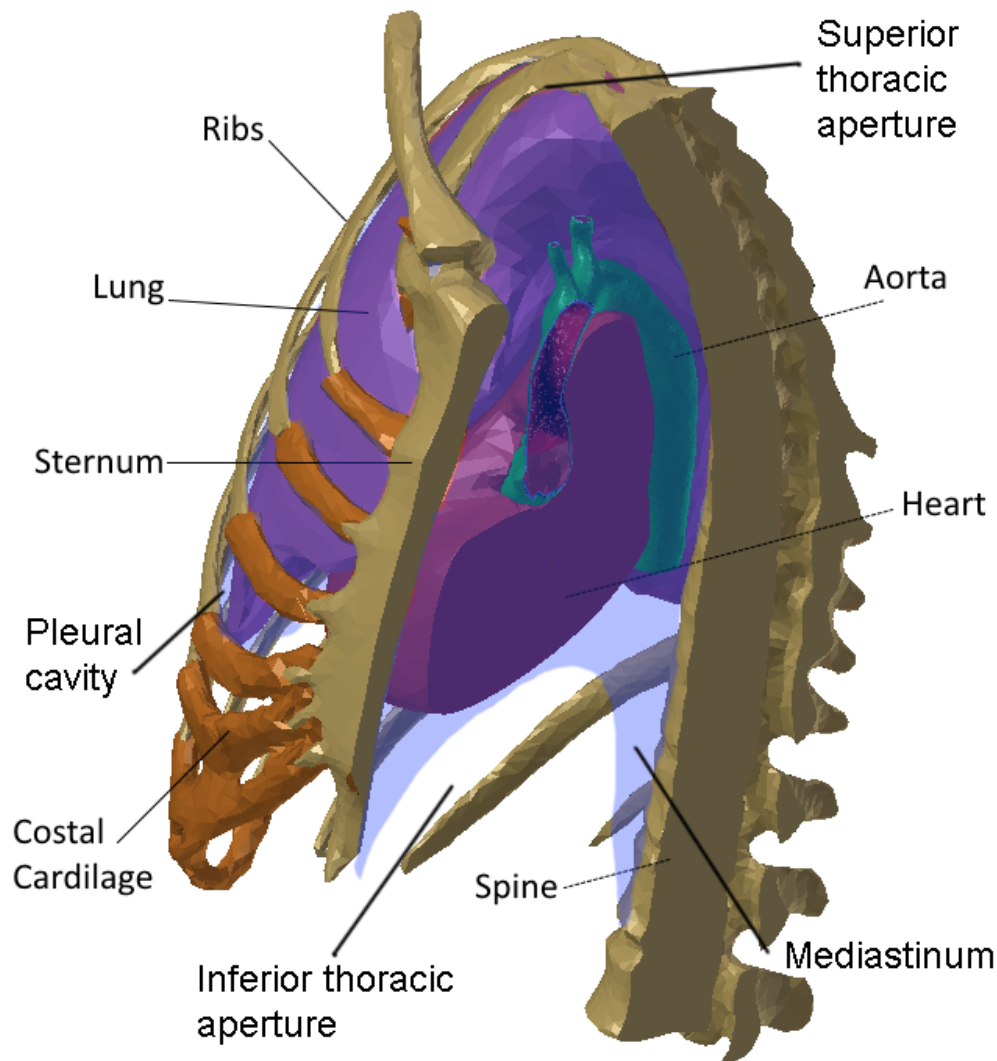


Figure 1.4: Anatomy of the thorax

- CONTROL AND COMMUNICATIONS - Through the bloodstream communication between tissues is performed by hormones; also the cardiovascular system secret control bio-active agents [Levick, 2013].

- REGULATION OF TEMPERATURE - The heart is in charge of controlling the bloodstream that reach all the body, the heart can variate the speed in way that through friction of the blood through the vessels produce heat [Levick, 2013].

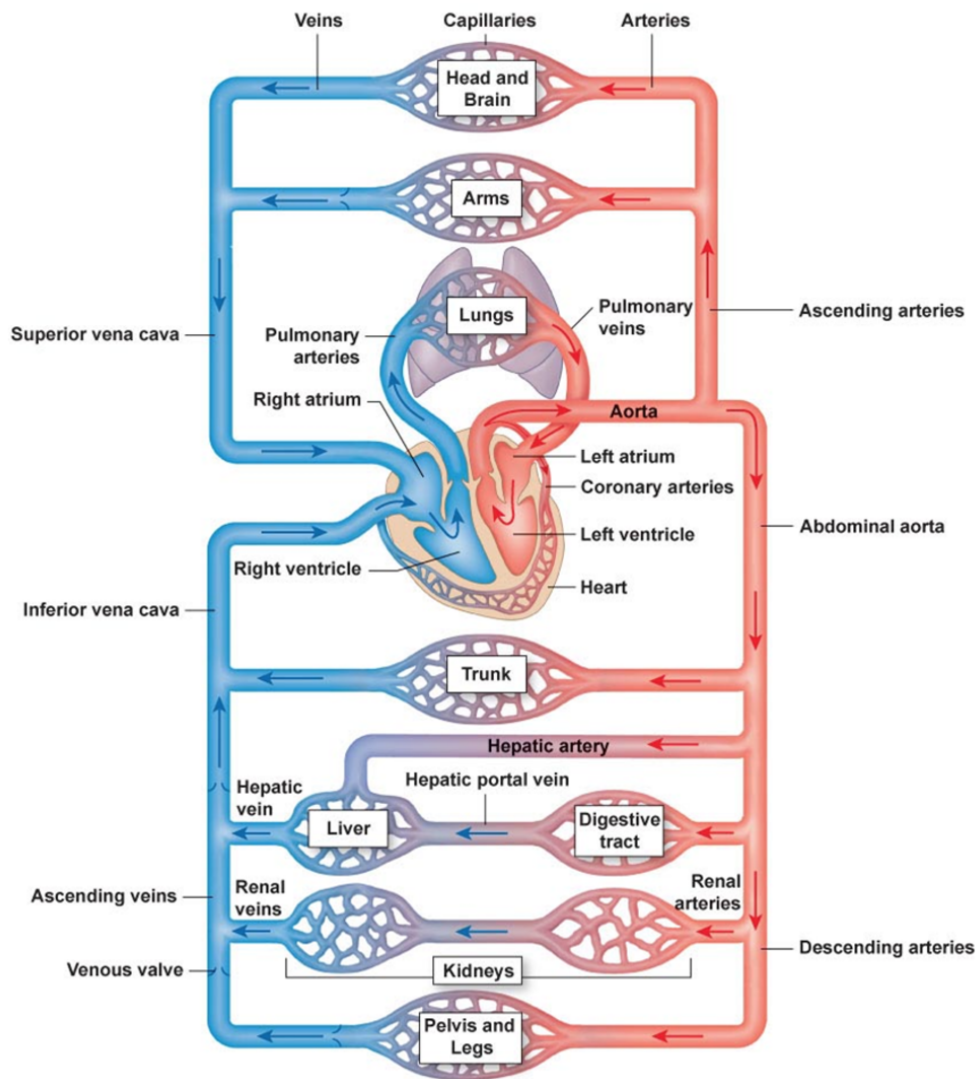


Figure 1.5: Circulatory system [cir, 2009]

Heart

The heart is constituted of a reclined pyramid shape, with the apex of the pyramid pointing front, down and to the left of the cavity.

The parts of the heart are defined by the different surfaces of the pyramid:

- **DIAPHRAGMATIC SURFACE** - Situated on the inferior part is the surface in which the pyramid rests, placed on the top of the diaphragm.

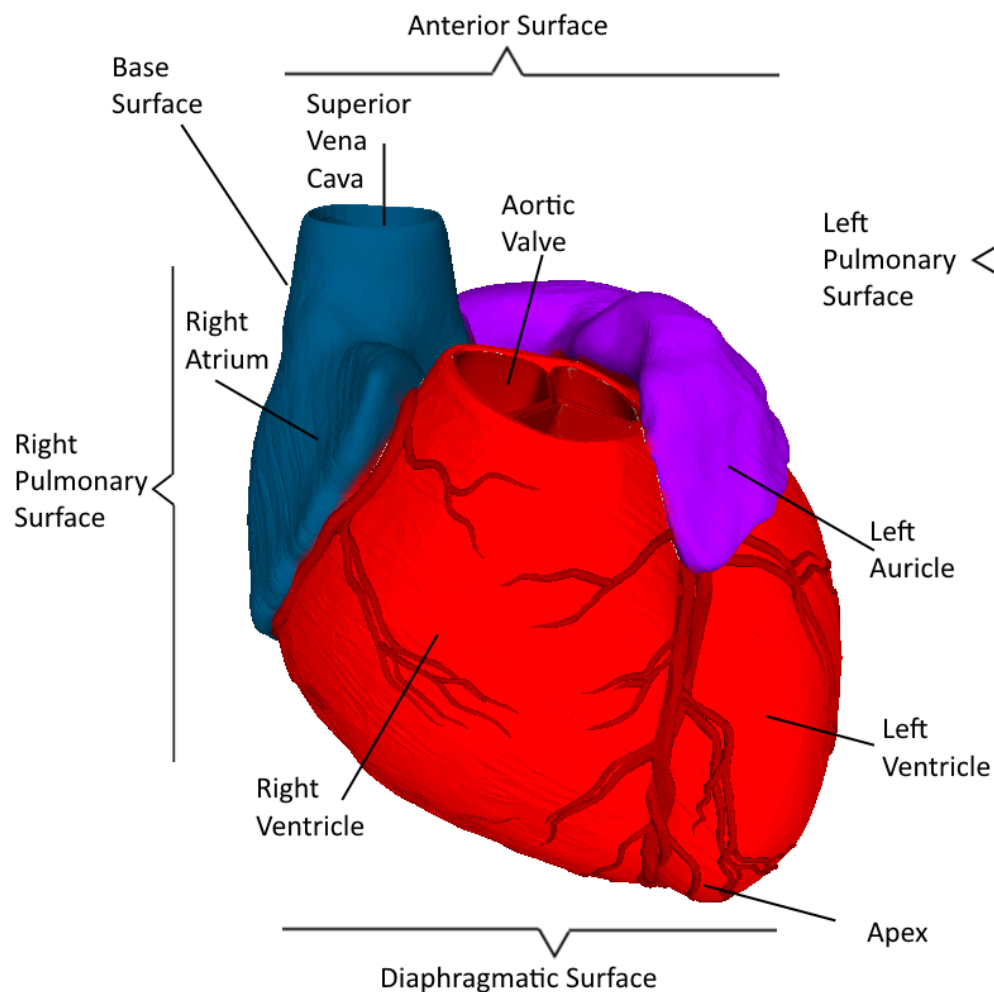


Figure 1.6: Anatomy of the heart [Okubo, 2009]

- ANTERIOR SURFACE - Situated opposite to the diaphragmatic surface, also known as sternocostal. Mostly consist of the right ventricle, additionally some of the right atrium and some of the left ventricle, respectively to right and left sides. At the left part of this surface, is where the aortic valve is connected, which is in charge of lead the blood flow to the aortic arch. On the right top of this surface are located the superior vena cava and the pulmonary arteries.
- RIGHT PULMONARY SURFACE - This side faces the right lung, it is broad and convex. On this side the right atrium is located.

- LEFT PULMONARY SURFACE - Located opposite of the right pulmonary surface, facing the left lung, it is also broad and convex. At this side the left atrium is located.
- BASE SURFACE - Situated at the posterior part, a quadrilateral shape and directed to the back. It consists of part of the left atrium, a small portion of the right atrium, and the proximal parts of the superior and inferior vena cava, and the pulmonary veins.
- APEX - Is located at the inferior part, pointing to the front, down and left of the chest

1.4.3 Great vessels

Figure 1.5 how the great vessels are connected to the heart. For description purposes, the mediastinum it is divided into superior and inferior, and the inferior section is subdivided by the pericardium into anterior, middle and posterior sections, these sections will be explained and located next:

- SUPERIOR MEDIASTINUM this zone starts from the superior thoracic aperture to a transverse thoracic plane, formed by a horizontal plane that starts at the sternum and passes through the disc formed by the junction of the fourth and fifth thoracic vertebrae.

From anterior to posterior the contents of this section are:

1. Thymus gland - located in front of the heart, organ of the immune system.
2. Great vessels.
 - + Veins - Brachicephalic and superior vena cava

- + Arteries - Aortic arch, ligamentum arteriosum (which is the remnant of the fetal ductus arteriosus), branchicephalic trunk, left common carotid artery, left subclavian artery
 - + Nerves - vagus and phrenic nerves and the cardiac plexus of nerves
3. Inferior continuation of the trachea anteriorly and oesophagus posteriorly and left recurrent laryngeal nerve
 4. Thoracic duct and lymphatic trunks.
- INFERIOR MEDIASTINUM this is situated at the inferior part of the transverse thoracic plane mentioned above, through the diaphragm, subdivided by the pericardium into middle and posterior:
- + MIDDLE MEDIASTINUM constituted mainly by the pericardium and it's contents, enclosed by the heart and roots of its great vessels, the terminal half of the superior vena cava besides to the ascending aorta.
 - + POSTERIOR MEDIASTINUM for this zone the organs which are enclosed are: the continuation of the aortic arch, known as descending aorta, the oesophagus to the right, the thoracic aortic plexus, the left lung pericardium and finishing with the abdominal aorta.

Anatomy of the aorta

Figure 1.8 shows the aorta which is the main supply of blood to the human body; it is the largest artery, with its origin at the left ventricle of the heart, where the oxygenated blood is pumped. The aorta is divided in two parts:

1. **Thoracic aorta.** For its study is divided in these different parts:

- (a) **ASCENDING AORTA**, a intrapericardial tubular segment of approximately 2.5cm in diameter. This section of the thoracic aorta, begins at the aortic valve, shown in Figure 1.7. This valve works as a check valve, which allows blood going out from the heart, but stops the flow going back to the heart. This section also contains the sinuses of valsalva.

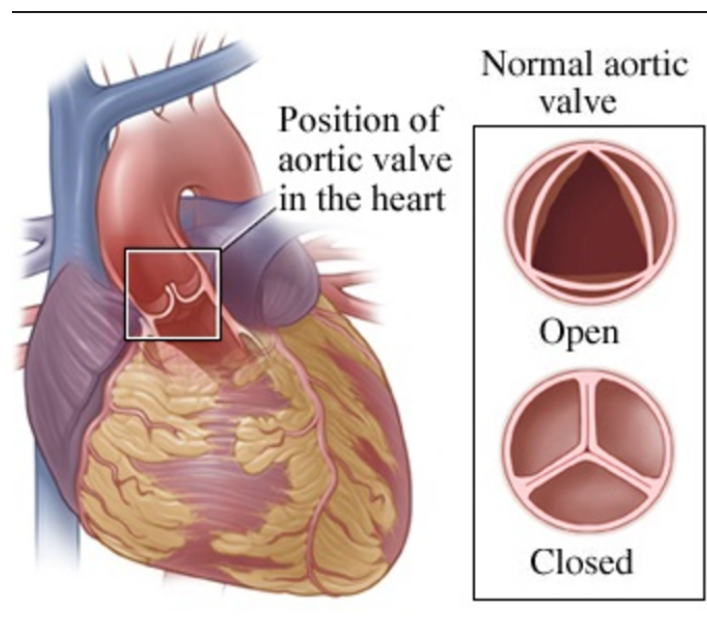


Figure 1.7: Aortic valve: connection of the aorta to the heart [Resourse, 2014]

- (b) **AORTIC ARCH**, almost immediately after the tubular segment of the ascending aorta, the aorta makes a curve, in a complicated three dimensional way (It arches superiorly, posteriorly and to the left, then inferiorly), giving origin to the aortic arch. It begins posterior to the second right sternocostal joint at the level of the sternal angle.

At the superior segment of the aortic arch, it subdivides into three different branches, shown in Figure 1.8 at the top of the aortic arch:

- i. BRACHIOCEPHALIC TRUNK - First and largest branch of the arch, arises posterior to the sternal manubrium, ascending superiorlaterally to the right side of the trachea.
 - ii. LEFT COMMON CAROTID ARTERY - Second branch of the arch, as well arises posterior to the sternal manubrium, slightly posterior and to the left of brachiocephalic trunk, it enters the neck passing posterior to the left subclavian joint.
 - iii. LEFT SUBCLAVIAN ARTERY - Third branch of the arch, arises from the posterior part of the arch, ascending laterally to the trachea and left common carotid artery through the superior mediastinum, it enters the root of the neck, and passes posterior to the left subclavian joint.
- (c) AORTIC ISTHMUS, This is a narrow region of the aorta, at the inside of the aortic arch, between the origin of the left subclavian artery and the ligamentum arteriosus which is a remnant of the fetal ductus arteriosus, which connects the root of the left pulmonary artery to the interior surface of the aortic arch. This region is the one that is affected in the event of BTAR. This is shown in Figure 1.8.
- (d) DESCENDING AORTA It runs straight down along the left of the vertebral column, on the left side of the inferior border of the body of the fourth thoracic vertebra and descends in the posterior mediastinum on the left sides from fifth to the twelfth thoracic vertebrae at the zone of the diaphragm. This is shown in Figure 1.8.

The descending aorta lies posterior to the left root of the left lung, pericardium and oapproximatelyesophagus. This parts connects the two sections of the aorta, thoracic aorta and abdominal aorta.

Table 4.1, shows a summary of the thoracic aorta and its branches, so that one can easily identify easily the location of each part, specifically the aortic arch where the Isthmus is located as the specific spot of BTAR.

Table 1.3: Aorta and its branches in thorax

Aorta section	Origin	Course	Branches
Ascending aorta	Aortic orifice of left ventricle	Ascends approximately 5cm to sternal angle where it becomes arch of aorta	Right and left coronary arteries
Aortic arch	Continuation of ascending aorta	Arches posteriorly on left side of trachea and esophagus and superior to left main bronchus	Brachiocephalic, left common carotid, left subclavian
Descending aorta (thoracic aorta)	Continuation of arch of aorta	Descends in posterior mediastinum to left of vertebral column; gradually shifts to right to lie in median plane at aortic hiatus	Posterior intercostal arteries, subcostal, some phrenic arteries and visceral branches (e.g., esophageal)

2. **Abdominal aorta** This region begins at the diaphragm, where it is divided in smaller vessels that are in charge of feeding abdominal organs, it course within a three vascular planes. The abdominal aorta ends at the height of the hip, where the aortoiliac bifurcation is located, giving off major visceral and the paired renal arteries.

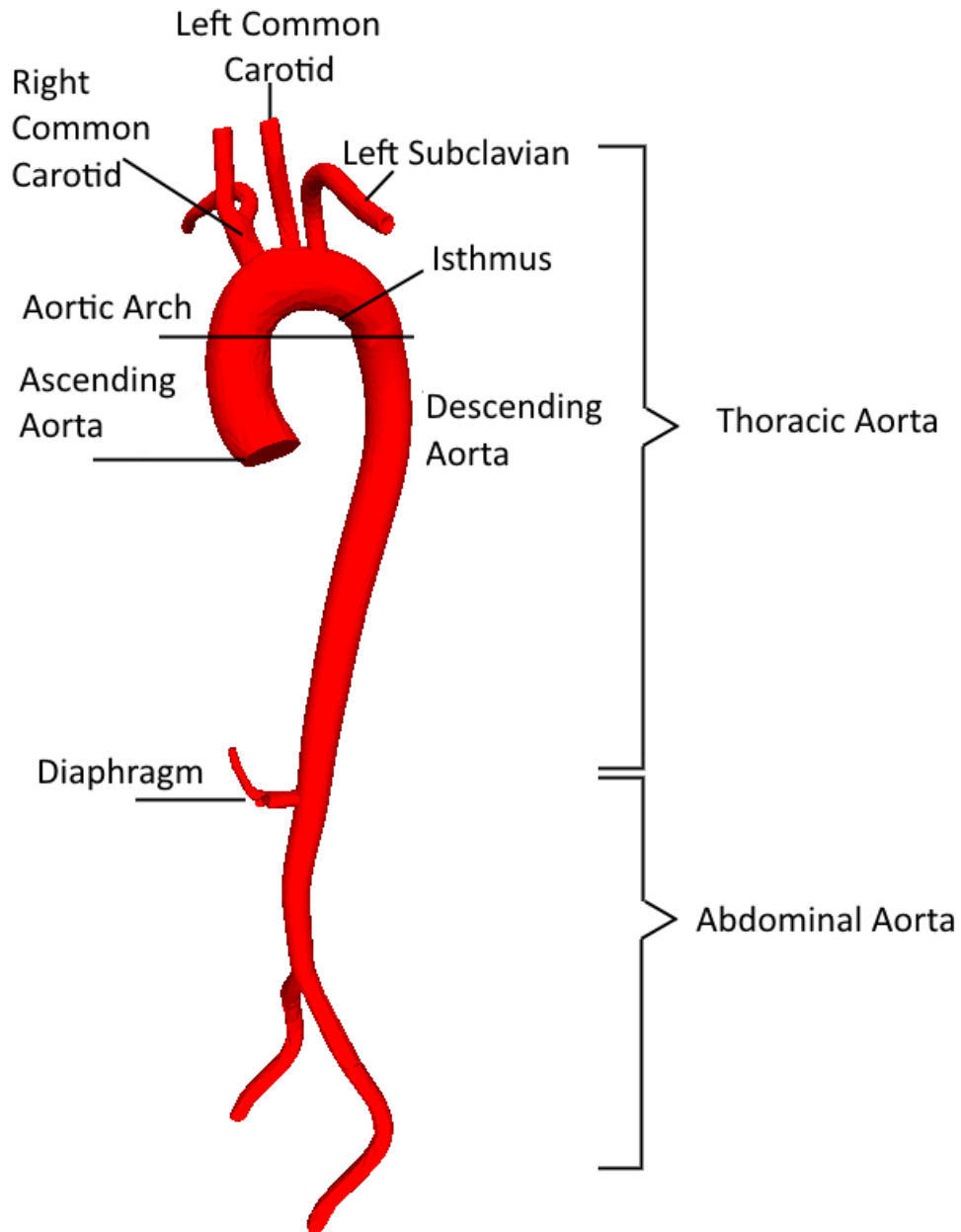


Figure 1.8: Aorta parts and location of the aortic isthmus [Okubo, 2009]

Blood vessels

Having identified the location of the great vessels, their structure shall now be explained in greater detail. The blood vessels are the pipelines of the body, conducting blood through all of the tissues, in this manner blood vessels contribute to homeostasis, providing communication between the body, exchange of nutrients and wastes in the different tissues and by adjusting the velocity and volume of blood flow can regulate the temperature of the body.

Depending on structure, location and function, blood vessels are classified in five main types:

1. ARTERIES - Subdivided into two kinds: large arteries and medium size arteries.
 - (a) LARGE Arteries which take blood out from the heart, then these vessels routes the blood flow into medium size arteries.
 - (b) MEDIUM Arteries are in charge of route blood to all the different regions of the body.
2. ARTERIOLES - Medium size arteries subdivide into the Arterioles which enter the tissue.
3. CAPILLARIES - After the arterioles enter the tissue the vessels has to divided into numerous tiny vessels that are called capillaries. The structure of capillaries allow the exchange of substances between blood and tissue.
4. VENULES - On the returning of the blood, venules are the beginning of the way back to the heart and lungs. Capillaries reunite and form venules which are small veins.
5. VEINS - These vessels take the blood from venules and route it back to the heart.

Basic structure of blood vessels

Among the different kinds of blood vessels, the structure could vary, but the basic design of the wall is constituted of three layers, changing design depending on structural and functional differences. These layers are also called tunics which are formed by different tissues:

- TUNICA INTIMA - Innermost coat, thin layer formed by flattened epithelial tissue. Among other tasks it works actively in different vessel-related activities: contractile state of the vessel's overlying smooth muscle, assisting with the capillary permeability, during tissue repair it guides cells from the vessel to the affected tissue, and its main task is to be a barrier that prevents the flow of blood to escape [Drake et al., 2014], this layer is configured by a framework of collagen fibres which gives significant tensile strength providing physical support, resilience for stretching and recoil.
- TUNICA MEDIA - Middle coat, layer formed by smooth muscle cells with an helical arrangement, built in a matrix of collagen fibres and elastin. Provides mechanical strength and contractile power to the vessel, for communication between intima and media layers, there are myo-endothelial cells sending signal from the internal elastic lamina to the smooth muscle cells [Holzapfel and Ogden, 2003].

The smooth muscle, part of the tunica media, regulates the diameter and the rate of blood flow. Therefore, in case of damage of the vessel, the smooth muscle will contract to reduce the loss of blood. Mechanically speaking, the muscle cells allow the vessel to stretch and recoil under the applied pressure of the blood.

- TUNICA ADVENTITIA - Outermost coat, outer covering, connective tissue lid with no definition of the outer limit. This layer contains nerves and tiny blood vessels, which supply the tissue of the vessel wall. Another important task is that fasten the vessel to surrounding tissues.

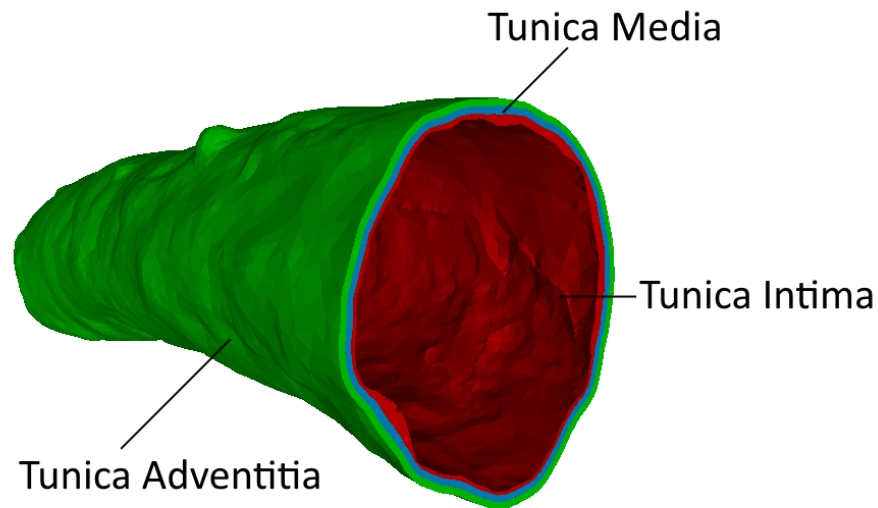


Figure 1.9: Vessel wall layers

1.5 Mechanism of aortic rupture

After determining the anatomy of the aorta, it is necessary to understand what occurs on the event of BTAR. The aorta fails in a transverse tear of the wall, at the Isthmus zone, on the intravascular surface of the intima layer of the aorta. This zone has the shortest curvature in relation to the aortic arch, hence is vulnerable to longitudinal stretch [Scali et al., 2015].

In 1947 Strassman [Strassmann, 1947] designate the isthmus as “The classic site”, their study shows an increased frequency of rupture at this zone, with 62% of the 51 cases of patients studied which presents BTAR.

Even though the trauma is at the same place and with similar characteristics, the mechanism of the wound has not been completely understood, leading to a variety of hypotheses, which either erroneously or incompletely explain the causes or mechanisms that lead to a BTAR. These hypotheses be categorised as follows:

1.5.1 Scar at the isthmus

In the human embryo the aortic arch and its branches develop from an essential bilaterally symmetric pharyngeal arch artery system, Figure 1.10(1). This is remodelled into a left aortic arch and (prenatally) a left Ductus Arteriosus (DA), Figure 1.10(2). During normal development, the early left subclavian artery crosses over the DA entrance, thereby creating the isthmus, which by definition is a piece of tissue connecting two larger parts, Figure 1.10(3). In this step the connection between the aortic arch with the descending aorta are developed [Moller and Hoffman, 2012].

When the aortic tissue is injured, it has to go through a healing process. Broadly speaking the tissue that is surrounding the injury start connecting both sides of the tear, this is performed by covering the wound with cells taken from the adventitia layer (outermost layer) into the intima (innermost layer), this cells are called fibroblasts (which are cells that produce collagen and other fibres), now that the wound is covered by fibroblasts, smooth muscle cells from the media grown in between the Intima and the adventitia layer. This process of healing produces a new scar tissue which change its stiffness and has different mechanical properties compared with the surrounding tissue [Brown, 1994].

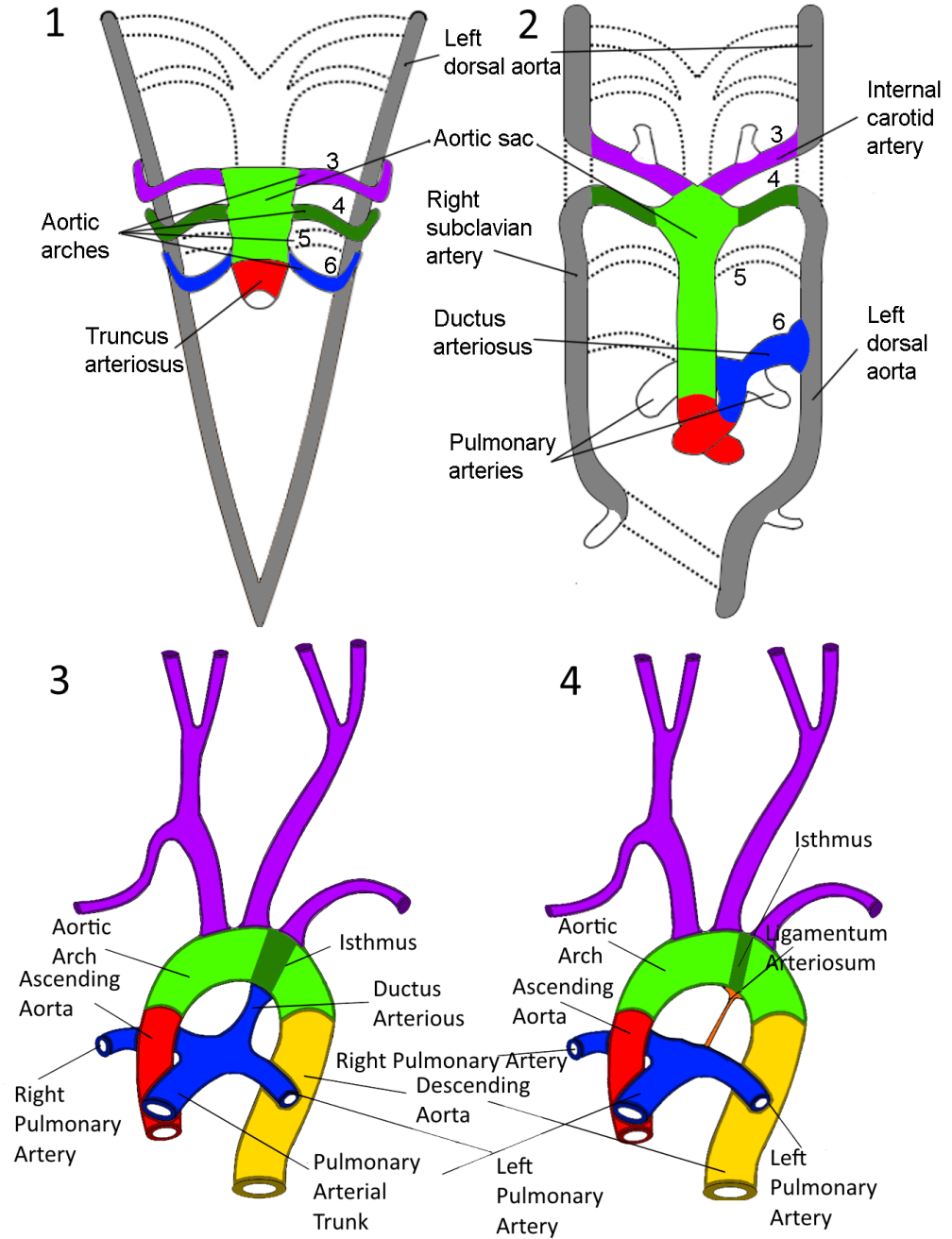


Figure 1.10: Development of the aortic arch

Putting together the development of the aortic arch and the way that the aortic tissue heals, if the closure of the DA could generate a scar of arbitrary dimensions, due to the healing process of the cardiovascular tissue the mechanical properties of the scar tissue could change. Therefore this hypothesis is explained:

1. In the development of the aortic arch system the growth of the DA, ligamentum arteriosus and isthmus zone leads to a merge of vascular tissue which results in a scar [Moller and Hoffman, 2012], with fibrosis resulting from the fusion of two materials. Therefore it is supposed that the tissue has a scar generated by the closure of the DA. Because of the healing process the scar has the material properties of the Adventitia.
2. In BTAR a sudden impact in the chest will compress all the organs inside of it, then the compression of the aorta will prevent the blood flow, generating an over pressure at the Isthmus zone where the scar is located, then there should be a concentration of stress and strain at the border between the patch and the Intima and Media layers

1.5.2 Archimedes lever hypothesis

This hypothesis is based on the explanation that Archimedes gave to the principle of leverage.

In 2006 Siegel et al. developed a computer simulation trying to validate the Archimedes lever hypothesis, experimenting with isolated human aortas, presenting as a result a rise of the blood pressure from 100 mm-Hg, to a level of 350 to 600 mm-Hg in a time of 50 to 100 ms after impact [Siegel et al., 2006].

This increment of the pressure level, inside of the aorta will define the ascending aorta and aortic arch as the input arm of the Archimedes lever. The left subclavian is working as the support of the beam, and the isthmus is working as the output arm of the Archimedes lever, having the rest of the descending aorta fixed to the spine. Shown in Figure 1.12.

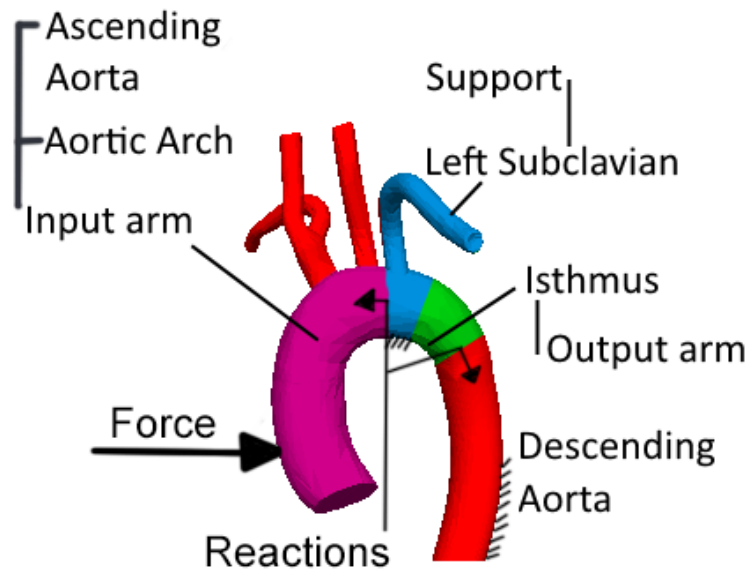


Figure 1.11: Representation of the aorta as a lever [Okubo, 2009]

In this moment the compression of the chest pressurises both arms of the lever, because of the distance in the input arm, the input force increases, and because of the fixation of the descending aorta to the spine, the isthmus, defined as the output arm, cannot move, causing a transverse tear at this spot.

1.5.3 Water hammer hypothesis

A pressure wave caused by a fluid which is suddenly forced to stop or change direction is known as water hammer effect also known as fluid hammer or hydraulic shock [Siegel et al., 2010].

Transferring this effect to the human body, the aorta, which is working as a pipeline, will be suddenly closed by the diaphragm at the aortic hiatus zone; the fluid, which is the blood, will find the way back through the same vessel and this will increase the pressure inside the aorta.

The flow will reflect at the first change of direction, which is the start of the descending aorta, at the isthmus zone, causing an instantaneous over pressure at the inside of the aorta producing a tear on the aortic wall, affecting the innermost wall of the vessel [Reid et al., 1999]. Figure 1.12 shows a representation of the water hammer effect in the aorta.

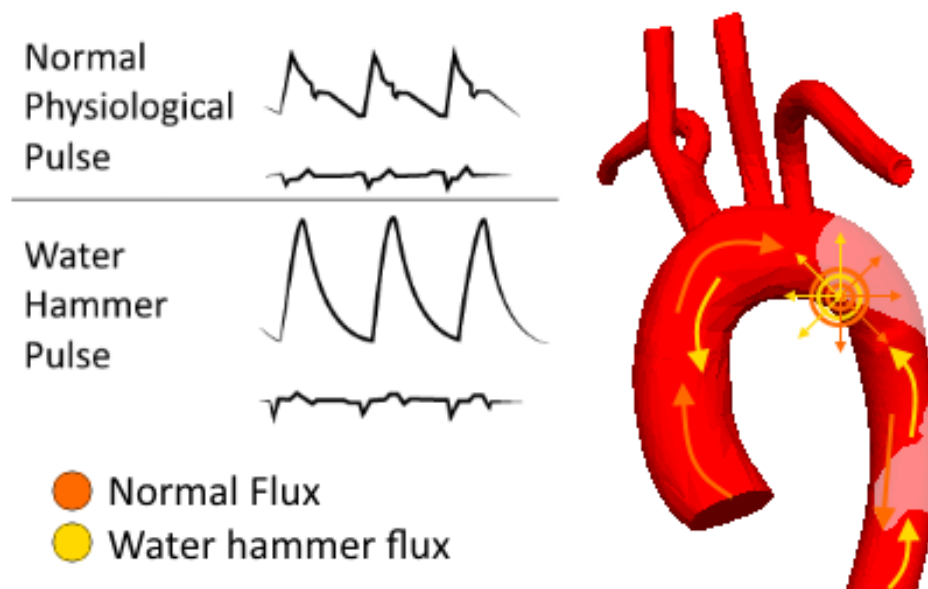


Figure 1.12: Aorta - water hammer [Okubo, 2009]

1.5.4 Osseous pinch hypothesis

Inside of the human chest there is no empty space, all the organs are packed inside of a box, which is formed by hard tissues: ribs, sternum and spine.

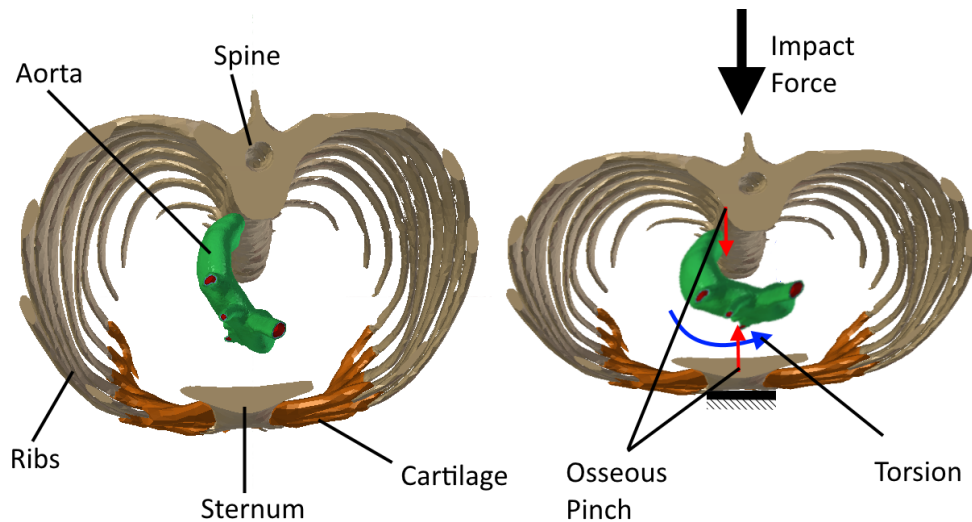


Figure 1.13: Osseous pinch

The mechanism of chest compression in a car crash, could be explained as follows: the sternum is stopped by the seat belt, the spine continues to move against the sternum. Inside the chest the soft tissue has no space to move so gradually will get compressed. The aorta is fixed to the spine cannot move, will be compressed from one side by the sternum and on the other side by the spine, this will generate that the arch move to the upper side of the rib cage, braking apart of its usual position.

The conjunction of forces could be explained as a compression of the sternum that generates torsion on the descending aorta, then a compression of the spine bones, the combination of these two compression forces will generate tension at the aortic arch.

These forces will damage the aorta by trapping it, the torsion at the descending aorta and the tension of the arch will stretch and shear the vessel, first producing a reduction of volume increasing the blood pressure, and then increasing the stress of the aortic wall at the isthmus region [Cohen et al., 1992]. Figure 1.13 shows the osseous pinch mechanism.

1.5.5 Multivariate hypothesis

The mechanism of BTAR is complex and it is feasible to think that the real mechanism must be a combination of simple mechanisms. Therefore, this section shall examine the relationship between each of the previously mentioned hypotheses [Richens et al., 2002].

On my personal suggestion a multivariate hypothesis which explains the mechanism that leads to BTAR, could be explained by the following mechanisms occur simultaneously and depend on the rate of compression:

- An impact on the chest will compress the ascending aorta, forcing the aortic arch to move upwards, stretching and twisting the descending aorta.
- A blockage at the descending aorta due to a sudden closure of the diaphragm, will initiate an impact pulse wave against the blood flow through the descending aorta.
- A collision of waves will be located at the isthmus, the normal blood flow from the ascending aorta and the water hammer wave from the descending aorta.
- An aortic rupture is initiated at the isthmus, due to the ascending aorta (input arm of the lever) is moving against the descending aorta, the subclavian artery restricts the movement of the vessel (support of the lever) and the force is focused on the inner part of the isthmus (output arm of the lever).

1.6 Mechanical background

In engineering it is important to characterise the materials which are subjected to loads, this characterisation will be used to predict the behaviour that the material will follow when is subjected to different scenarios. Before any engineering analysis, it is important to know the loads to which the material should be exposed.

For knowing the mechanical properties of materials two tests should be analysed, first a quasi-static loading and second a dynamic loading. It has being proved that a dynamic loading could change the behaviour of the material [Macaulay, 2012].

A quasi-static test is defined by a load that is applied slowly, as its name states, the load should be almost static. Inversely, for a dynamic test, the load should be applied fast. In a way to define the different ranges of loads, a rate of deformation is suggested by Macaulay M.A. [Macaulay, 2012] in Figure 1.14 which shows the different strain rates that will define the kind of load, i.e. dynamic or static.

For the propose of this research, because it will be dealing with car crashes, the use of dynamic loads is necessary. Hence the simulation shown on the following chapters will be subjected to dynamic loads.

After defining the kind of loading that should be applied to the test. The material properties should be determined, it has been mentioned that this research will be based on the Finite Element Method (FEM). Therefore the basic information for these kind of simulations are the mechanical properties and the material model for each of the parts involved on the test.

The human body is structured of many, and very complex, materials. In this manner, human tissues are usually divided into two large groups, hard tissue and soft tissue

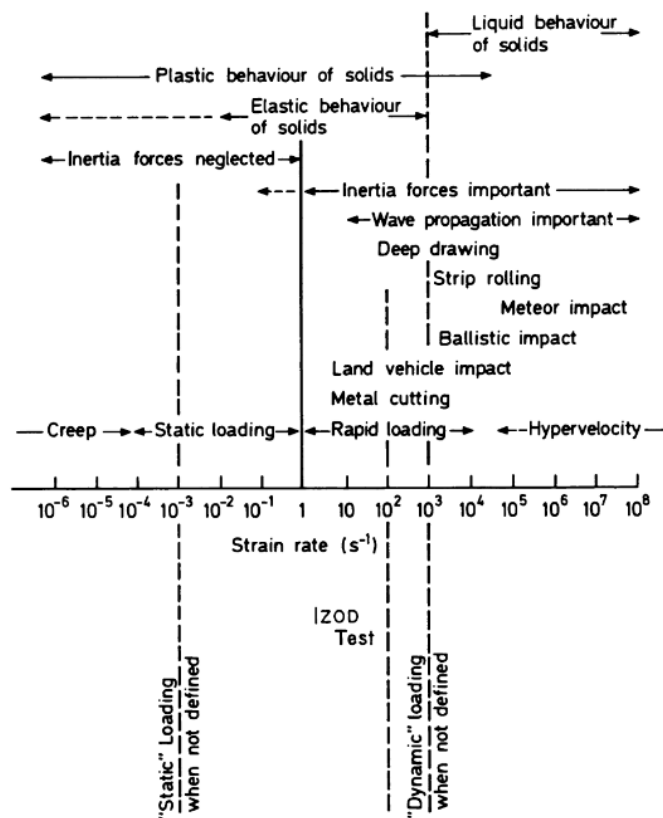


Figure 1.14: Range of strain rates found [Macaulay, 2012]

- a HARD TISSUE characterised by containing mineral (calcium), bones and teeth.
- b SOFT TISSUE these kind of tissue are not containing mineral, i.e., lungs, heart, blood vessels, among others.

Therefore the inclusion of mineral distinguish the mechanical properties and mechanical behaviour between both groups [Meyers et al., 2008].

1.6.1 Material properties and material model

To identify the behaviour of human tissue, different formulations for material behaviour should be analysed:

1. **LINEAR - ELASTIC** - This formulation is used for materials which during loading can deform with a linear behaviour and when the loads are removed the material returns to its original shape, through the same linear behaviour, the strain depends only on the stress applied.

2. **HYPOELASTIC** - This formulation is used for materials which during loading can deform with a non-linear behaviour and when the loads are removed the material returns to its original shape, through the same non-linear behaviour applying for small strains. As well as the **LINEAR - ELASTIC** materials the strain depends only on the stress applied. This formulation is used to approximate the behaviour of loadings which exceed the **LINEAR-ELASTIC** limit.

3. **VISCOELASTIC** - When the strain depends not only on the stress applied, instead depends on temperature and strain history.

In contrast to the hypoelastic formulation, that the unloading follows the same non-linear behaviour. Viscoelastic formulation change the range of behaviour zones and temperature due to the molecular structure of the solid.

Figure 1.15 shows the different transitions for a visco-elastic material. At a lower temperature a viscoelastic formulation presents a “Glassy” behaviour where the material gets brittle exhibiting a stiff response. After the denominated “Glassy transition temperature”, where the behaviour of the material shows a drop in modulus, changing the material behaviour from the stiff (glassy) behaviour to a rubber-like (elastic) behaviour, where the stress does not depend strongly on strain rate history.

The viscoelastic formulation includes a range of different behaviour, depending on temperature, a stiff behaviour, passing through the denominated glass transition temperature, and to the rubber-like behaviour. Hence the behaviour of a viscoelastic material depends on temperature, strain history and loading rate.

4. **HYPERELASTIC** - This formulation is used for materials which are subjected to very large strains and their reaction is elastically, with a non-linear behaviour, showing large shape changes. As it is shown in Figure 1.15 above the “Glass transition temperature”, the material exhibits a rubber-like behaviour, close to a ideally elastic response, and allowing the stress to not be strongly dependent on the strain rate or history. Therefore a hyperelastic formulation intends to approximate this “rubbery” behaviour without the dependence on temperature, but which includes a dependence in strain history and loading rate.

5. **QUASI-LINEAR VISCOELASTIC THEORY** - For the specific case of biological tissue Y.C. Fung suggested that soft tissue is a non-elastic material, thus the history of strain affects the stress reacting as a different response between the loading and unloading of the tissue [Fung, 1993].

A common link between studies suggest that the material could be modelled as locally homogeneous, isotropic and linearly viscoelastic material, as states the latter based on “Quasi-linear Viscoelastic Theory” (QLV) [Hemmasizadeh et al., 2013b; Carew et al., 1968; Liu et al., 2011]

It is important to say that hard tissue and soft tissue shows different mechanical properties, and mechanical behaviour, mainly due to that hard tissue contains mineral [Meyers et al., 2008].

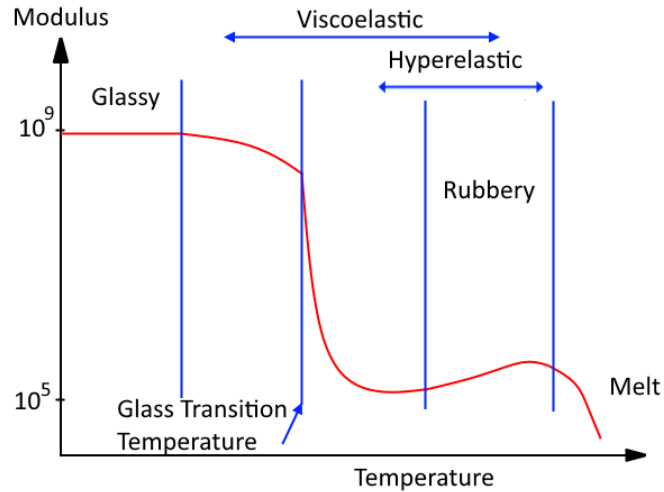


Figure 1.15: Hyperelastic - viscoelastic zones [Bower, 2009]

1.6.2 Hard tissue

The boundary conditions for the simulation will include the interaction with hard tissue. It is important to note that hard tissue will be modelled as having elastic and isotropic behaviour [Nsiampa et al., 2011].

1.6.3 Soft tissue

Soft tissue shows a complex behaviour and high deformation ability, in this study the material is approximated using the hyperelastic formulation [Meyers et al., 2008].

The main object in this study is the reaction at the Aorta. Even though the aorta has been considered as an anisotropic, viscoelastic and incompressible material [Dobrin, 1978].

In this study, the simulation will include living aortic tissue, which is usually treated as a pre-stretched material [Holzapfel et al., 2000a]. The range of temperature will surpass the denominated glass transition temperature, considering it as a rubber-like material, discarding the temperature dependency of the viscoelastic formulation.

Therefore the most appropriate material model in LS-DYNA is the simplified rubber/foam material(MAT_ 181_ RUBBER/FOAM), which is a simplified “Quasi”-Hyperelastic rubber model defined by a single uniaxial load curve or by a family of uniaxial curves, at discrete strain rates [Hallquist and Others, 2013b].

With the option of failure, a strain based failure surface is defined suitable for incompressible polymers that models failure in both tension and compression.

1.7 Simulation background

Whole body impacts with real human tissues, could be conducted but are extremely difficult to perform. Also the available specimens for testing are obtained from corpses, which have died from diseases of the cardiovascular system, these will alter the behaviour of the specimen.

Knowing that, the tissues that are the focus of this research, belong to the cardiovascular system, an experimental analysis with corpses will increase the probability of observing damage tissue, therefore the results cannot be reliable. For this reason the reproduction of a real tissue into a computational model which can mimic a real tissue is the best option [Robinson, 1994]. For a reproduction of the tissue it is suggested to use numerical simulations.

The Finite Element Method (FEM) uses numbers to solve algebraic expressions, and it is used in engineering to solve boundary value problems, this technique is one of the most widely used numerical methods.

The FEM is based on the idea to divide a complex problem into small and simpler problems. The path of a curve in space could be explained by small straight line segments, while the segments are smaller the description of the path of the curve should be more accurate. These division of a curve into small segments is called discretization, because of the discretization of the problem the solution given is approximated.

In recent years the use of high performance computers with software that can approximate the solution of a complex numerical equations have been leading to popularise this technique in the process of fabrication of products, being a crucial part for the testing of the final product [Liu and Quek, 2013], as well as in other branches of engineering in a way to approximate the solution for displacements, stress, strain, among others, that a structure is subjected among the different loading that is exposed.

The solution of a continuum problem using the FEM follows a step-by-step process [Rao, 2010; Liu and Quek, 2013] which is mainly divided in three parts, namely: Pre-processing, Processing and Post-processing:

- Pre-processing

Step 1: GEOMETRY MODELING

To analyse the reactions of a load applied to a structure, the first step is obtaining the geometry. Being a computer based method, the geometry to be analysed, should be generated in a Computer Assisted Design (CAD) software.

In the case of engineering structures that are usually composed by multiple geometries, the generation of the structure could be determined by the complexity of the geometry.

For biological structures, the segmentation of medical images is getting popularity, this process is explained on the following chapters of this thesis.

Step 2: GEOMETRY DISCRETIZATION

The step after generating the geometry or model, is to divide it into small pieces. This is usually executed by generating a grid attached along the geometry. On the intersections of the grid, there are nodes and the space between the nodes is called element.

The generation of this mesh will discretize the geometry, therefore it will set the accuracy of the approximated solution.

Step 3: MATERIAL PROPERTIES AND MATERIAL MODEL

As it was explained in the section above, it is important to identify the behaviour of any material to different kind of loads. In FEM, the definition of the behaviour and properties is of great concern, depending on the test performed are the requirements of the properties.

Depending on the nature of the test different properties are required, for example in an analysis of the structure the input data should have the Young's modulus, bulk modulus, shear modulus, among others, depending on the test nature; for thermal analysis, thermal conductivity; and so on. This will establish the relation between the simulation with the real material.

Step 4: EXTERNAL CONDITIONS

External conditions are considered as the ones that are not intrinsic of the material, these involve the environmental circumstances that the structure will be subjected, among the external conditions are included:

- BOUNDARY CONDITIONS These determine the border line of the test, by define constrains or supports, that the specimen is subjected.
- INITIAL CONDITIONS These determine the conditions before the test that the specimen has been subjected.
- LOADING CONDITIONS These determine the kind, localisation, quantity, frequency of the loads applied during the test.

- Processing

Step 5: CALCULATIONS

The processing of data should follow the geometry generation, discretization and determining the external conditions, to start with the calculations of the equations generated by the discretization of the continua.

- GENERATION OF EQUATIONS

Depending on the relevant desired analysis to be performed, different formulations are proposed. In this research because the nature of the approach is for solid and structures during dynamic loads, the approach of the FEM will be selected. This approach is based on the Taylor series.

Also because on later formulations the inclusion of a fluid and a Fluid Solid Interaction is involved the Smoothed Particle Hydrodynamics formulation is selected, which will be explained in detail in further chapters.

During this step the software depending on the approach selected will define stiffness matrices and load vectors for the elements. After will assemble the equations to be solved for each element to obtain equations of equilibrium. Because in this thesis work it is selected a FEM approach, the equations generated are of the form:

$$KD + M\ddot{D} = F \quad (1.1)$$

where K is the global stiffness, M is the mass matrix, D is the displacement vector and F is the force vector, it should be noticed that the displacement and force vectors applied to the entire problem.

- SOLVING EQUATIONS

During this step the equations generated with Equation 1.1, has to be solved, to obtain the displacements.

Being a non-linear dynamic problem, the procedure has to involve a stepping process involving a modification of the matrix. In this manner the FEM is divided into two methods for integration, implicit and explicit.

- IMPLICIT integrations take the evaluated time step based on the last time step and on the conditions imposed on the following time step. The conditions on the next time step are calculated with the use of another numerical method.
- EXPLICIT integrations take the evaluated time step based only on the last time step evaluation.

Once that the displacement of each node is already known, the element stress, strain and other specific evaluations can be computed using the mechanical equations.

- Post-processing

The post processing of data is the analysis and processing of the results of the calculations performed by the FEM simulation.

In terms of software that are based on the FEM, there is a huge range to choose from. Considering that on this research, dynamic loads, non-linear elastic materials and fluid interactions will intervene, the package selected that fulfil the expectations is LS-DYNA from Livermore Software Technology Corporation.

LS-DYNA is a general-purpose software based on the FEM, capable of simulating complex real world problems. It is competent in the use of highly nonlinear materials and transient dynamic finite element analysis, including fluid analysis as well as rigid body dynamics, quasi-static simulations, fluid solid interactions, thermal analysis, among others.

Among the material library included, it presents biomaterials, including material model of the heart, lungs and for soft tissue. It is used by automotive, aerospace, construction, military, manufacturing and bioengineering industries.

Beside LS-DYNA, the software that will be used to discretize the geometry is HYPERMESH from Altair, because of the control that gives to design and personalise the proper mesh and elements for the geometry of the specimen.

1.8 Literature review

In this chapter, BTAR has been defined and reviewed, showing the most important hypotheses which explain the internal mechanism that leads to this injury. Also an introduction of the anatomy of the thorax, including the structure and parts of the cardiovascular system, and specifically the anatomy of the aorta which is the focus point on this research.

A background of mechanics and numerical approximations is introduced, in a way to understand the mechanical theory and the tests evaluated in this thesis work.

Now is the time to establish the starting point for this research, accordingly studies about of the understanding of the internal mechanism of BTAR has been reviewed and the most representatives will be mention and explain in this section.

It has been found that mechanical test to biological tissues can be roughly classified into two kind of studies i.e. Experimental test and Numerical Tests.

1.8.1 Experimental test

Experimental studies with real tissue can be performed, as an attempt to understand the mechanical behaviour of soft tissue. Even though experiments with human tissue can be done, it is simpler to use animal tissue to perform mechanical tests.

To get the mechanical properties of any material or to simulate an incident to a complete structure. In this study, swine tissue is the topic under consideration.

Pearson R. et al. [Pearson et al., 2008], in an attempt to explain the internal mechanism of BTAR, developed an experiment with samples from three different parts of the aorta, i.e. ascending aorta, descending aorta and aortic isthmus. The aim of this experiment was to show a discrepancy on the thickness, rupture pressure or ultimate stress, of the tissue among the different parts.

Even though Pearson R. et al. found a difference in wall thickness among the tested specimens, there was no difference in rupture pressure and for the ultimate stress, the descending aorta showed greater values compared with the isthmus. Accordingly, the conclusion of these experiments, even though that the wall thickness variation is considerable, it is not a determining factor of the localisation of BTAR.

Schmoker J. et al. [Schmoker et al., 2008] actively promotes the Archimedes lever hypothesis as an explanation for the mechanism of BTAR. For this experiment four aortas filled with blood, were tested in a Pneumatic trauma device, showing:

- Determines the lesion as an Intimal - to - outer wall progression, proportional to the impulse force and always in transverse direction.
- For the damaged specimens, the intima and media layers at the aortic isthmus were injured and were identical to those documented in humans.
- An impulse of 827.37 kPa produced a critical load to the aorta.
- Hypertension may play a role in lesion expansion, after injury.

Numerical simulations should be compared with these data obtained through experimental analysis with real tissues, to establish the link between both (experimental and numerical analysis) and also these experiments will establish the starting point of the numerical analysis.

1.8.2 Numerical methods

Although an experimental study can be performed for real tissue, because of the fact that has to be with dead tissue, could result in a change of the mechanical properties. Otherwise for tests of the mechanical reaction of a specific tissue within the body, being experimental it increases the difficulty to be developed.

Experimental studies with dead bodies, simulating a car crash have being developed, showing that it is difficult, or sometimes even impossible to include all the voluntary and involuntary reflexes of the human body (breathing, heart beating, blood flow, among others). Therefore the use of numerical simulations as the FEM technique, it facilitates the development of complex test, as the reaction to the human body involved in a car crash.

In 2006 Ismailov R.M., presented a mathematical model that presented the internal risk factors of an aortic rupture, using multi-phase equations solved applying the finite-difference method. The study includes the coefficient of resistance, Reynolds and Dean numbers, shear stress and velocity inside of the aorta [Ismailov, 2006].

A shear stress of 0.04 kPa is needed to damage the interior surface of the vessel.

An increment from $0.12 - 0.14 \text{ kPa}$, on the shear stress of the plasma is due to rouleaux, increasing the possibility of BTAR. Rouleaux are defined as chains of blood cells that become stacked together [Caro, 2012].

The geometrical particularities in coronary arteries may predispose them to delayed rupture trauma [Candell et al., 1979]

1.8.3 Blunt thoracic trauma followed by aortic rupture (BTAR)

Research which simulates a fully dynamic FEM model has been reviewed, establishing the starting point of this research. The most helpful restrictions and results are mentioned in this section, to keep them in mind as a way to validate or compare results with other researchers on the field.

To get a tear inside the vessel, it is proposed to use a three layered model for the aortic tissue, with different mechanical properties and thickness, for each layer. Richens and Zhao determine that the rupture occurs on the inner side of the aortic arch and the rupture is a very clear separation of the aortic wall [Richens et al., 2004; Zhao et al., 2008].

The advantages of using a three layered model, is that the rupture of the aortic wall will start at the innermost layer and develop towards the following layers [Siegel et al., 2010]. Also it will show the real direction of the tear, noting that Lee S. H. et al., reported a fragmented tear instead of a tear transverse to the vessel, because they used a one thick layer model [Lee and Kent, 2007].

The model should be shown an interaction between solid and fluid, with a Galerkin formulation. This will determine if the aorta gets stiffer with an increment of blood pressure, explained by the Archimedes lever hypothesis. Siegel established that before the incident, the intra-aortic measured pressure is around 13.33 kPa and in the $50 - 100 \text{ ms}$ after the crash, the pressure increase to levels of $40 - 80 \text{ kPa}$ [Siegel et al., 2010].

Richens and Zhao modelled the blood using a Lagrange fluid material code [Richens et al., 2004; Zhao et al., 2008]. On another simulation, Siegel uses the Galerkin FEM formulation to simulate the blood [Siegel et al., 2010]. And finally Lee S.H. et. al [Lee and Kent, 2007] separate their simulations into two solvers, one for the fluid and the second for the structure, modelling the blood as a non-Newtonian fluid.

As limitations of the studies mentioned, the aorta is modelled with only one layer with isotropic shell elements. Even though that Lee S.H. et. al [Lee and Kent, 2007] used an anisotropic, visco-elastic and incompressible material, its model was also one thick layer. Another limitation is the fluid, the closer simulation with fluid is the one of Lee S.H. [Lee and Kent, 2007], but uses two different solvers.

In conclusion, to create a novel FEM simulation of a fully dynamic model of the aorta, which tests the mechanism that leads to BTAR, it is important to generate a three layered model of the aortic tissue, use anatomical boundary conditions and use a fluid solid interaction for the blood.

1.9 Sequence of chapters

The main aim of this research is to understand the mechanism which leads to BTAR and as such, a multivariate hypothesis is proposed. Therefore to explain in detail each part of the mechanism, this thesis is divided into chapters, which explain the proposed mechanisms and justify the decisions for applying the resources used. The sequence of the chapters that this thesis will have are mention below:

- The mechanical properties for the soft tissue has an important role on this research, therefore the second chapter of this thesis, shows a study that validates the mechanical properties used for the aortic tissue. The validation is in three ways, experimental, analytical and numerical, by the recreation of an experimental bubble inflation test, done by Pearson et. al. [Pearson et al., 2008].

A scar at the isthmus zone will weaken the tissue at this zone. A bubble inflation simulation is added to this chapter, it is simulated a specimen of aortic tissue with the insertion of a patch varying stiffness and patch size, to demonstrate the affectation of the tissue with an insertion of a patch.

- Two ways for geometry generation are analysed in the third chapter, showing advantages and disadvantages of both. Also a methodology is developed for the use in FEM for cardiovascular biomechanics, this will facilitate following studies.
- To test if there is a relation between hypertension and the structural weakening of the aorta. Chapter four analyses the geometry of the thoracic aorta subjected to a pressure range which includes the hypertension stages. This chapter is based on the idea that Ismailov [Ismailov, 2006] states, in which the geometrical particularities, of the vessel, may predispose it to delayed rupture trauma [Candell et al., 1979].
- To test the remaining mechanisms, Chapter five analyses a geometric approximated model of the aorta, using two different numerical techniques (for fluid and for solid models). Testing a range of speed, in a way to analyse the reaction of the aortic tissue with the inclusion of the heart and real boundary conditions.
- The compilation of all the studies explain the mechanism proposed in this thesis. Chapter six shows the highlights of the different chapters, relating them as an explanation of a multivariate mechanism.

Chapter 2

Biaxial comparison of aortic tissue and stiffer patch by a bubble inflation test

2.1 Introduction

In car crashes the most common cause of death after head injury is Blunt Thoracic Trauma followed by Aortic Rupture (BTAR) [Pavlidis et al., 2011]. A feature of this injury is the high frequency of the site of rupture at the aorta, which is just distal to the left subclavian branch in an area known as the Isthmus. It is observed on a wide range of acute deceleration conditions, as opposed to other locations within the different parts of the vascular system.

Pearson R. et al. [Pearson et al., 2008] developed an experimental study with the purpose of understanding the prevalence in this specific location of BTAR, in Pearson's study, tissue samples were extracted at different zones of the aorta, i.e. ascending aorta, descending aorta and the isthmus.

With the aim to identify if there is a considerable difference between each section (i.e. ascending aorta, descending aorta and isthmus), Pearson R. et al. tests each sample in a bubble inflation test. For these tests, samples were cut from the selected sections, then each sample was clamped at its circumference using a O-ring and inflated to a spherical shape with pressurised air [Pearson et al., 2008].

The present work is based on the experimental study of Pearson. With the supposition that the weaker part of the aorta is positioned at the isthmus zone, explaining the high incidence of this being the site of rupture regardless of the external compression forces.

In the development of the aortic arch system, the growth of the ductus arteriosus, ligamentum arteriosus and isthmus zone (Figure 1.10), leads to healing of vascular tissue which results in a scar [Moller and Hoffman, 2012]. A fibrosis scar located on the aortic wall will weakness the tissue at the boundary between the scar and the aortic wall.

A sensitivity analysis of the difference of DA scar size and material properties will define if there is a stress concentration at the isthmus section, that could trigger BTAR.

This study is based on the Finite Element Method (FEM) and has the aim to find a correlation between geometry and material properties of the configuration of a specimen, since using this kind of analysis is easier to redefine material properties and even geometry, in order to generate a sensitivity study.

2.2 Rationale

As it was mentioned on section 1.5.1 of this thesis:

- The DA, ligamentum arteriosus and isthmus zone (Figure 1.10, leads to a scar on the aortic wall [Moller and Hoffman, 2012]. The healing process the scar has the material properties of the adventitia.
- In an over pressure at the Isthmus zone where the scar is located, could lead to a concentration of stress and strain at the border between the patch and the intima and media layers.
- Another major objective of this chapter is to validate the material properties of the aorta, that will be used for further simulations.

2.3 Methods

A scar on the aortic wall located at the isthmus, will generate a fibrosis tissue. In order to simulate this scar, a patch in the centre of the specimen is added.

A FEM sensitivity study with a control of patch diameter and material properties is proposed. Because producing an experimental study with these different specimens would be very difficult. The FEM technique offered control of these parameters. Therefore the following methodology is proposed:

1. Generate a tri-layered FEM specimen using CREO, which is a computer assisted design (CAD) software. This specimen will have the dimensions of the sample used in the experimental bubble inflation test conducted by Pearson [Pearson et al., 2008].
2. Identify the constitutive behaviour of aortic tissue, justify the material properties and material model for the aortic tissue.

3. Validate the input data with the experimental study of Pearson. The different parts of the tri-layered specimen are assembled (Figure 2.1), the shell circle is clamped and the layers are inflated to a spherical “balloon” using uniform pressure on the bottom of the specimen (Figure 2.1). In this way a state of equibiaxial tension is achieved at the bubble pole (Figure 2.3).

Each of the layers has different material properties, and the loading and boundary conditions are based on the experimental study.

4. Generate seven models with the insertion of a patch, changing the patch diameter from 1mm, 2mm, 3mm, 4mm, 5mm, 6mm and 7mm (Figure 2.9).
5. The stiffness of the patch will increase from the stiffness of the adventitia layer, to 190% in intervals of 10%. Because the material properties of the scar is different, to the rest of the surrounding tissue, and the scar is produced from adventitia cells.
6. Apply a bubble inflation simulation test, to the specimens generated, and compare results.

2.4 Generation of the model

Using the software CREO to design the models and HYPERMESH to create the FEM mesh, four parts were generated and assembled into the model, as shown in Figure 2.1,

1. INTIMA (red part in Figure 2.1), a solid square of 4 cm^2 and 0.27 mm of thickness, which is the inner layer of the tissue, with a quad mesh of 12609 elements.

2. MEDIA (blue part in Figure 2.1), a solid square of 4 cm^2 and 0.36 mm of thickness, which is the middle layer of the tissue, with a quad mesh of 19454 elements.
3. ADVENTITIA (green part in Figure 2.1), a solid square of 4 cm^2 and 0.40 mm of thickness, which is the outer layer of the tissue, with a quad mesh of 19534 elements.
4. BOUNDARY (yellow part in Figure 2.1), As a way to constrict the movement upwards of the specimen, but allow sliding of the tissue to generate the bubble, a solid shell circle is created, with the dimensions: inner diameter of 3.2 cm , outer diameter of 4 cm with a round corner of 2 mm of diameter, with a quad mesh of 1080 elements.

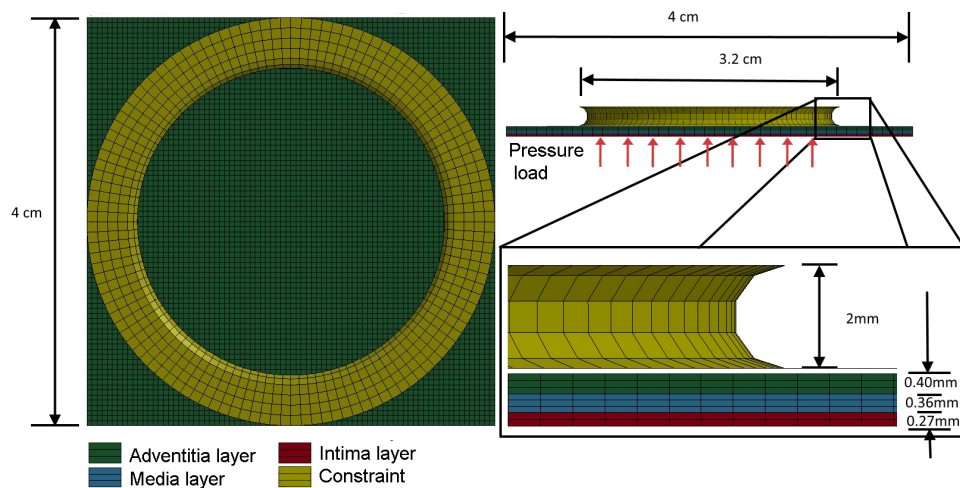


Figure 2.1: Dimensions of the specimen for the bubble inflation test

2.5 Constitutive behaviour of aortic tissue

On account of the complex behaviour of aortic tissue and high deformation ability, the material is approximated using a hyperelastic formulation.

The tissue will be considered as a rubber-like material, discarding the temperature dependency of the viscoelastic formulation. Because a living aortic tissue is usually treated as a pre-stretched material [Holzapfel et al., 2000b], therefore the range of temperature will surpass the denominated glass transition temperature.

The most appropriate material model in LS-DYNA is the simplified rubber/foam material (MAT 181), which is a simplified “Quasi” - Hyperelastic rubber model defined by a single uniaxial load curve, at discrete strain rates [Hallquist and Others, 2013a].

The definition of the uniaxial load curve, which relates the stress to time, is obtained by a nano indentation test reported by Hemmasizadeh, A. et al. [Hemmasizadeh et al., 2013a]. Two load curves of force against time from Hemmasizadeh are used for the material model MAT 181. One curve is for the Intima and Media layers and the other is for the adventitia layer. These curves are shown in Figure 2.2, and represent the loading rate dependency.

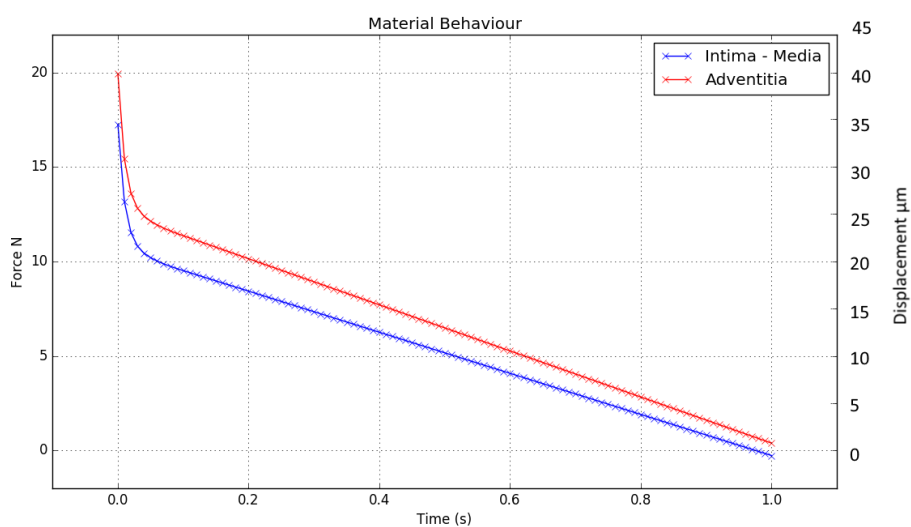


Figure 2.2: Material behaviour curves

2.6 Validation of the material model

The most appropriate way to understand the mechanical behaviour of any material is to subject it to mechanical tests. In this study comparisons of the FEM model with both an analytical model and with the experimental bubble inflation test [Pearson et al., 2008] are compared.

2.6.1 Analytical comparison

The analytical model follows the relationship for a pressurised spherical vessel to calculate the ultimate tensile stress [Charalambides et al., 2002]:

$$t_t = t_0 \left(1 - \frac{h^2}{r^2}\right)^{-2} \quad (2.1)$$

t_0 = Original thickness

r = Original radius

h = Height of the bubble (Z displacement)

$$R = \frac{a^2 + h^2}{2h} \quad (2.2)$$

R = Radius of the bubble

$$\sigma = \frac{PR}{2t_t} \quad (2.3)$$

σ = Ultimate tensile stress

P = Rupture pressure

t_t = Thickness at the pole of the bubble

2.6.2 Experimental comparison

Bubble inflation test

To obtain the mechanical characteristics of soft tissue a sample should be tested in a biaxial tensile test, there are different types of this kind of test as: biaxial plane extension of cruciform samples [Iadicola et al., 2014], rotatory clamp technique [Hachmann and Meissner, 2003], among others.

In this study the test that is evaluated is known as Bubble-inflation test, that seems to be the best way that a biaxial test can be held, because of the simplicity of its mechanism [Charalambides et al., 2002], this method has long been used for the characterisation of synthetic polymers, especially rubber and polymer melts by many researchers [Charalambides et al., 2002], [Mohan and Melvin, 1982], [Joye, 1972]; it is of great importance that the bubble shows the equi-biaxial zone at the bubble pole [Reuge et al., 2001].

Figure 2.3, shows the bubble inflation test, with a 3-dimensional shape and all the data that the study can produce, in order to get the mechanical properties of a material during a biaxial test.

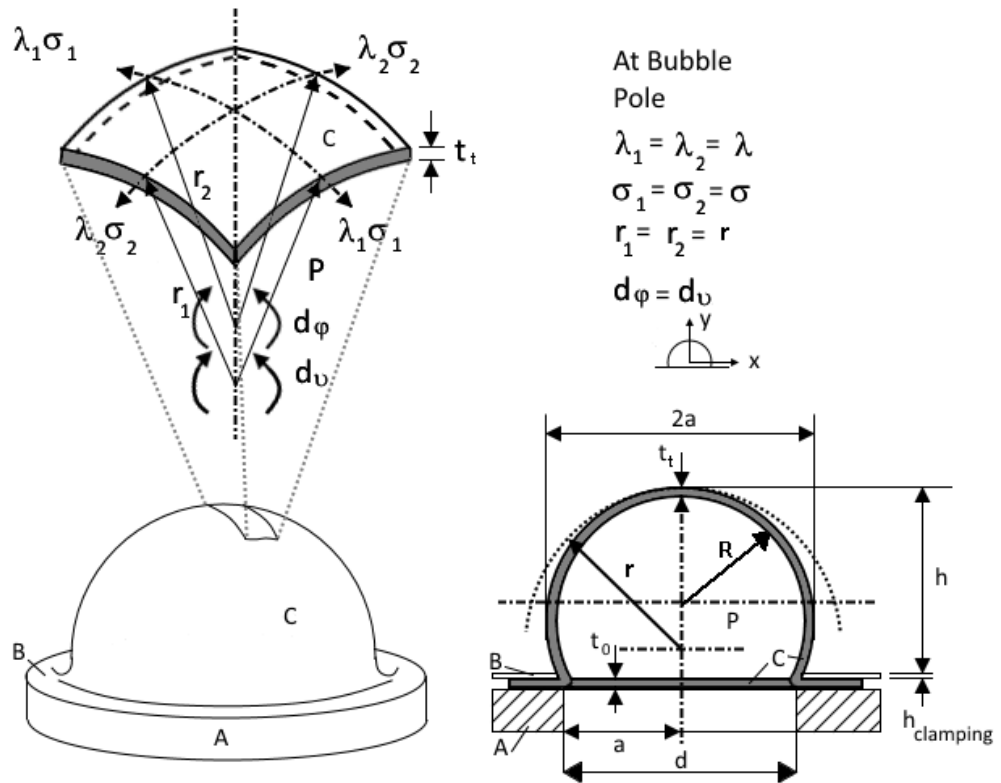


Figure 2.3: Bubble inflation test. A - inflation orifice, B - clamping orifice, C - specimen sheet, P - pressure, t_0 - original thickness, a - initial radius, h - bubble height, t_t - thickness at bubble pole, d - diameter, r - radius of curvature, σ - engineering stress λ - stretch ratio [Johannknecht and Jerrams, 1999]

2.6.3 Results

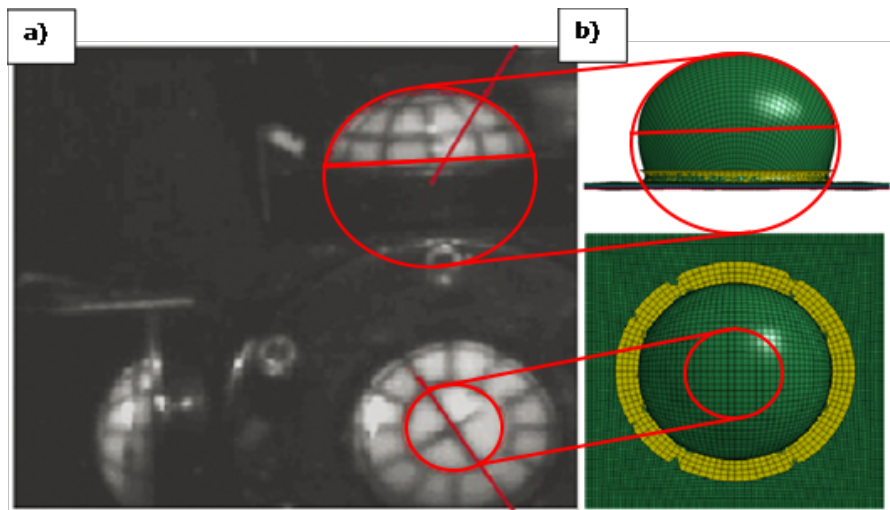


Figure 2.4: Comparison of experimental VS FEM test of the isthmus zone. (a) Experimental from Pearson [Pearson et al., 2008], (b) equivalent FEM images.

Figure 2.4(a) shows an image taken during the bubble inflation test of Pearson, just prior to rupture, compared to the FEM simulation 2.4(b). This section will demonstrate that the bubble on Figure 2.4(b) is an accurate recreation of the shape of the experimental bubble on Figure 2.4 (a).

Three different ways of comparing the results are given, i.e. rupture pressure, ultimate tensile stress and radial extension. The experimental data of the isthmus zone and analytical calculations, are compared with the FEM model results.

Rupture pressure

From the experimental study are measured three values for the rupture pressure, a maximum value of 335.3 kPa , an average value of 287 kPa , and finally a minimum value of 238.7 kPa . Comparing this to the analytical calculations, using equation 2.3, three values are evaluated, a minimum of 240 kPa , average of 270 kPa and a maximum of 300 kPa . These values are shown in Figure 2.5.

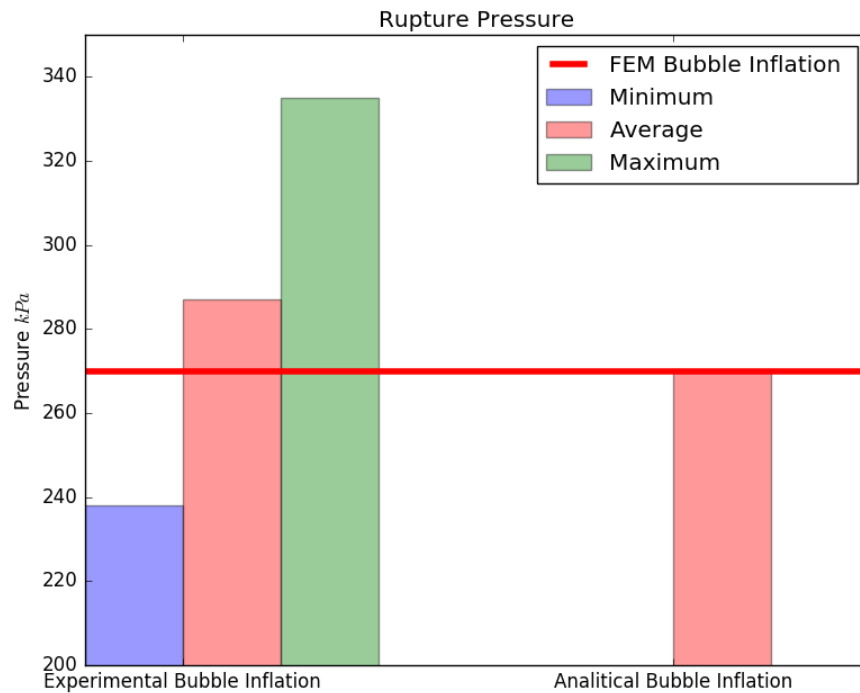


Figure 2.5: Comparison using the rupture pressure

Because this simulation is not using a failure criteria, with the values taken in the experimental study and the analytical calculation, the average value of 270 kPa is used as the ultimate value for the rupture pressure, included also in Figure 2.5.

Ultimate tensile stress

The comparison of ultimate tensile stress is shown in Figure 2.6. For the experimental test the values are taken exactly from the reference [Pearson et al., 2008].

For calculating the ultimate tensile stress Pearson use the variables of rupture pressure (P), initial membrane thickness (t_0), initial innermost circle diameter (d_0), diameter of innermost circle in frame prior to rupture (d), radius of curvature prior rupture (R). Using these variables to calculate the hoop stress (σ_{HE}), which is used to calculate the ultimate tensile test (σ_E) [Pearson et al., 2008].

Radial extension

$$\lambda = d/d_0 \quad (2.4)$$

Hoop stress

$$\sigma_{HE} = PR/2t_0 \quad (2.5)$$

Ultimate tensile stress

$$\sigma_E = \sigma_{HE} \times \lambda^2 \quad (2.6)$$

In the FEM simulation, Von-Mises stress of twelve elements from the centre of the bubble (four from each layer), were calculated to give the average value, the minimum and the maximum value. Because the material model does not have failure criteria, Von-Mises stress will give the yield criteria, for the ultimate tensile stress.

The analytical values were calculated from the spherical pressure vessel relationship, using equation 2.3, with the values of rupture pressure shown in Figure 2.6.

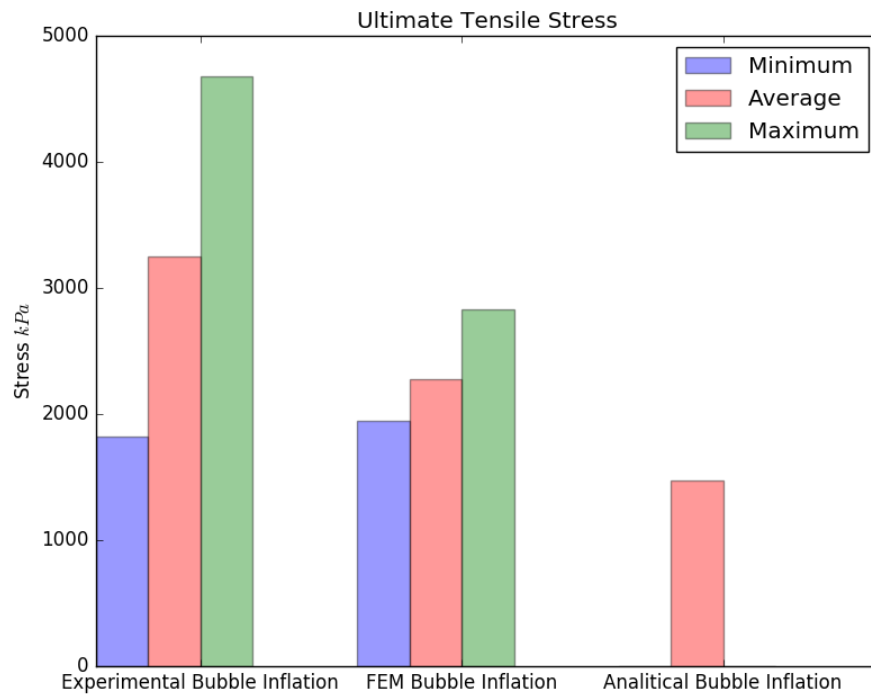


Figure 2.6: Comparison using the ultimate tensile stress

Distortion on the mesh of the zone restricted by the solid ring began after 270 kPa . Even though no failure criterion was used, this distortion affects the values at the equi-biaxial zone, located at the pole of the bubble.

Radial extension

Figure 2.7 shows the comparison of radial extension, for the experimental test. For the results of the FEM test, because the values of a radial extension are not given in the FEM, an analytical calculation using equation 2.2 enabled radial extension to be calculated from the bubble Z-displacement.

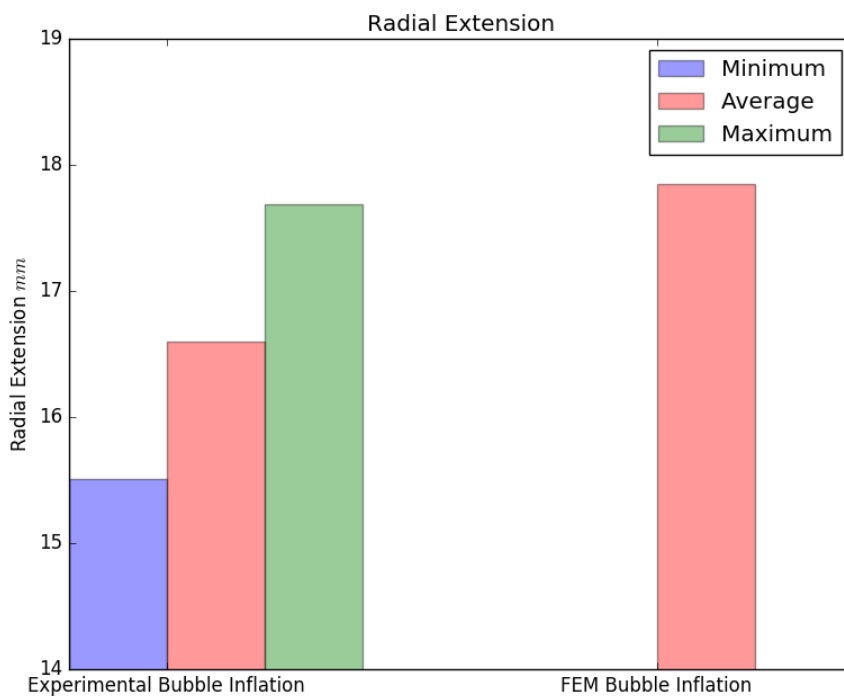


Figure 2.7: Comparison using Radial Extension

2.6.4 Conclusion

Good agreement with all three comparatives is obtained. In the first comparison, the rupture pressure of the isthmus region does not exceed the maximum value of the experimental test and is not lower than the minimum value.

For the ultimate tensile stress comparison, the value of the FEM simulation is closer to the analytical calculation but is still in the range of the experimental test.

The radial extension comparison shows a difference of 1.79% between the higher experimental radial extension and the FEM value obtained. Thus the FEM model is validated with these results and can be altered to the next test and will produce accurate information.

2.7 The use of the FEM to predict bubble inflation with a stiffer patch

Having validated the FEM model with the experimental data for the bubble inflation test, the model is now used to investigate the effects on stress of a stiffer patch inserted in the bubble. Using the same nominal mechanical behaviour and material properties, as for the aortic bubble inflation model, the geometry of the specimen is changed in a way to simulate a scar on the vessel wall. Usually a scar is formed by the closure of the DA, which has a diameter of approximately 5 mm [van Vonderen et al., 2014], Figure 2.8 shows the location of this vessel.

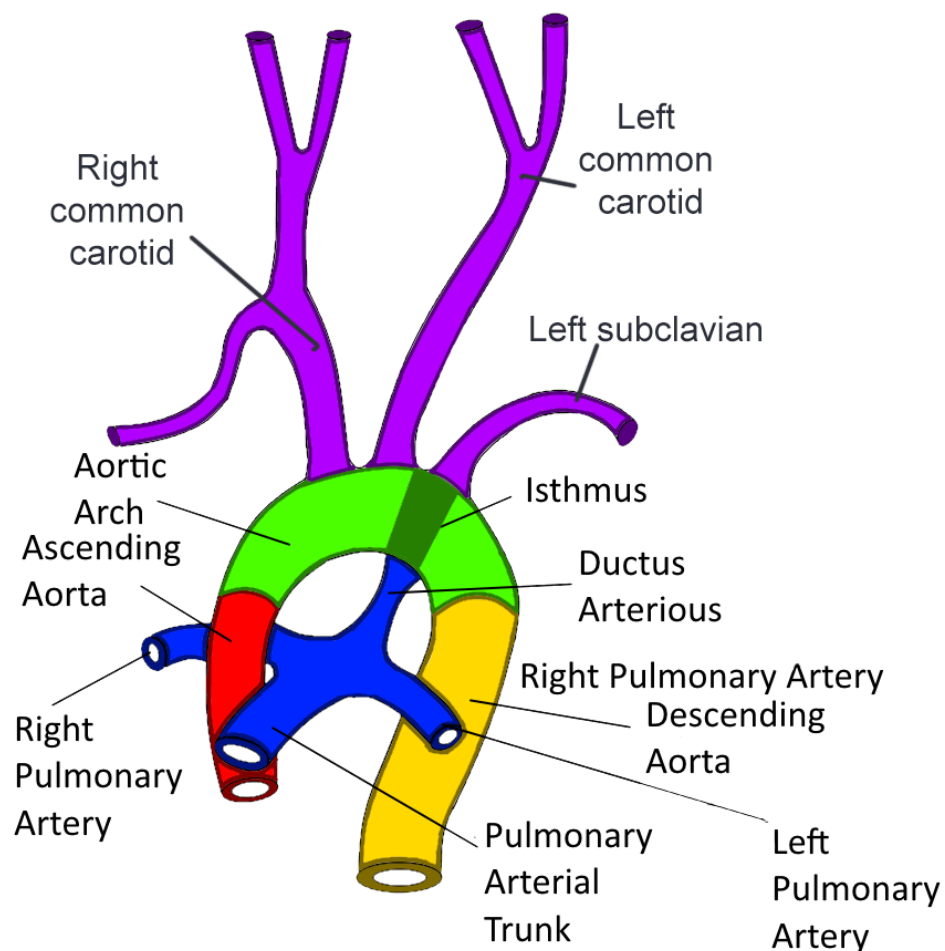


Figure 2.8: Location of the ductus arteriosus

Following the briefing of section 2.4 of this chapter, seven models were designed, changing size of the patch of each one, and a further ten simulations changing the stiffness of the patch.

2.8 Results

In this study two dimensions were altered, first the diameter of the patch (which simulates the size of the DA scar) and second the stiffness of the patch (which simulates the material properties of the DA scar). In the interest of showing which of these variables affects more the tissue. Two sensitivity studies are developed, comparing the reaction of the Intima later, at the border between the patch and the tissue (on the side of the tissue).

These two variables (i.e. stiffness and diameter) were chosen to compare which of them can affect more to the mechanical reaction of the tissue at the isthmus zone.

The two studies are:

1. VARIATION OF DIMENSIONS. Values of Von Misses effective stress and strain are compared across the inflating bubble, varying the dimensions of the patch but but keeping its stiffness constant.
2. VARIATION OF STIFFNESS. Values of Von Misses effective stress and strain are compared across the inflating bubble, maintaining constant dimension of the patch.

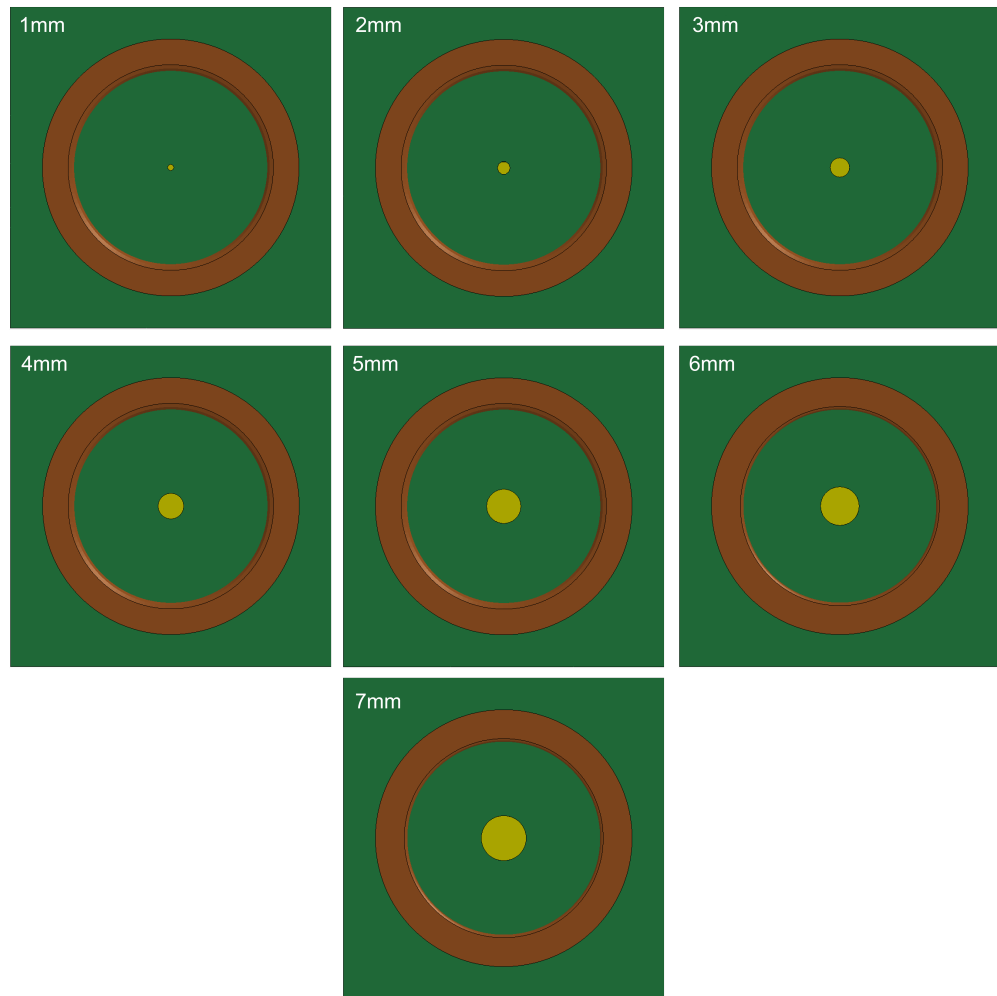


Figure 2.9: Specimens showing the different diameter of patches from 7 *mm* down to 1 *mm*.

Figure 2.10 shows two different plots, using the values of stress and strain obtained in the simulation, first for the variation of dimensions of the patch, and second, for the percentage change in stiffness of the patch. This figure also shows on the abscissa axis, the size of patch or the percentage of stiffness, and on the ordinates a value called the intensity factor which is used here as a synonym for stress or strain concentration factor, depending upon context.

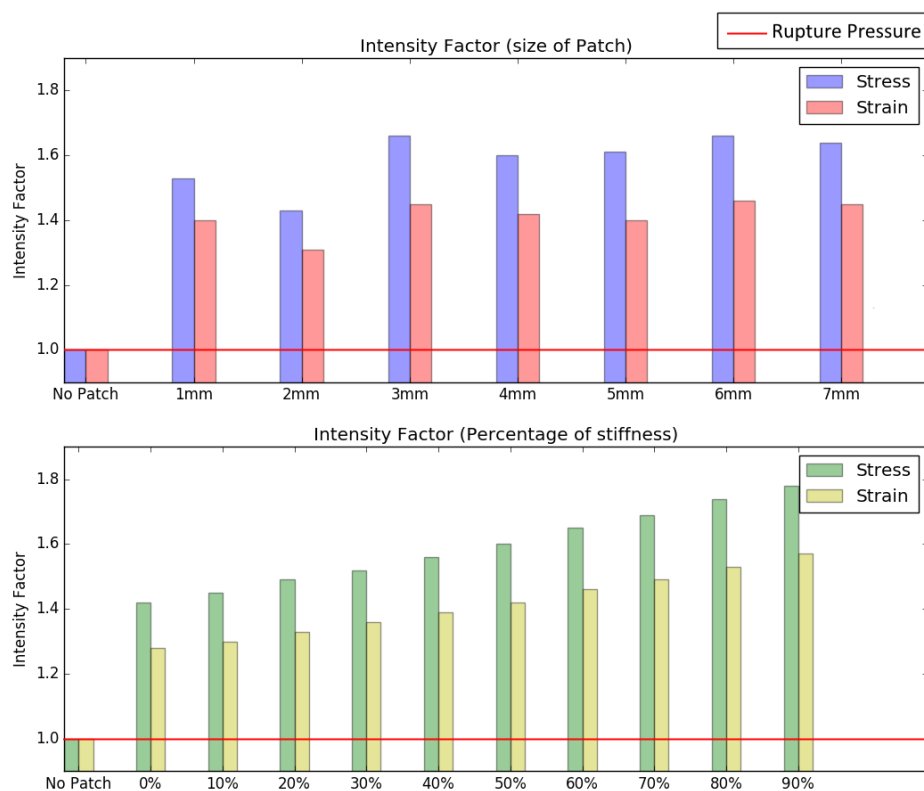


Figure 2.10: Intensity factor for stress and strain, varying dimensions and stiffness of a patch in a bubble inflation test.

In a patch which variate the stiffness in a linear increment of stress and strain its shown. Therefore, meanwhile the patch is stiffer the values for stress and strain are higher.

For the variation of diameter of the patch shown in Figure 2.9, four focus points of interest are enumerated:

1. The highest concentration of stress and strain is achieved in the specimen with a 1 *mm* patch diameter, showing an intensity factor of 1.53 and 1.40 for stress and strain respectively, compared with the 2 *mm* patch diameter which has 1.43 and 1.30 for stress and strain respectively.

The values of the 2 *mm* patch, are closer to the lineal increment of the study in which the stiffness variate, at an increment of 10% with values of 1.44 for stress and 1.29 for strain.

2. The bubble with a patch of diameter of 3 *mm* presents the highest concentration of stress and strain with a value of intensity factor of 1.66 and 1.45 respectively.
3. From 3 *mm* on, the values of intensity factor are fluctuating until achieve a lineal increment, where it can be said that the bubble is behaving with the mechanical properties of the patch.
4. The sixth step with a value in diameter of 6 *mm* achieve the same values of the third which are the maximum values of both studies.

2.9 Discussion

The material model and properties of each layer of the aorta were validated within these simulations. Since the input data were taken from published literature, a comparison with a experimental analysis and analytical calculations will validate the data, and ensure the use of it in other FEM simulations.

A high concentration of stress and strain, between the first specimen and the second, is observed in both studies. This is due to the insertion of the patch, and due to the mechanical properties of the patch, which are taken from the adventitia layer being stiffer layer.

For the study in which the stiffness where the variable, a parabolic increment with the increment of the stiffness is observed, this is due to the non-linear behaviour of the tissue. This behaviour implies that the change in diameter affects the mechanical behaviour of the specimen to a greater extent than the change in stiffness.

When both studies have the same increments of stress and strain the bubble is behaving in greater degree as the mechanical properties of the patch, that can be seen in the simulations referring to 7 mm diameter and 60% of stiffness.

Accordingly with the analysis shown in this chapter, a small diameter scar due to a closure of the DA, could lead to a high concentration of stress and strain at the isthmus zone.

The tissue will get weaker due to a break at the intima and media layer, with the addition of a fibrous tissue, therefore if the vessel is subjected to a high inside pressure, the border between tissues will show a concentration of stress and strain.

The scar tissue gets the properties of the Adventitia layer which is stiffer than the others, in consequence this could lead to make the material of the intima or media layers brittle and initiate a tear inside of the vessel.

This reaction of the tissue could not be observed in the experimental study done by Pearson, because the samples were taken from healthy young specimens, and they were not in the search of samples with a scar due to the closure of the DA. An experimental study of this kind need a high number of samples of the same diameter of scar in this zone and a non destructive way to see the material properties of the scar.

2.10 Conclusion

At the isthmus zone a scar a scar is usually present, due to the closure of the DA which connects the pulmonary trunk to the aorta. Both the diameter of this scar, and also the mechanical properties, could vary, due to the type of healing of each individual. In spite of this BTAR initiates at this zone, therefore in this chapter a sensitivity study is proposed to test the insertion of a scar in this zone of the aorta.

Therefore with the insertion of a patch with different material properties and diameter, in a bubble inflation test of the aortic tissue, a concentration of stress and strain is observed, if the scar is closer in diameter to the thickness of the tissue (the diameter of the scar is 1 *mm*, the thickness of the aorta is 1.03 *mm*), at this size of patch the highest concentration of stress and strain is observed. This could be an explanation for one of the mechanisms of BTAR.

Chapter 3

Comparison of geometric approximation and anatomically segmented model of the aorta using the Finite Element Method

3.1 Introduction

FEM simulation of organic tissues has become important in the design of medical devices, as a non-destructive test for human tissue. To perform a FEM simulation a geometry has to be generated.

Two ways to generate a geometry of any organic tissue, for the use in FEM, are explored. One is to generate an approximated geometry of the tissue, using a Computer Aided Design (CAD) software. The alternative is to use a software which can segment 3D medical images. In this way the dimensions of the specimen are as accurate as the input data. Usually the input data is taken from Computed Tomography scan (for hard tissue) or Magnetic Resonance Imaging (for soft tissue).

The advantages of using an approximated geometry specimen, includes the simplicity of its creation and the speed in a simulation, due to its symmetry and uniformity [Spirka et al., 2014].

The segmentation of 3D medical images, can be used to generate an anatomically precise model, this model will be more accurately shaped, but it requires significantly more computational power for FEM simulations, in comparison to the geometric approximated specimen.

The shape of any structure will influence the distribution of stress and hence the strain reaction of the specimen in general, within the range of the internal mechanical properties of the material. Therefore, in any engineering analysis (including FEM) it is of great significance to have an accurate representation of the geometry that will be analysed.

Taking this into consideration, an accurate geometry has to be designed, in association with a good quality mesh, in order to reduce error in the prediction of the analysis. An essential variable is the element size of the mesh, considering that while the topography of the mesh gets closer to the real geometry, the mesh requires smaller elements. A smaller element mesh will increase the cost in terms of processing power and time.

This chapter shows a comparison of a Geometric Approximated Model (GM), with a simple geometry; against a Segmented Model (SM), which is a precise anatomical specimen. In order to find the advantages of a segmented model in cardiovascular biomechanics.

3.2 Methods

To ensure that a simulation is accurate and uses as fewest resources as possible, a sequence of a trustworthy FEM simulation is shown in Figure 3.1. This could be used as a guide line for applying the FEM technique, to simulate engineering problems in biomechanics.

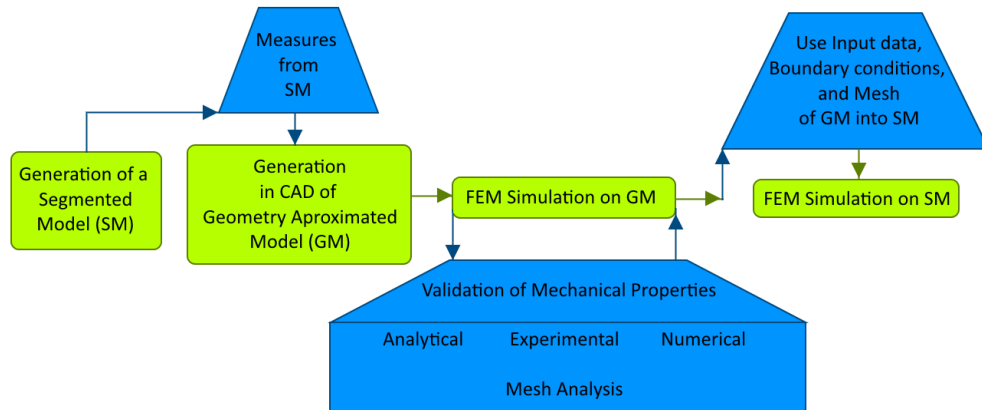


Figure 3.1: Procedure to generate a complex FEM simulation using a geometric approximated and a segmented model

In the following sections this methodology will be applied, explained and tested, for comparing the two geometries mentioned above.

In general, the proposed procedure is:

1. With the use of 3D medical images, generate a geometry, based on this geometry sketch a GM CAD model.
2. Verify the mechanical properties and material model selected with a three way validation, i.e. experimental, analytical and numerical.
3. Certify that the mesh has an accurate topology (size and type of elements) as to check analysis convergence, through a FEM Mesh analysis of the GM.
4. Verify the boundary, load and contact conditions, through a complete simulation with the GM.
5. Apply the input data of the GM, into the SM simulation.

The models represents a 10 *mm* long segment of the human aorta, with three layers, using hyper-elastic rubber-like mechanical properties [Hemmasizadeh et al., 2012], verified in a bi-axial bubble inflation test (tested in Chapter 2).

Both specimens will be loaded with an internal variable pressure, which will simulate the reaction of the aorta to the beating of the heart, being that the aorta is an elastic tube, the beating of the heart will generate a pressure wave that will travel through the aorta. Using the software LS-DYNA (Livermore Software Technology Corporation), based on the FEM to simulate two different pressure curves:

1. HIGH PRESSURE RANGE. Using as the highest value the rupture pressure defined in the previous chapter. With values from 0 – 2025 *mmHg* (0 – 270 *kPa*).
2. NORMAL PHYSIOLOGICAL PRESSURE RANGE. Low pressure curve with values of 0 – 170 *mmHg* (0 – 22.7 *kPa*).

Using the following equations to calculate the percentage of error between GM and SM:

$$\% \sigma \text{ error} = \left| \frac{\sigma_{GM} - \sigma_{SM}}{\sigma_{GM}} 100\% \right| \quad (3.1)$$

$$\% \varepsilon \text{ error} = \left| \frac{\varepsilon_{GM} - \varepsilon_{SM}}{\varepsilon_{GM}} 100\% \right| \quad (3.2)$$

$$\% S \text{ error} = \left| \frac{S_{GM} - S_{SM}}{S_{GM}} 100\% \right| \quad (3.3)$$

Where:

σ : Von-mises stress

ε : Von-mises strain

S : Resultant displacement

Using the sub-index GM for the geometric approximated model and the SM for the segmented model.

3.3 Generation of specimens

The segmentation of images depends on the quality of the input data, and the contrast of the part to be segmented out.

Computational Tomography (CT) scans are usually used for the segmentation of bone, due to the quality that hard tissue represents on the image, facilitates to distinguish it with the rest of the tissues shown in the image.

The use of Magnetic Resonance Imaging (MRI) scans, gave a good resolution for distinguish soft tissue.

Because in this simulation the aorta will be treated as a three layered vessel, in an MRI image these layers are not distinguishable, therefore to get a clearer image of the three layers, the use of a different source of image data is necessary.

The visual human project is a set of high resolution photographic images, of a healthy middle aged man, that was frozen after execution by lethal injection and cut in slices, then a high resolution photograph was taken of each slice [Spitzer et al., 1996]. These images were loaded in the software MIMICS V17 (Materialize), which can segment the images and generate a STL (STereoLitography)file.

Even though that it is possible to identify the three layers of the aorta on this high resolution images, on some of them it is not possible to distinguish clearly between layers, with the result that the thickness of each layer is not constant.

Consequently the following procedure was used to segment a 10 *mm* portion of the Descending Aorta

First segment out the inside of the aorta, using the liquid within the lumen. Then this section (as a STL file), was exported to the software 3-Matic V9 (Materialize), and from the lumen, the layers of the aortic wall were added: 0.027 mm for the Intima layer, 0.036 mm for the Media layer with and 0.040 mm for the Adventitia layer [Holzapfel et al., 2005].

Adopting the largest diameter of the previously segmented model, the GM was generated using the CAD software PTC CREO Parametric, a cylinder of 15 mm diameter and 10 mm long was generated. The SM specimen has two branches on its side, therefore two small cylinders were generated on the side of the GM specimen.

This specimen is also built from three layers, each layer has the same thickness as the SM model (i.e. intima 0.027 mm , media 0.036 mm , adventitia 0.040 mm), these parts were assembled as a three layered model.

Figure 3.2 shows the architecture of the two specimens, on the left side the GM and on the right the SM.

The GM specimen was exported to HYPERMESH (Altair) to create the FEM mesh that will be applied in both models.

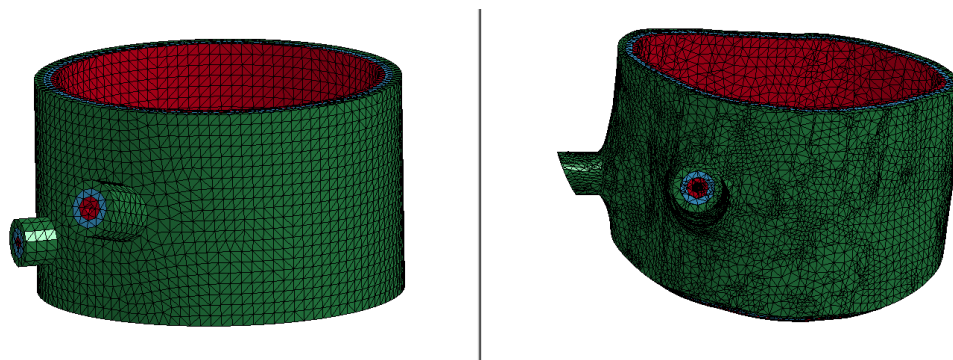


Figure 3.2: Geometric approximated model (GM) left, segmented model (SM) right

3.4 FEM mesh analysis

In order to discard the possibility that the element size of the mesh alters the distribution of results, in this section, an analysis of different size element meshes is performed.

To have an accurate mesh for both models, the GM is subjected to a normal physiological pressure of $0 - 170 \text{ mmHg}$ ($0 - 23 \text{ kPa}$), with the input data which is presented in Table 3.1.

Using HYPERMESH (Altair), the GM specimen was meshed with R-Trias elements (square elements split into two right angle triangles), this shape of element was selected because it could be applied to both models. Eight different size of elements were tested: 0.200 mm , 0.250 mm , 0.300 mm , 0.325 mm , 0.350 mm , 0.375 mm , 0.400 mm , 0.500 mm .

In Figure 3.3, stress values are compared from elements selected from a particular area, two disturbances are located, one at 0.300 mm and the second one at 0.375 mm , these two values are $\approx 4\%$ lower than the last measure, due to the approximated error, the discontinuity could be due to irregularities among these sizes of elements, therefore the stress values droop.

The mesh with 0.325 mm element size shows the best convergence of the element sizes compared, shown in Figure 3.3, therefore the results will not be conditioned by the element size, using the lowest computational resources.

The mesh for both specimens, SM and GM, will be R-Trias elements with a size of 0.325 mm , respecting the separation of the three solid layers.

This mesh generated 91327 elements for the complete GM specimen. The SM specimen the mesh consisted of 105013 elements.

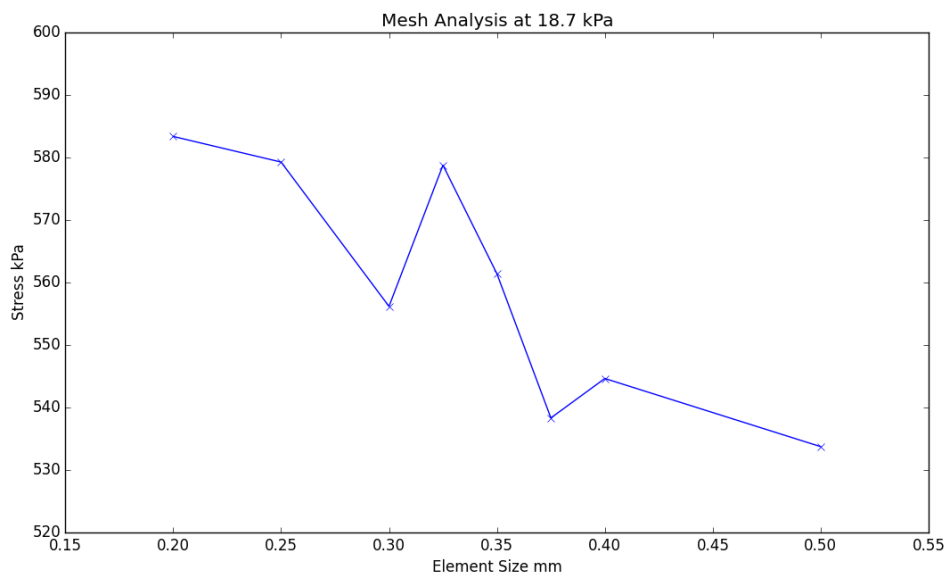


Figure 3.3: FEM mesh analysis, comparing element size of 0.200 *mm*, 0.250 *mm*, 0.300 *mm*, 0.325 *mm*, 0.350 *mm*, 0.375 *mm*, 0.400 *mm*, 0.500 *mm*, at a pressure of 18.7 *kPa*

For the SM specimen the way to generate the FEM mesh was, first using the STL mesh as base to generate surfaces, then based on the surfaces a solid will be generated. Then this solid will be the base of a mesh with R-Trias elements with a size of 0.325 *mm*.

These two models were exported to LS-DYNA to start the FEM simulation. with the data shown in Table 3.1

Table 3.1: Input data for FEM simulation of aortic tissue

Condition	Specification	Value	Units
Boundary	Z axis displacement was not allowed in upper and lower borders	-	-
Contact	Intima as master segment	Tied nodes to surface	-
	Media as master segment	Tied nodes to surface	-
Control	Termination	0.001	s
Load	Segmented set inside intima layer	0 - 300	<i>kPa</i>
Material 181 Simplified Rubber / Foam	Density	1000	$kg \cdot m^{-2}$
	Linear bulk modulus	2×10^5	<i>Pa</i>
	Damping coefficient	0.4	-
	Shear modulus	703×10^5	<i>Pa</i>
	Limit Stress for frequency independent	703.33002	<i>Pa</i>
	Possion's ratio	0.5	-
	Intima, material behaviour	Figure 2.2	-
Media, material behaviour	Figure 2.2	-	
Adventitia, material behaviour	Figure 2.2	-	

3.5 Results

The number of elements differ from 91 327 of the GM to 105 013 of the SM, due to the difference of architecture complexities. It is important to emphasise that the maximum size and kind of element used in this comparison was the same.

The most outstanding point between the two simulations was that the SM took 30 *hr* against the GM which took 10 *min*, using a computer with an Intel® Core™ i7-3820 quad core, hyper threaded CPU @ 3.60 *GHz* processor and 16.0 *GB* of memory.

The difference in run time is associated to the uniformity in element size, due to the simplicity of the GM specimen, the element size is constant, in comparison with the SM specimen that its complexity suggest smaller elements for some areas.

A collection of data from specific sections should be analysed using an engineering analysis and a deformation comparison. Because both geometries are not regular and have different deformation depending on the zone that are measured.

Therefore data was collected from three different zones: two selected zones with high concentration of stress and strain, and a representative zone which will work as a comparable deformation of the rest of the specimen, shown in Figure 3.4. This selected sections are:

- The root of the smallest branch, dividing the results for each layer.
- The root of the biggest branch, dividing the results for each layer.
- The opposite wall of the smallest branch, dividing the results for each layer.

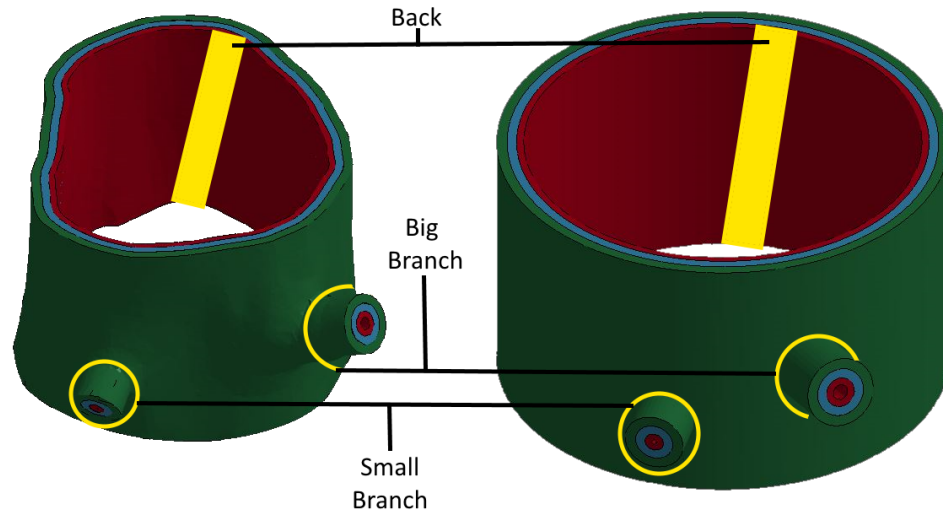


Figure 3.4: Specific Sections for the acquisition of data

For each of these sections values of Stress, Strain and Resultant Displacement are measured. These values will be compared between both specimens to quantify the discrepancy.

The elements were separated first in layers, then in sections and finally in steps of the test. Mean values of Von-Mises stress, Von-Mises strain and resultant displacement for each section and each layer were compared using equations: 3.1, 3.2, 3.3, respectively. The GM specimen is selected as the real value and the SM specimen is selected as the approximated value.

These comparisons generate the results which will be shown and explained in the following sections.

3.5.1 Comparison at high pressure range

This evaluation shows the results at the maximum tensile stress of the tissue, observed by Pearson [Pearson et al., 2008]. The simulation is evaluated first on a high pressure range, then to a normal physiological pressure range.

The first evaluation is the deformation comparison. This would give a global view of the physical appreciation within each layer, it is shown in Figure 3.5 a) b).

For a particular view, an analysis of each one of the specific sections is performed and shown in Figure 3.5 a), b), c).

These two analyses will support the validation to use segmented models.

Deformation comparison

Figures 3.5 a), b), c), show a comparison of the percentage of error for Displacement, Strain and Stress (y axis) for each one of the different pressure steps (shown on table 3.2, x axis), showing the reaction on each one of the layers.

Table 3.2: Range for High Pressure Range

Time (<i>ms</i>)	Rupture Pressure (<i>kPa</i>)
0.1	30
0.2	60
0.3	90
0.4	120
0.5	150
0.6	180
0.7	210
0.8	240
0.9	270

An increment of pressure of 30 *kPa* leads to a 90% of displacement error at the beginning of the test.

The displacement within the three layers, among the selected zones does not show considerable discrepancy, Figure 3.5 shows that the layers follow the same error path and value in displacement for each layer on each zone.

The back zone (Figure 3.5 a) showing a constant decreasing slope until the end of the test, and a parabolic curve which also decrease until 210 *kPa*, which maintain 40% of error for 240 *kPa* and a small increment in the last step.

The small branch (Figure 3.5 c) maintains a constant slope for the first steps, until a pressure of 120 *kPa* having a less steep slope for the next step of 150 *kPa* and then it recovers the same slope than the beginning until the end of the test.

For the error in stress, shows the smallest error reaching values of 10% for pressures of 210 – 240 *kPa*. The Intima layer (red line) shows less error between specimens, followed by the Media (green line) and then the Adventitia (blue line) which achieves 80% error at the first step. The three selected zones shows a decreased steadily until the pressure of 240 *kPa* and then rise on the last step.

The percentage of error in strain, shows the highest discrepancy between layers, having the Intima layer (red line) lower values, then the Media layer (green line) and the Adventitia (blue line) being the highest of the three.

The back zone (Figure 3.5 a) is the more constant decreasing with values no lower than 35% for the Intima layer increasing at the end of the test. The big branch zone (Figure 3.5 b) is the one that has more constant values for the Intima layer from 80 – 40%, Media layer from 80 – 50% and the Adventitia from 80 – 60%.

For the Intima layer, at the small branch zone (Figure 3.5 c) is the one which both specimens get closer but in comparison to the other layers there has a more marked difference.

In Figure 3.6 a) and b) it is shown the difference in appearance at the beginning of the test (60 kPa) for the three zones, then after 120 kPa, the SM specimen is getting a more cylindrical shape, closer to the GM specimen.

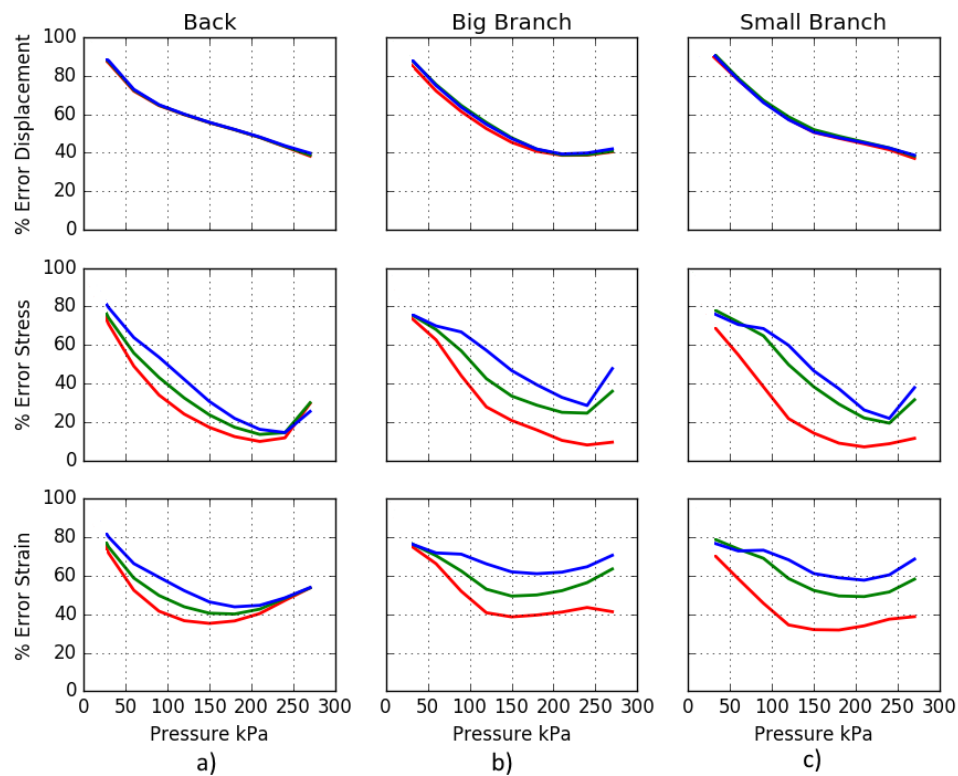


Figure 3.5: Comparison for percentage of error - Pressure for mechanical deformation, stress and strain for each layer for specific sections at rupture pressure (a)back (b)big branch (c)small branch; for intima (red), media (green) and adventitia (blue) layers

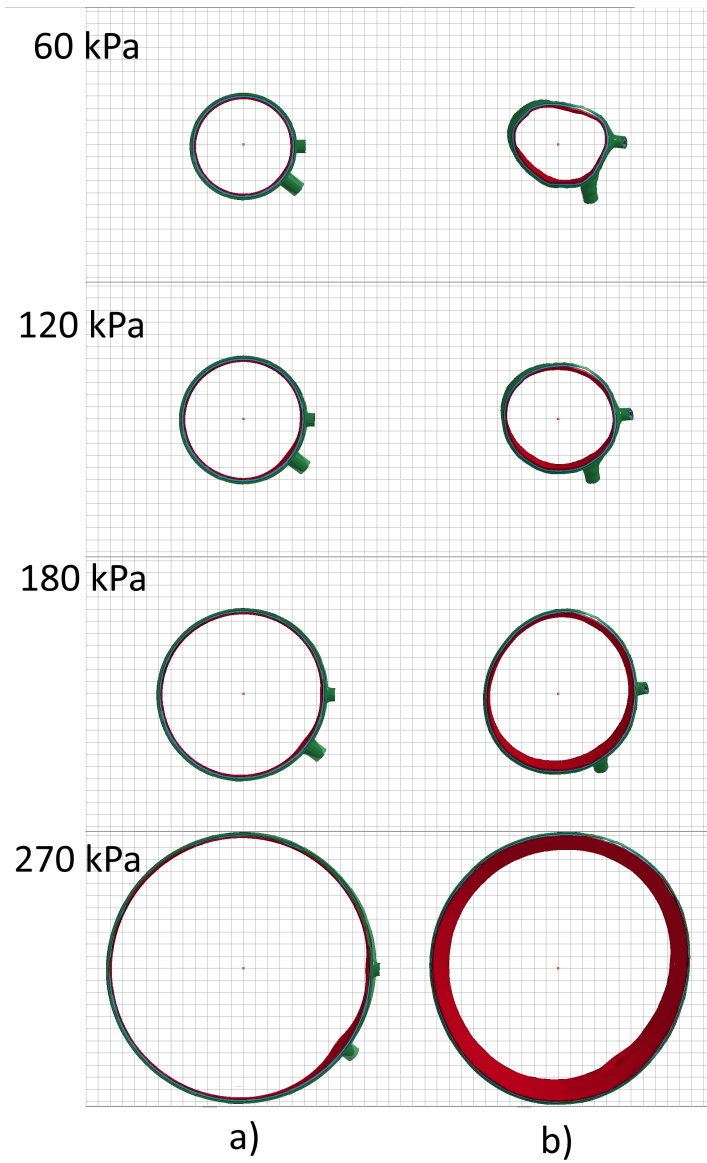


Figure 3.6: Comparison of shapes between (a) Geometric model, (b) Segmented model. Subjected to a rupture pressure range.

Discrepancies between the two models became smaller at higher pressures as the aorta distends and become more circular, above 100 *kPa* the SM geometry overestimate stress by 10 – 40% and strain by 30 – 60%. With these outcome of the simulation, it can be concluded that:

1. Another simulation using a lower pressure range is important to understand what is happening before 30 *kPa*
2. Considerable difference in the architecture between specimens will be seen, hence, values of Deformation and Strain have to be handled with care.
3. The big branch and back zone has a higher difference error at the first step, thus at low pressure these zones has to be analysed carefully.
4. It is important to look at the change in shape for the normal physiological pressure range, specifically when the SM shape gets closer to a quasi-cylindrical shape, in this case the percentage of error will decrease.

3.5.2 Comparison normal physiological pressure range

After the analysis of the previous set of simulations in a high pressure range, a comparison for a low range is essential; because in the last test the highest percentage of error was observed at the beginning of the test. This range is defined as a Normal Physiological Pressure Range due that marks the limits of a pressure that the aortic tissue physiologically should resist.

Specific deformation comparison

Figures 3.7 and 3.8, exhibits the comparison of the reaction between a GM and a SM specimen subjected to a Normal Physiological Pressure range. This range includes changes in blood pressure due to Systole (compression of the heart)[Chobanian et al., 2003], shown in Table 3.3:

1. Optimal blood pressure ($< 120 \text{ mmHg} - 16.0 \text{ kPa}$)
2. Normal blood pressure ($120 - 129 \text{ mmHg} - 16.0 - 17.2 \text{ kPa}$)
3. High normal pressure ($130 - 139 \text{ mmHg} - 17.3 - 18.5 \text{ kPa}$)
4. First grade of hypertension ($140 - 159 \text{ mmHg} - 18.7 - 21.2 \text{ kPa}$)
5. Second grade of hypertension ($160 - 179 \text{ mmHg} - 21.3 - 23.9 \text{ kPa}$)
6. Third grade of hypertension ($\geq 180 \text{ mmHg} - 24.0 \text{ kPa}$)

Table 3.3: Normal physiological pressure range

Time (<i>ms</i>)	Normal Physiological Pressure (<i>kPa</i>)	Normal Physiological Pressure (<i>mmHg</i>)
0.1	10.6	80
0.2	12.0	90
0.3	13.3	100
0.4	14.7	110
0.5	16.0	120
0.6	18.7	140
0.7	20.0	150
0.8	21.3	160
0.9	22.7	170

For the steps under the optimal blood pressure ($< 16.0 \text{ kPa}$), small difference in displacement between layers is shown. For the big branch zone, values are close to zero, shown in Figure 3.7 (b)(Displacement). After this pressure the error between models becomes distinguishable.

The movement between layers is close as the high pressure range, showing the same displacement comparison within the three layers.

The back zone (Figure 3.7 a) is the most affected for the displacement values, presenting a dramatically drop after 140 mmHg (18.7 kPa) having the highest value of error of the test, as the high pressure range simulation. The displacement falls after 140 mmHg in all the other zones at the displacement measure.

When the blood pressure is at the value between optimal blood pressure and first grade of hypertension ($14.7 \text{ kPa} - 110 \text{ mmHg}$, $16.0 \text{ kPa} - 120 \text{ mmHg}$, $18.7 \text{ kPa} - 140 \text{ mmHg}$), the error starts to increase for all the measured values.

This increments are focused on the back zone (Figure 3.7 a) and the small branch zone (Figure 3.7 c), the adventitia layer (blue line) is the most affected within the three zones, for stress and strain.

The small branch zone (Figure 3.7 c) shows a more constant range of error for each layer for the three measures.

The pressure of 18.7 kPa (140 mmHg) is the key value, as it is where the error between models stops increasing. In literature this pressure is considered to be as isolated systolic hypertension; defined by the value where the systolic pressure (compression of the heart) is high and the diastolic pressure (relaxation of the heart) is normal.

The value of 140 mmHg is consider the lower limit of hypertension [Chobanian et al., 2003]. In Figure 3.6 b), it could be seen that the shape of the SM specimen change its shape closer to the GM model (Figure 3.7 a)).

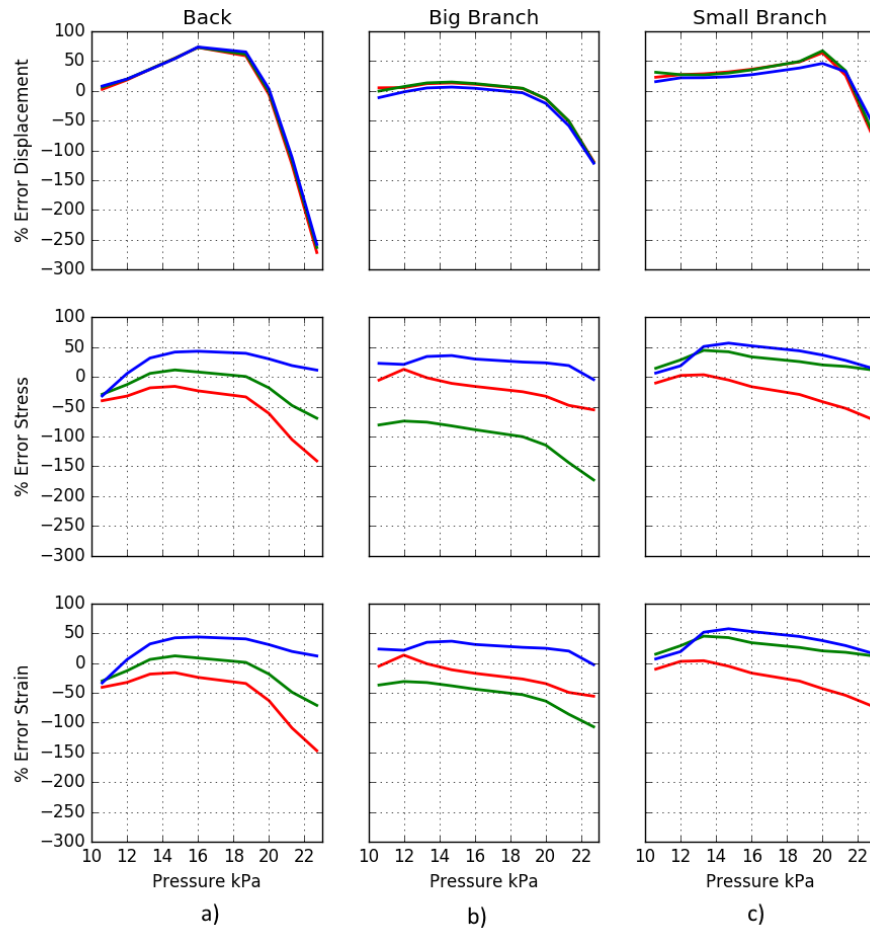


Figure 3.7: Comparison for percentage of error - Pressure for mechanical deformation, stress and strain for each layer for specific sections at normal physiological pressure. (a)Back zone, (b)big branch (c)small branch; for intima (red), media (green) and adventitia (blue) Layers

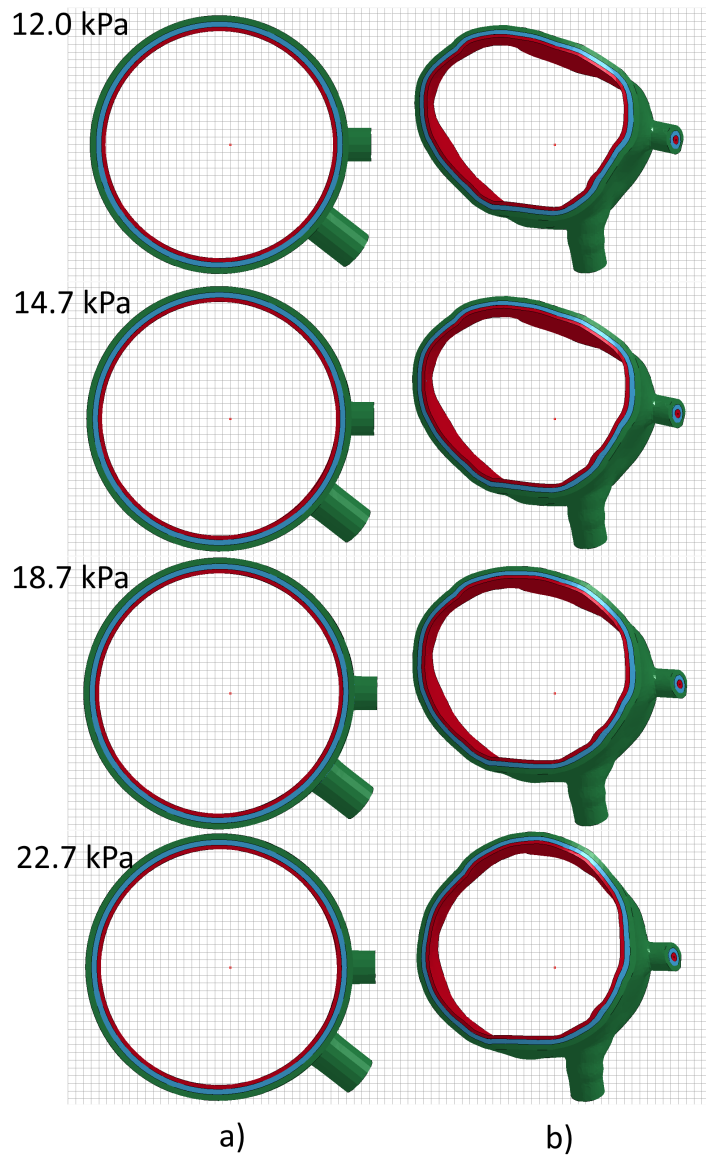


Figure 3.8: Comparison of shapes between (a) Geometric model, (b) Segmented model. Subjected to a normal physiological pressure for mechanical deformation, stress and strain for each layer for specific sections.

3.6 Discussion

This chapter shows a simulation which reinforces the generation of geometries through the segmentation of medical images. These could be applied in the use of a numerical simulation using the FEM, applied to cardiovascular biomechanics.

For the high pressure range, the first part of the test shows the highest error values, where the difference in shape of both specimens is appreciable, with the increment of pressure the shape of the SM gets closer to the GM specimen, therefore the difference between models decrease.

After 150 *kPa* the error in stress and displacement is still decreasing, in comparison with the strain at 150 *kPa* shows a positive tendency.

For the selected zones, the small branch zone is where the difference is higher between the two architectures, in this high pressure range.

In conclusion for this first comparison, the change of shape of the specimen is where the error between models shows higher difference.

A normal physiological pressure range simulation is proposed due of the high increment of error seen at the beginning of the high pressure range simulation.

The errors at the beginning of the test have an approximately constant slope until the pressure achieves the called optimal blood pressure, when the pressure reach the value of 14.7 *kPa* (110 *mmHg*).

At this pressure all the errors increase in value, for the displacement at the back zone continue increasing until 16 *kPa*, where starts going down and then at 18.7 *kPa*, where it presents a steep fall until the end of the test.

The displacement of the big branch maintains around the same value of 0 – 10% error until the pressure of 18.7 *kPa*, where it also shows a drop. And finally for the small branch increase the values until the same step of 18.7 *kPa*.

At 18.7 *kPa* of pressure, the SM instantly starts to behave as the GM simulation, the percentage of error decreases from ≈ 50 – $\approx 100\%$, the SM shows a physical change of cross - section closer to a circle.

For the comparison of errors involving the three layers of the aorta, the values remain close, and increase after the same point of 140*mmHg*.

A high concentration of error in the small branch is focused, at the middle and last steps. The Adventitia is the most affected of the layers

Comparing the two simulations:

1. It is shown that the shape of the curves in Figure 3.5 and Figure 3.7, do not follow the same path, and the percentages of error does not match. This is because of the formulation of the material, being a hyper-elastic model in which strain depends on the time that the specimen has being loaded. On the tables of range of pressure it is shown the time where the load was charged.
2. It can be seen that the error range changes between layers, the adventitia layer shows the more affectation between the three layers. This is due that the load is applied uniformly to the intima layer, and the others received the reaction of this layer, if an error is generated at the intima, it will carry on to the next layers.
3. First comparison suggest that the rupture pressure has the highest error in stress. The error in strain starts to increase after 150 *kPa*.

For the normal pressure range the increment of percentage of error is low until 14.7 *kPa*, 16.0 *kPa*, 18.7 *kPa* where it has a dramatic increase of error for the displacement.

4. Second comparison of the three layers, even though the values of error at the normal physiological pressure range are higher than the rupture pressure range, the tendency for the normal physiological pressure is to increase as the first steps of the rupture pressure range
5. Third comparison the Adventitia layer and the root of the small branch are the specific sections with highest values.

In a increment of inner pressure, the Adventitia layer is the most affected of the three layers, if the aorta is subjected to a high pressure range the discontinuities of the shape are the ones which can cause problems and in a low pressure range all the general shape of the Adventitia layer could cause problems.

3.7 Conclusion

In conclusion, these studies highly supports the segmentation of 3D medical images for the use in cardiovascular biomechanics applied to FEM simulations.

A simulation with a GM specimen should be performed first to assure that the input data, like boundary, contact and load conditions, mesh topology, material model, mechanical properties, among others are the accurate data for the simulation, since now the error between them is measured. The methodology showed in 3.1 must be used in the following chapters, to reduce mistakes in the input data, for a simulation with a SM specimen, which takes more time.

Even though the SM has greater bio-fidelity than a GM model, the reduction in computational resources by the use of the GM gives flexibility to the complexity of the material model selected and facilitates the inclusion of other formulations such as smoothed particle hydrodynamics (SPH) and the use of a fluid solid interactions (FSI).

Chapter 4

Increment of blood pressure raises the possibility of aortic rupture, due to Blunt Thoracic Trauma

4.1 Introduction

The previous chapter supports the segmentation of 3D medical images for the generation of a 3D model for the use in cardiovascular biomechanics. Two ways to generate a 3D model of the aorta were compared using the Finite Element Method (FEM).

The border line between hypertension and normal blood pressure is 140 *mmHg* at the systole (compression of the heart), also this systolic blood pressure represents a higher risk factor for cardiovascular diseases [Chobanian et al., 2003].

At the pressure of $140 \text{ mmHg} \approx 18.7 \text{ kPa}$ last chapter shows that the aortic tissue start to change its cross section to a circle, behaving closer to the geometric approximated model.

Therefore in this Chapter an increment of blood pressure is simulated into the thoracic aorta, using the FEM, in order to test the architecture of the aorta at the different stages of systolic blood pressure (BP), showing that the increment of BP could affect the mechanical behaviour of the architecture of the Thoracic Aorta.

A segmented model of the aorta formed by three layers is subjected to a variation of inside pressure, from $0 - 180 \text{ mmHg} \approx 24 \text{ kPa}$, in steps of 0.1 ms of time, this will simulate the mechanical behaviour of the aorta subjected to a stressful situation when the BP is rising.

Four zones of the aorta are analysed in this study, of a way to show the change of architecture of the vessel, from the Ascending Aorta, Descending Aorta, Internal and External Isthmus.

4.2 Rationale

As a justification for selecting a study with an increment of pressure range and the association between blood pressure with Blunt Trauma, three points are analysed:

Firstly, the American Medical Association on its Seventh Report of the Joint National Committee on Prevention, Detection, Evaluation and Treatment of High Blood Pressure (JNC7), establish that *"In persons older than 50 years, systolic blood pressure (BP) of more than 140 mmHg is a much more important cardiovascular disease (CVD) risk factor than diastolic BP"* [Chobanian et al., 2003].

And also in relation with prevention of hypertension states that, “*Individuals with a systolic BP of 120 – 139 mmHg or a diastolic BP of 80 – 89 mmHg should be consider as pre-hypertensive and require health - promoting lifestyle modifications to prevent CVD*” [Chobanian et al., 2003].

Secondly, for the past 30 years researches have suggested that an increment of adrenaline will activate the sympathetic nervous system increasing the blood pressure [Mancia et al., 2013].

Finally, the second most common cause of death in a car accident is when the chest gets compressed and this leads to a tear inside of the aorta which sliced the vessel through the perimeter of it, allowing blood flow spilling outside the vessel, this is known as Blunt Thoracic Trauma followed by Aortic Rupture (BTAR).

Even though the mechanism of BTAR has not been explained at all, the Archimedes lever principle of leverage is one of the hypotheses that has been used to explain the mechanism of this injury. The principle of leverage is explained as a force has the potential to be amplified if it is applied to one side of a “lever” resting on a pivot.

As a way to connect these three statements, I proposed this rationale:

1. *If a person is involved in a car crash, would reach a state of stress due to the accident, the human body will react with an increment of blood pressure.*
2. *If the BP will increase until a risk factor ($< 140 \text{ mmHg} \approx 18.7 \text{ kPa}$), the architecture of the aorta will change and a concentration of stress could be localised at the inner aspect of the aortic isthmus.*
3. *The chest gets compressed and the aorta deforms, the arch gets closer to a “U” shape tube, due that the ascending aorta moves against the descending aorta. An increment of BP will force the inner part of the arch to move against the inside wall.*

4. Being that the BP is in values of hypertension, the aorta will act as a solid beam, and because of the Archimedes lever hypothesis, these will lead to a concentration of stress focused on the inside wall of the Isthmus zone. Adding the increment of BP a peak of concentration of stress is reached, leading to the collapse of the tissue at this position: the innermost layer of the inner part of the aortic isthmus.

A study which evaluates the architecture of the aorta is proposed and analysed in the subsequent sections, in order to test this rationale.

4.3 Methods

The increment of internal pressure is based on the following stages of blood pressure presented on the seventh report of the joint national committee on prevention, detection, evaluation and treatment of high blood pressure [Chobanian et al., 2003]:

1. Optimal blood pressure ($< 120 \text{ mmHg} \approx 16.0 \text{ kPa}$)
2. Normal blood pressure ($120 - 129 \text{ mmHg} \approx 16.0 - 17.2 \text{ kPa}$)
3. High normal pressure ($130 - 139 \text{ mmHg} \approx 17.3 - 18.5 \text{ kPa}$)
4. First grade of hypertension ($140 - 159 \text{ mmHg} \approx 18.7 - 21.2 \text{ kPa}$)
5. Second grade of hypertension ($160 - 179 \text{ mmHg} \approx 21.3 - 23.9 \text{ kPa}$)
6. Third grade of hypertension ($\geq 180 \text{ mmHg} \approx 24.0 \text{ kPa}$)

To simulate the reaction of the aorta during an increment of BP. The different stages of hypertension were divided in eleven steps, shown in the Table 4.1

Table 4.1: Range of pressure to be simulated

Time <i>ms</i>	Increment of Blood Pressure <i>kPa</i>	Increment of Blood Pressure <i>mmHg</i>
0.1	0.0	0
0.2	10.7	80
0.3	11.9	90
0.4	13.3	100
0.5	14.7	110
0.6	16.0	120
0.7	18.7	140
0.8	20.0	150
0.9	21.3	160
1.0	22.7	170
1.1	24.0	180

This measure refers to the contraction of the heart (Systole), when the blood flows from the heart through the aorta. The increment of BP inside of the vessel could be due to stressful situations, as in the event of a car crash.

One peculiarity of BTAR is that failure happens in a specific spot of the aortic arch, located at the inner part of the aortic isthmus.

Images from the visual human project were selected [Spitzer et al., 1996], including the different zones of the thoracic aorta, i.e. Ascending Aorta, Aortic Arch and Descending Aorta.

These data were loaded and segmented in the software MIMICS V17 (Materialize), using the software 3-MATIC V9 (Materialize) the segmentation of this zone was expanded into three different layers. First the intima layer, with a thickness of 0.027 mm , then the media layer with a thickness of 0.036 mm and finally the adventitia layer with a thickness of 0.040 mm [Sommer et al., 2008].

These three geometries generate an assembly which was exported to HYPERMESH (Altair) to generate a FEM mesh, with the specification shown in Table 4.1.

After generating the FEM mesh, the geometry was exported to LS-DYNA with the input data shown in Table 4.2. This will be the program which calculate the using the Finite Element Method.

Table 4.2: Input Data for FEM simulation of aortic tissue

Condition	Specification	Value	Units
Contact	Intima as Master Segment Tide Nodes to Surface Media as Master Segment Tide Nodes to Surface	-	-
Control	Termination	0.001	s
Load	Segmented Set Inside Intima Layer	0 - 24.0	<i>kPa</i>
Material	181 Simplified Rubber/Foam	-	-
	Density	1 000	$kg \cdot m^{-2}$
	Linear Bulk Modulus	2×10^5	<i>Pa</i>
	Damping Coefficient	0.4	-
	Shear Modulus	703×10^5	<i>Pa</i>
	Limit Stress for Frequency Independent	703.33002	<i>Pa</i>
	Possion's Ratio	0.5	-
	Intima Material Behaviour Curve (Chapter 2 Figure 2.2)	-	-
Media Material Behaviour Curve (Chapter 2 Figure2.2)	-	-	
Adventitia Material Behaviour Curve (Chapter 2 Figure 2.2)	-	-	
Mesh	Number of Elements	861 512	-
	Number of Nodes	287 333	-
	Type of element - R-Trias (square elements split in two right angled triangles)	0.325	<i>mm</i>

4.4 Results

To analyse the thoracic aorta has been divided in four different zones, shown in Figure 4.1:

1. Ascending aorta (ASA, shown in red)
2. External aortic isthmus (EAI, shown in green)
3. Internal aortic isthmus (IAI, shown in black)
4. Descending aorta (DSA, shown in blue)

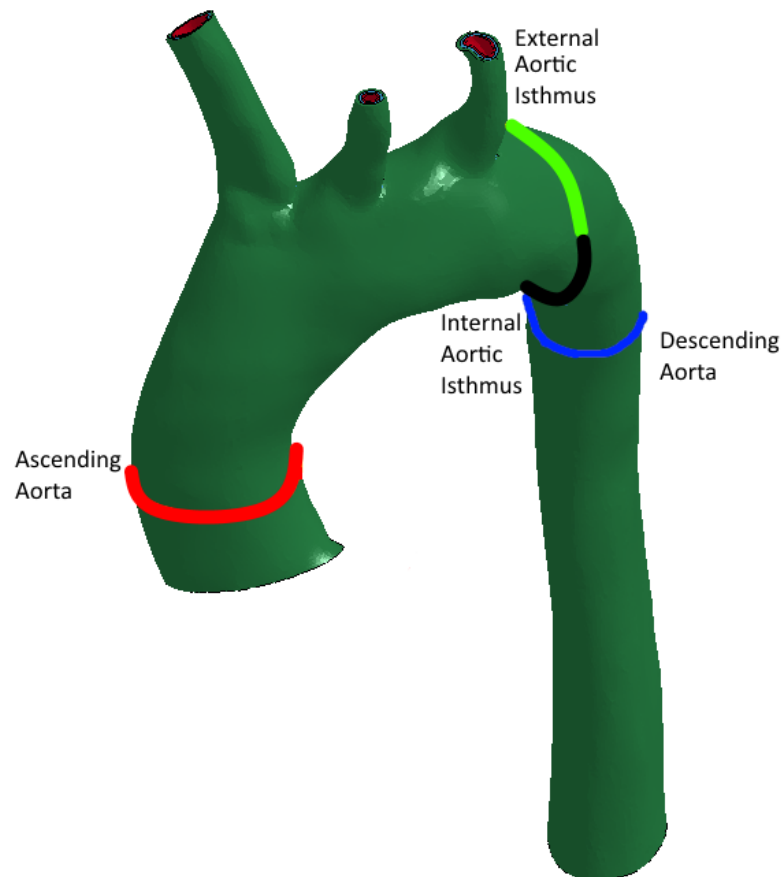


Figure 4.1: Selected zones of the aorta, for the data acquisition

The aortic isthmus was divided in two: external and internal zones, as shown in Figure 4.1, the external part of the isthmus (EAI) will be the control measure, since its displacement is constant (green in Figure 4.2; and the inner part of the isthmus is where the incidence for BTAR is located.

Results from displacement (Figure 4.2), Von-Mises strain (Figure 4.3) and Von-Mises stress (Figure 4.3) (Yield criteria as in Chapter 2), are analysed for each layer (Intima, Media, Adventitia). These results were plotted for only two values of pressure, from normal blood pressure ($120 \text{ mmHg} \approx 16.0 \text{ kPa}$) to first grade of hypertension ($140 \text{ mmHg} \approx 18.7 \text{ kPa}$) to show the difference in reaction, between the Intima layer and the other layers, and the internal part of the aortic arch and the other zones.

For the displacement comparison, a constant increment for these values is shown in Figure 4.2. The IAI (black line) zone for the Intima layer shows a small negative displacement, for the Media nearly to no displacement and for the Adventitia shows a positive displacement with small values. The EAI (green line) shows closer to zero displacement for the three layers among the measures taken.

The displacement for the ASA (red line) zone, even though that is the highest values, is the zone with more movement freedom, anatomically speaking.

The adventitia layer is thickest and the stiffest of the layers, the displacement is expected to be higher on the straight zones of the aorta (ASA and DSA) than on the arch (EAI and IAI).

The strain is compared on Figure 4.3.

Higher values of strain are handled by the IAI zone in comparison with the EAI, being clear on the three layers of the tissue. The EAI zone is again the control measure and shows constant values among the layers.

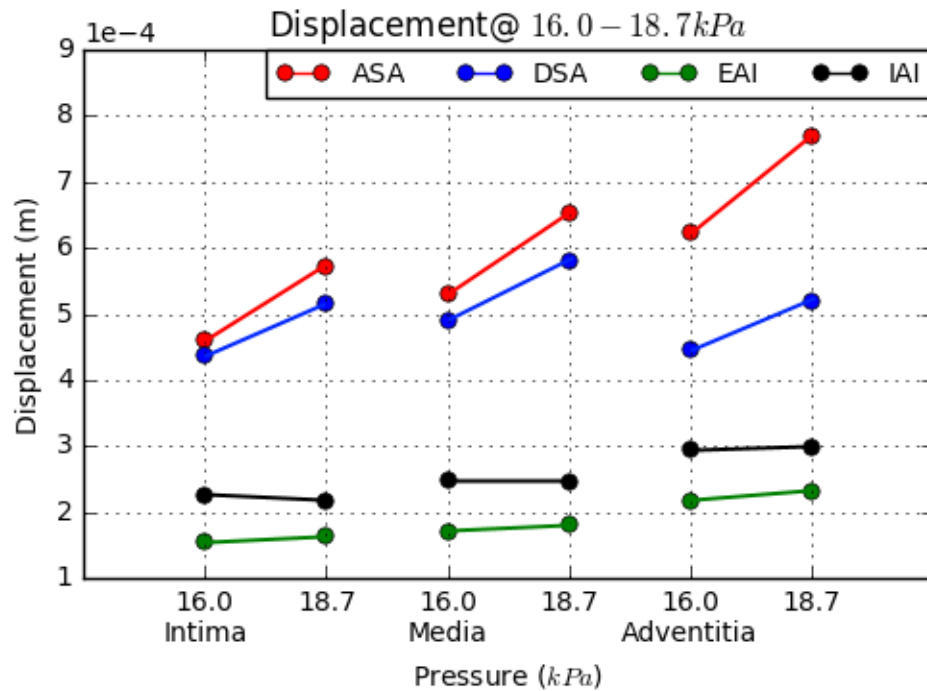


Figure 4.2: Displacement ascending aorta, descending aorta, external and internal aortic isthmus; intima, media and adventitia layers; normal physiological pressure

For the Intima layer, it is clear that the highest values are for the ASA zone, being the DSA on the first part of the test the highest concentration. It is important to point out the IAI zone that shows the same slope as the ASA and the EAI is the constant comparison for the different zones. For the intima and media layers, the DSA and the ASA values are closer.

For the adventitia layer, it is clear that the ASA zone has the highest concentration of strain compared with each zone and also compared with each of the layers. But also on this layer the IAI zone is where the values reach the deformation of the DSA, having a higher concentration on this zone.

Figure 4.4 shows the stress values against the increment from normal pressure to the first grade of hypertension, inside of the thoracic aorta.

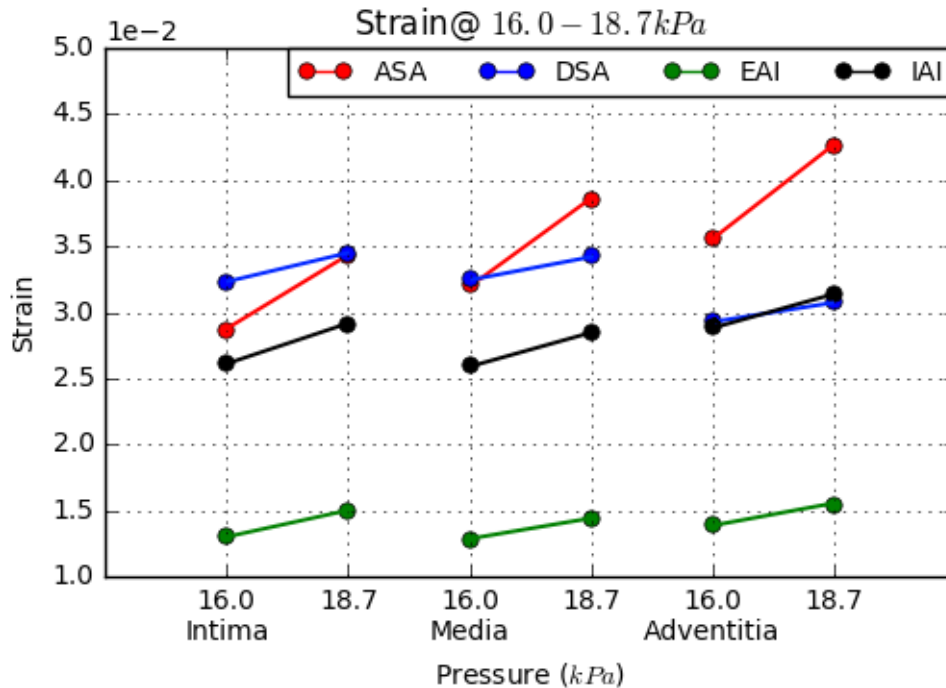


Figure 4.3: Strain ascending aorta, descending aorta, external and internal aortic isthmus; intima, media and adventitia layers; normal physiological pressure

The Intima layer shows a marked concentration of stress at the IAI, pointing out that due of an increment of internal pressure, the innermost layer of the internal part of the aortic isthmus will be weaker in comparison to the other zones and layers.

The highest value of stress is observed at the DSA zone, after reaching these values, the stress values decrease.

There are not big difference between zones at the media layer, showing not a big difference of stress values between zones.

For the three layers the ASA, DSA and EAI zones shows the expected behaviour, the IAI have anomalies, reduced to a concentration of stress with the highest values at the Intima layer, not at the adventitia as would be expected.

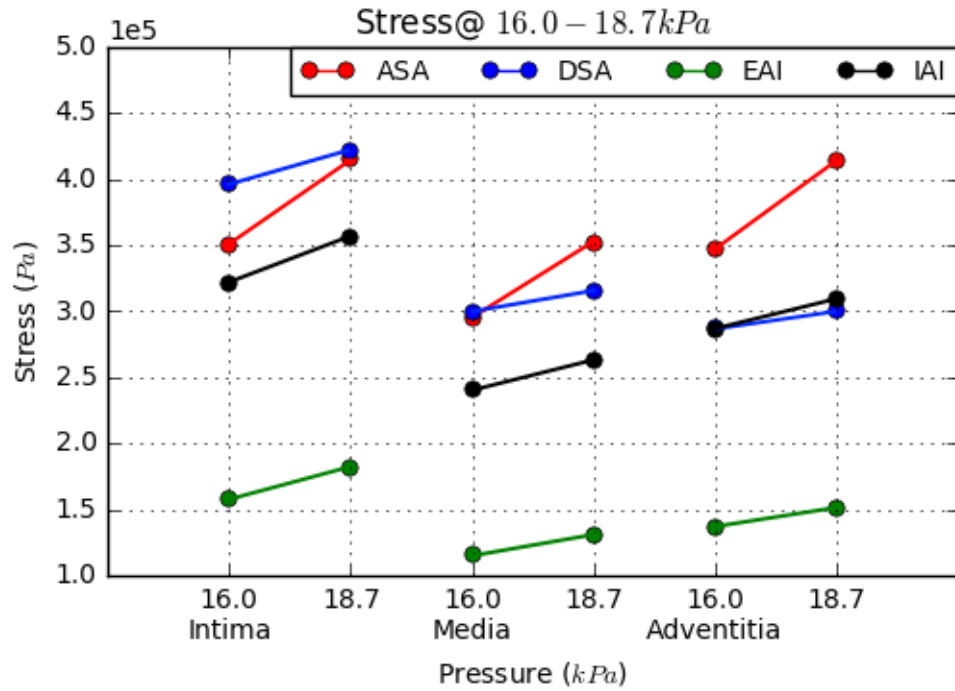


Figure 4.4: Stress ascending aorta, descending aorta, external and internal aortic isthmus; intima, media and adventitia layers; normal physiological pressure

As the displacement Figure (4.2), the stress Figure (4.4), the path for each layer of each zone is a constant slope until the sixth step where the pressure reaches the values for normal blood pressure ($16.0 \text{ kPa} - 120 \text{ mmHg}$), having a smaller slope for the first grade of hypertension ($18.7 \text{ kPa} - 140 \text{ mmHg}$), and after that, the slope droops until the end of the simulation. It is shown a difference for the ASA zone that the curve is different than the other zones.

The previous chapter showed that when the aorta is subjected to an increment of pressure, changes its cross section into a circular shape. When BTAR takes place, the ascending aorta move against the descending aorta, and the arch gets compressed changing its shape and getting closer to a tube with a “U” shape.

Now a geometric three walled “U” shape tube, was subjected to the same test as the segmented model of the aorta. This will show the reaction of a aorta that changes complete cross section to a circle, and the ascending aorta moves against the descending aorta changing the shape of the arch.

Figure 4.5 shows a section through the sagittal plane of both models, displacement vectors are drawn to sketch the direction of movement of the walls.

Three steps are studied in this Figure 4.5, the value of the optimal blood pressure ($16.0 \text{ kPa} \approx 120 \text{ mmHg}$), the border of hypertension (or first grade of hypertension)($18.7 \text{ kPa} \approx 140 \text{ mmHg}$) and the third grade of hypertension($24.0 \text{ kPa} \approx 180 \text{ mmHg}$).

The first comparison shows has closer behaviour, but the geometric model shows higher values of displacement.

The second comparison the IAI zone of the geometric model change the displacement direction to the inside of the vessel. But in comparison, the segmented model shows higher values of displacement, compared to the neighbour area and also in general with the values of the geometric model.

The last comparison the direction of displacement of the geometric model, at the aortic arch, changes completely at values of the third grade of hypertension. The IAI of the segmented model starts to change direction of the displacement, as the geometric model.

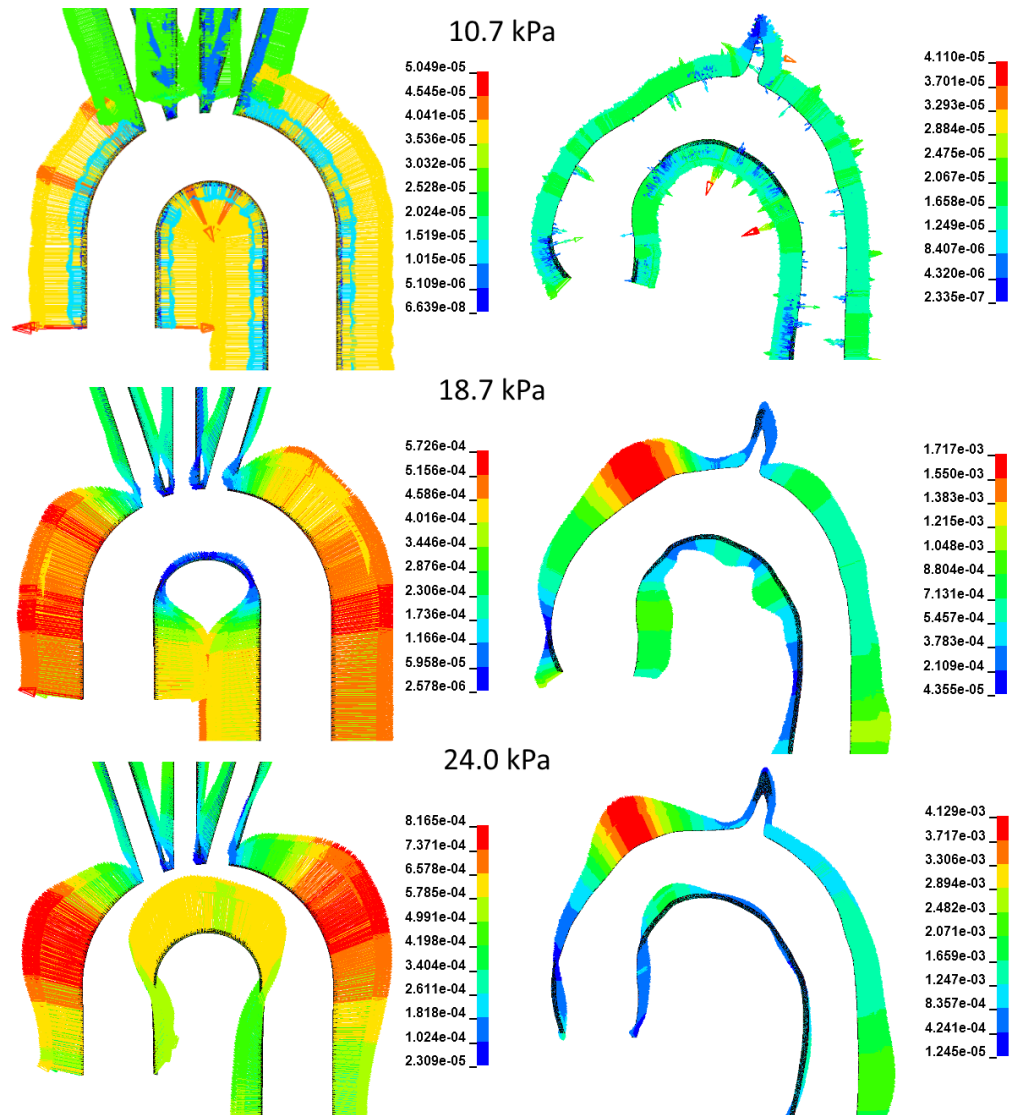


Figure 4.5: Comparison of displacement, in meters, for a "U" tube Vs. thoracic aorta

4.5 Discussion

These simulations shows the response of the architecture of the thoracic aorta when hypertension grades are achieved. A concentration of stress is weakening the internal wall of the inner aspect of the aortic isthmus, and the shape of the aorta impede movement at this zone.

In a hypertension stage the aorta changes its cross section closer to a circle, in the event of BTAR the compression of the aorta deforming in a high range the architecture of it, closer to a “U” shape tube. So these deformations will force the inner part of the arch to move to the inside of the vessel increasing the stress of the Intima layer

This explains why during a blunt thoracic trauma followed by aortic rupture the injure starts as a tear on the inner most layer at the aortic isthmus.

The first part of the results shows the graphical representation of the displacement, stress and strain, of each layer when is affected by a normal physiological pressure range.

The second part of the results shows a comparison with an elastic tube in a “U” shape, which shows the importance of the change of shape of the aorta at the specific spot of the isthmus within the internal aspect.

The American Medical Association on its JNC7 states, a risk of a CVD increases at a pressure of 18.7 kPa (140 mmHg)[Chobanian et al., 2003]. Pressure used as a comparison among all the figures.

The graphs show that the values for the ASA remains changing, but for the DSA, EAI and IAI the values are stable. These behaviours are for the three graphs displacement (Figure 4.2), stress (Figure 4.3)and strain (Figure 4.4).

The IAI shows a marked concentration of stress of 0.4 MPa at 18.7 kPa closer to the DSA zone with 0.35 MPa . With the difference that in displacement the DSA has higher values at this pressure, $0.6 \times 10^{-3} \text{ m}$ for DSA, and $0.2 \times 10^{-3} \text{ m}$ for IAI.

Comparing the three layers, in all of the figures, the adventitia and media layer, follow almost the same path on the three comparisons and for the selected zones.

For the intima layer the displacement and strain values are lower than the other two layers. Comparing the stress values between layers, the intima layer shows higher concentration.

These simulations shows the behaviour for only eleven steps. It could be proposed a further study with a higher range of steps, in a way to evaluate if the results are increasing or stabilising.

It is important to mention that this could be observed as an explanation of the Archimedes lever hypothesis, when the ASA moves against the DSA due to BTAR the arch will change shape, and the IAI zone will move up against the blood flow. The pressure will increase due to the reduction of diameter of the aorta.

4.6 Conclusion

The results demonstrate that the architecture of the vessel could be compromised when is deformed due to an increment of blood pressure or a compression of the vessel. If the blood pressure increases to higher values approaching hypertension levels ($140 \text{ mmHg} \approx 18.7 \text{ kPa}$) at this moment the vessel starts yielding and the shape changes to a circular shape and shows a concentration of stress at the IAI.

The possibility of aortic rupture due to BTAR will increased due to a compression of the chest, which will be represented as a displacement of the inner aspect of the isthmus, to the inside of the vessel, will explain why BTAR starts with a tear at the Intima layer at the isthmus zone.

This higher levels of BP allows the aorta to act as a solid beam supporting the Archimedes lever hypothesis mechanism of BTAR.

Chapter 5

Simulation of a frontal impact load applied to a geometric approximation model of the human chest.

5.1 Introduction

The second main cause of death in a car crash is BTAR [Pavlidis et al., 2011]. Many hypotheses on this subject has been developed to understand the internal mechanism of this injury.

Two hypotheses are included in this chapter to explain the internal mechanism of BTAR, the first is the Archimedes lever, which explain the mechanism as a collapse of a beam subjected to high load; the second hypothesis is Osseous Pinch, in which the lack of space inside of the chest impede movement of the descending aorta, the heart and the aortic arch moves against the descending aorta, shearing and stretching the vessel.

This chapter explains in detail a numerical simulation of an impact load, to a geometric approximated model which recreates the mechanical reaction of the chest to a different range of velocities. The main advantage of this method is that is a non-destructive test, and different tests could be applied to the same model.

5.2 Rationale

In chapter one section 1.5.5, a multivariate hypothesis is proposed which combines the different hypotheses of the mechanism of injury of BTAR that have been proposed, following this reasoning:

Explain that the aorta works as an Archimedes lever, in an arrangement of a beam and a column, where the beam is formed by the aortic arch and ascending aorta, and the column is formed by the descending aorta.

The osseous pinch hypothesis states that the column (descending aorta) is constricted by the spine.

The beam (ascending aorta and aortic arch) will be considered as a cantilever beam having the part of the column (descending aorta) as the clamped end.

Originated by the osseous pinch a force is introduced at the far end of the ascending aorta (at the aortic valve), the force will generate a shearing moment, due to the distance between the application of the force and the clamping zone. This will create a concentration of stress at the centroid of the geometry of the thoracic aorta.

Because the aorta is consider as a tube of rubber like material, which is filled by a fluid, the force that is compressing the ascending aorta and the lack of movement at the descending aorta will also cause compression, leading to stretching and shearing of the aortic arch.

The aortic arch is fixed at the heart by the the pulmonary trunk, adding the attachment of the heart to the lack of space in the human chest this will constrain movement, leading to a concentration of stress and strain at the inner aspect of the aortic isthmus.

5.3 Methods

The method will be based on the Finite Element Method (FEM). For a geometrically approximated model of the human chest, which would include elements that recreates organs and bones which interacts with the aorta as boundary conditions, shown in Figure 5.1:

The geometries were created in the CAD software Parametric CREO, and after were meshed in HYPERMESH.

In previous chapters was invalidated the use of a geometric approximated model of human tissues for the use in cardiovascular biomechanics.

But also one of the conclusions of the comparison shown in chapter three is that the cross section of the segmented model of the aorta gets closer to a circle, when is subjected to an internal pressure. And in chapter four, the highest concentration of stress and strain is achieved when the cross section of the aorta is similar to a circle, when the BP reached hypertension values.

It is also observed, in chapters three and four, that the reaction of geometric models follow similar paths, for deformation, stress and strain, that the ones established by the segmented models, the geometric models show higher values. Therefore, geometric approximated models could be used to prove that load concentrations are located at specific zones, but to prove which specific load will generate a concentration, a simulation with a segmented model should be performed.

The comparison of chapter three, shows that a simulation with a geometric approximated model will take less computer resources than using a segmented model, also the input data for a geometric approximated model could be used for future simulations with a segmented model.

These are the reasons why in this chapter a geometrically approximated model of the human chest is simulated; to understand the mechanical behaviour of the arrangement of organs inside of the human chest, and set a guideline for future work.

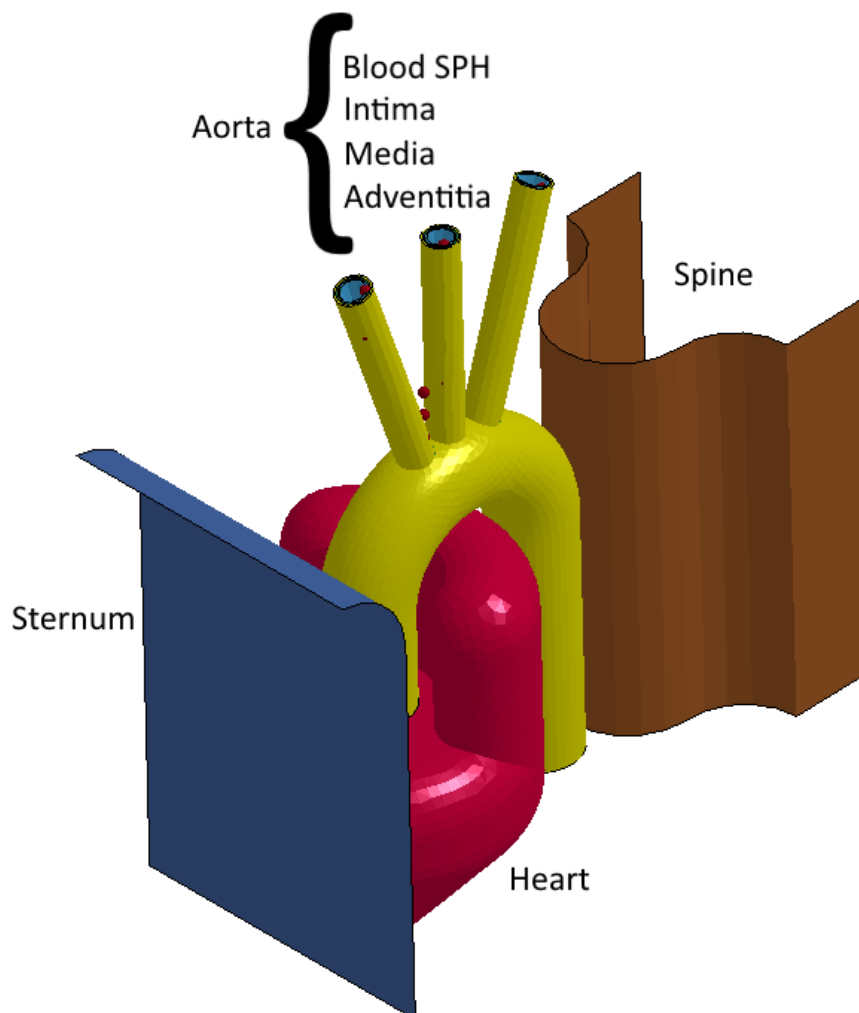


Figure 5.1: Geometric approximated model of the human chest for numerical simulation

1. AORTA - As in previous chapters, the aorta is designed as a geometric approximated model, adhering three different layers with their own thickness and mechanical properties.
2. BLOOD - Inside the aorta, is included another part, which will be characterised as blood, calculated as a multidimensional problem, when it is subjected to external forces reacts with strong distortions of the continuum under consideration thus a delimitation of the fluid - solid interaction [Stein et al., 2004] should be considered.
3. HEART - One solid piece of elastic material with rubber-like material properties is designed, which represent the heart, including the superior vena cava, pulmonary trunk, left and right pulmonary arteries, left and right pulmonary veins, left atrium and right atrium and the inferior vena cava.
4. BONES - SPINE AND STERNUM - These elements are chosen to be solid shell parts with mechanical properties and material model of bone.

5.3.1 Aorta properties, material and model

The focus part of this study is the aorta, for the FEM simulation a model of the aorta has been evaluated in the previous chapters. Figure 5.4, shows the model that it will be used as the object of study, captioning the different parts of the aorta that are included.

In order to get accuracy on the dimensions of the model, a geometry was segmented from 3D medical images, following the method explained on Chapter 4 and then measured to design the approximated geometry in a Computational Assisted Design (CAD) Software.

Table 5.1 presents the input data that have been used for the FEM simulation for this part.

Table 5.1: Input data for FEM simulation of aortic tissue

Condition	Specification	Value	Units
Boundary	Brachiocephalic artery Left common carotid artery Left subclavian artery Descending aorta	Z axis displacement was not allowed in upper and lower borders	-
Contact	Intima as master segment Media as master segment	Tied nodes to surface	-
Control	Termination	0.001	s
Load	Segmented set inside intima layer	0 - 24.0	<i>kPa</i>
Material	181 Simplified rubber/foam	-	-
	Density	1 000	$kg \cdot m^{-3}$
	Linear bulk modulus	2×10^5	<i>Pa</i>
	Damping coefficient	0.4	-
	Shear modulus	703×10^5	<i>Pa</i>
	Limit stress for frequency independent	703.33002	<i>Pa</i>
	Possion's ratio	0.5	-
Mesh	Intima Material behaviour curve (Chapter 2 Figure 2.2)	-	-
	Media Material behaviour curve (Chapter 2 Figure 2.2)	-	-
	Adventitia Material behaviour curve (Chapter 2 Figure 2.2)	-	-
Mesh	Type of element - R-Trias (square elements split in two right angled triangles)	0.325	<i>mm</i>

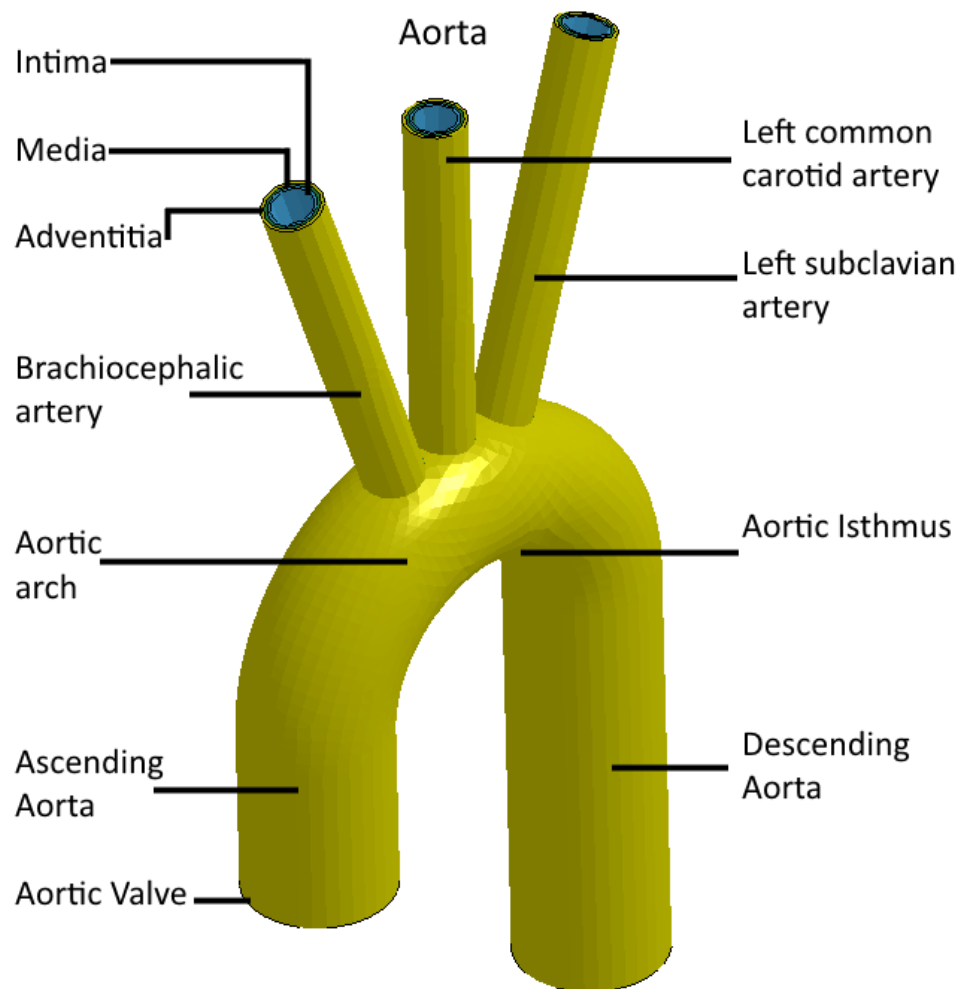


Figure 5.2: Geometric approximated model of the aorta for numerical simulation

Figure 5.2 shows the geometrically approximated model that has been used for the numerical simulation, in this figure also it can be identified the three different layers (i.e. Intima, Media, Adventitia) and also the different parts of the aorta, from the aortic valve, through the ascending aorta, aortic arch, aortic isthmus and descending aorta; it is important to mention that this model has the upper branches of the aorta which are the brachiocephalic artery, left common carotid artery and the left subclavian artery.

The vessel will be full with blood, therefore a plane which obstructs the flow, but allows movement of the solid parts, will be added to the model at the endings of the aorta (i.e. branchiocephalic artery, left common carotid artery, left subclavian artery and descending aorta).

5.3.2 Blood properties, material and model

To understand and simulate the reaction of a flexible tube full of liquid, it is necessary to use a representation of the blood in a numerical method. Therefore a different numerical formulation has to be proposed, in order to solve the equations that a problem with fluids generate.

The formulation has to include an interaction between solid and fluid which has to be allowed to move, in this manner two ways to analyse this interaction in FEM has been compared:

1. ALE Arbitrary Lagrangian - Eulerian formulation

This is an approximation based on large deformations of the domain and allow the fluid mesh higher deformations with lower loads. Starting from the idea of having two mesh domains one that is the reference mesh which will predict the reaction of the fluid and the second domain is the material domain, after a third domain will be introduced with the merge of both domains. These allow moving boundaries, large deformations and interface contact problems, this formulation needs a good mesh moving algorithm [Souli et al., 2000], [Le Tallec, 2001], [Souli and Zolesio, 2001].

2. SPH Smoothed - particle hydrodynamics meshless formulation

This formulation is a Meshless Lagrangian technique usually applied to represent fluids. With the use of moving particles each one is used as an interpolation point. These particles interact between them and also there is a requirement to have a fluid solid interactions with the other elements on the simulation [Jackson and Fuchs, 2010].

In this study the SPH method is selected to simulate the blood, as shown in Figure 5.3, for having the following advantages.

The mesh that is used to approximate a solid in FEM when subjected to large deformations could exhibit discontinuities or mesh tangling, hence the results will not be accurate. In this manner an adaptive mesh refinement code could be integrated to the main simulation.

The SPH method evaluates each particle using their particular properties and interaction to the other particles using their weight and average positions. Therefore each particle is recalculated (smoothed) at each iteration, hence the SPH code includes the adaptation of the particles (mentioned above).

Because the method recalculates the average positions each iteration, the interaction between solid and fluid is also applied naturally with the method

Being a Meshless method it is feasible to apply for complex geometries, as in this case of filling of the aorta.

Table 5.2, shows the material model and mechanical properties that represent blood in the simulation

In table 5.2, it is shown a Equation of state, equation 5.1 [Hallquist and Others, 2006], because is the simulation of a fluid the way to define pressure for compressed materials using equation

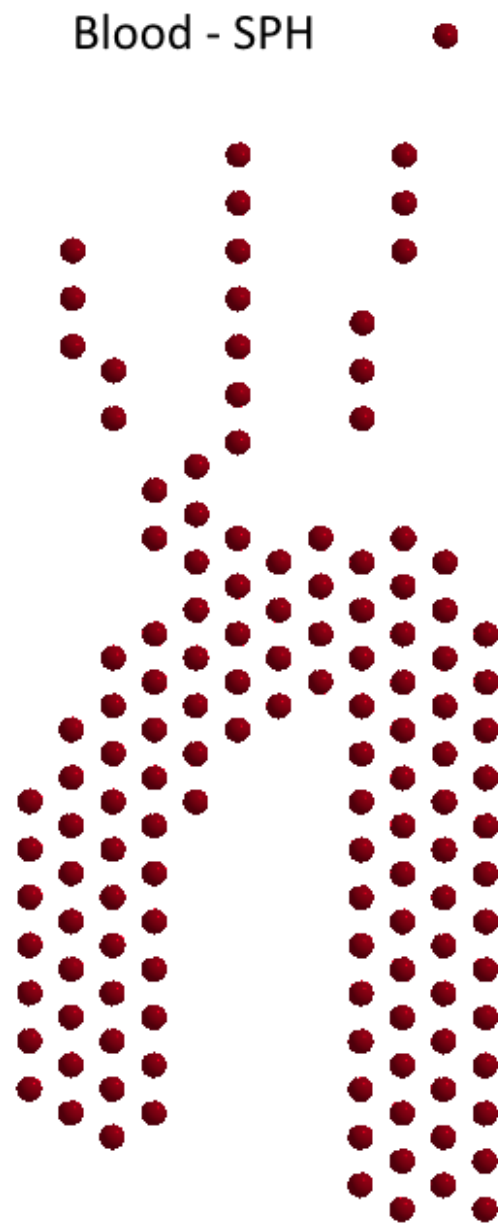


Figure 5.3: Geometric approximated model of the blood for numerical simulation

Table 5.2: Input data for FEM simulation of blood

Condition	Specification	Value	Units
Fluid solid interaction (FSI)	Blood - master element Aorta and heart - slave element	-	-
Material	Mass density Viscosity coefficient	1060.00 0.003	$kg \cdot m^{-3}$ $Pa \cdot s$
Equation of State	Gruneisen C S_1 γ_0 E_0	1657.00 1.49 200.00 2000.00	$m \cdot s^{-1}$ - - -
Mesh	Type of element SPH	222	No of particles

$$p = \frac{\rho_0 C^2 \mu \left[1 + \left(1 - \frac{\gamma_0}{2} \mu - \frac{\alpha}{2} \mu^2 \right) \right]}{\left[1 - (S_1 - 1) \mu - S_2 \frac{\mu^2}{\mu+1} - S_3 \frac{\mu^3}{(\mu+1)^2} \right]^2} + (\gamma_0 + \alpha \mu) E \quad (5.1)$$

Where

C - The intercept of the $V_S - V_P$ curve (in velocity units)

S_1, S_2, S_3 - Unit less coefficients of the slope of the $V_S - V_P$ curve

γ_0 - The unit less Gruneissen gamma

α - The unit less volume correction to γ_0

$$\mu = \frac{\rho}{\rho_0} - 1$$

5.3.3 Heart properties, material and model

The ascending aorta is attached to the heart through the aortic valve, and inside the aortic arch are located parts of the heart and different vessels which connect to the heart, i.e. right atrium, right pulmonary artery, superior vena cava, left pulmonary artery, pulmonary trunk, left pulmonary veins and left atrium.

Figure 5.4 shows a geometrically approximated model of the heart and vessels which are connected to the heart or pass inside the aortic arch, others than the aorta, conformed of all the parts mentioned above and the left and right ventricles, and the apex, shaped in a big mass.

In this study the aortic valve is closed and the heart model is full of blood, thus is modelled as a solid elastic mass. Using the same material properties and material model as the Adventitia layer of the aorta, shown in the Table 4.1.

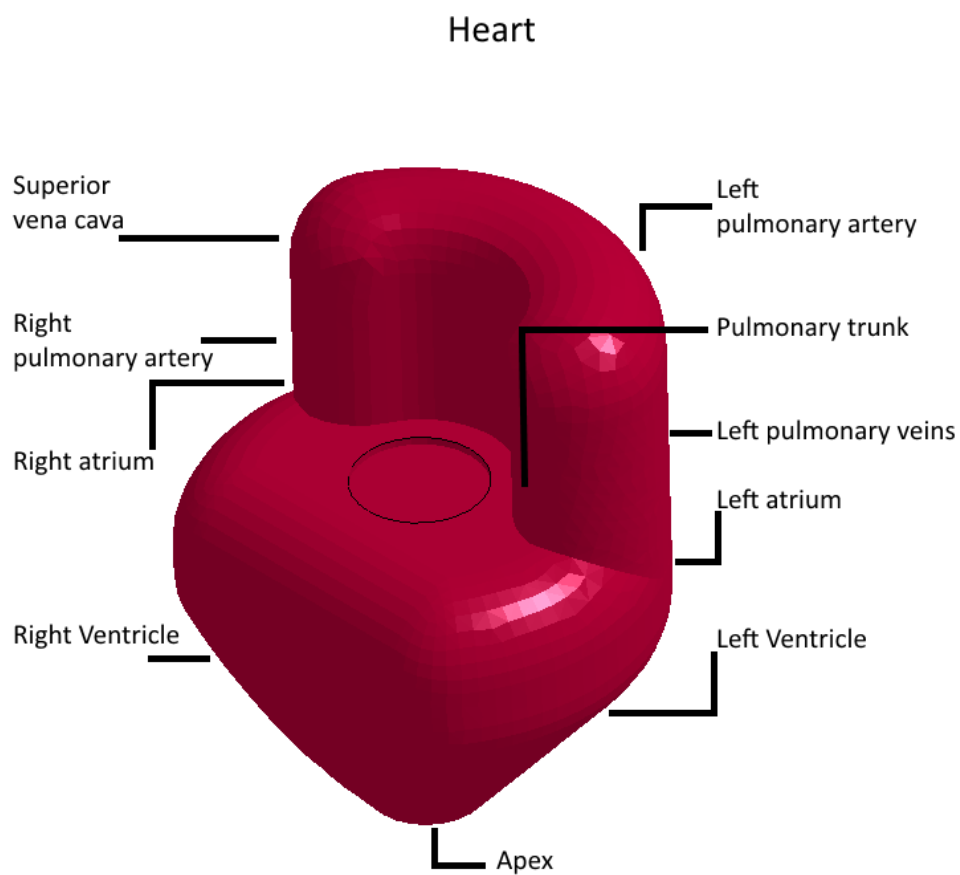


Figure 5.4: Geometrically approximated model of the heart for numerical simulation

5.3.4 Bone properties, material and model

When a compression of the chest is taking place, the sternum (left Figure 5.5) will first impact the heart, thus the Ascending aorta, that is facing the sternum and is attached to the heart, would be the first section of the aorta which reacts to the compression.

On the other side of the aorta, is located the Descending aorta which is attached to the body through the thoracic spine (right Figure 5.2), at the lower border of the fourth thoracic vertebrae.

Both of these structures are bone thereby the material is simulated as rigid solid, due that the reactions of bones are beyond the scope of this thesis and due to the significantly larger rigidity of the bone parts compared to the soft tissue. Input data in Table 5.3

The sternum will work as an evenly distributed load for the impact, and the spine will give the support boundary for the back of the descending aorta.

Table 5.3: Input data for FEM simulation of bone

Condition	Specification	Value	Units
Contact	Surface sternum - master segment Aorta and Heart - Slave Element	-	-
Material	020 Rigid	-	-
	Mass Density	7870.00	$kg \cdot m^{-3}$
	Young's Modulus	$2.7e^9$	Pa
	Poisson's ratio	0.28	-
Mesh	Type of element Controlled Quad-elements	Sternum - 24 Spine - 66	No of Elements

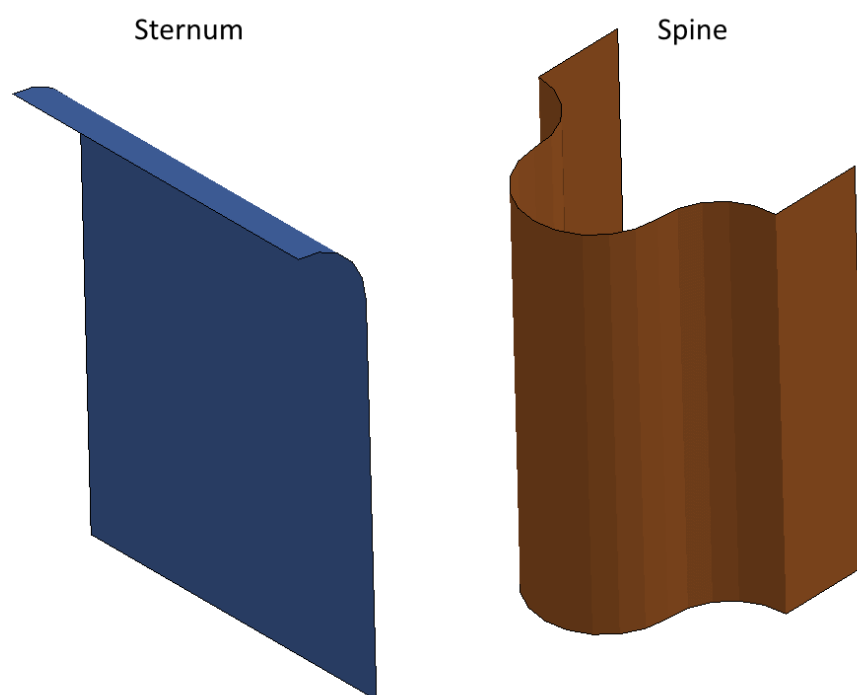


Figure 5.5: Geometric approximated model of the sternum and spine for numerical simulation

5.3.5 Specifications for the simulation

Now that all the material models, mechanical properties and boundary conditions of the test has been explained, the specifications of the simulation needs to be clarified.

In order to simulate the chest compression, a velocity will be loaded to the sternum, it will be loaded with an initial velocity, (following Table 5.4) then, after 0.0002 s, the sternum is stopped and the reaction of the internal organs will continue until 0.002 s. Twenty three steps are recorded in order to obtain values of displacement, pressure on the aortic wall, stress and strain, for each of the different layers of the aorta.

A range of velocities was designed in order to test the reaction of the aorta subjected to different impact loads. Gabauer D.J. et al [Gabauer and Gabler, 2008] compare the crash injury metrics using event data recorders, showing results with belt and air bag restrained, and air bag restrained only. For longitudinal occupant injury velocity (OIV) of $10 \text{ m} \cdot \text{s}^{-1}$ the probability of occupant injury is 10% increasing to 40% – $15 \text{ m} \cdot \text{s}^{-1}$, 80% – $20 \text{ m} \cdot \text{s}^{-1}$ and 100% – $25 \text{ m} \cdot \text{s}^{-1}$. For this reason the velocities selected are:

Table 5.4: Range of Impact Velocity

$\text{m} \cdot \text{s}^{-1}$	$\text{mi} \cdot \text{h}^{-1}$	$\text{km} \cdot \text{h}^{-1}$
10	22.37	36
15	33.55	54
20	44.74	72
25	56.00	90

5.4 Results

To start analysing the results of these test in the range of velocities that are suggested, elements are selected from specific zones, shown in Figure 4.1, including:

1. Ascending aorta (ASA)
2. Descending aorta (DSA)
3. External aortic isthmus (EAI)
4. Internal aortic isthmus (IAI)

In a time from 0 – 2.0 *ms*, 20 measurements are taken from each selected zone and each layer. The first set of graphs shows median values for these measurements.

These will determine which of the selected zones shows critical behaviour and if the values achieve the ultimate tensile stress shown in chapter 2 Figure 2.6, this will mark the critical zone.

To show the maximum displacement achieved in an event of BTAR, a comparison of displacement in three dimensions is shown in Figure 5.6 for the intima layer, Figure 5.7 for the media layer and Figure 5.8 for the adventitia layer, also showing the selected zones.

Figure 5.6 shows the reaction at the intima Layer, it can be seen that all the increments of the displacement are linear with initial velocity. The first moving zone is the ASA, being the zone that allows more movement. The IAI zone shows higher displacement values, in comparison with the EAI zone among all the range of velocities. The displacement values of the IAI zone are closer to the DSA than the values of the EAI.

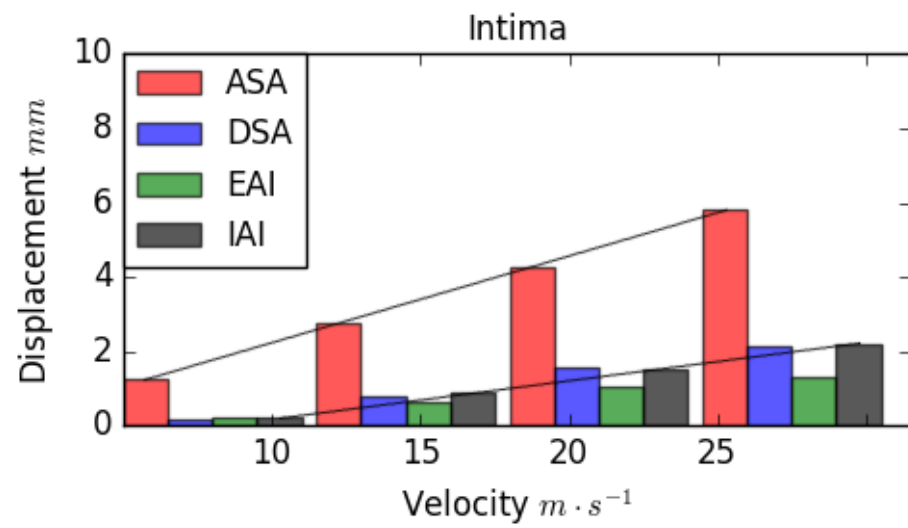


Figure 5.6: Displacement at intima layer, selected zones / velocity range 10 – 25 $m \cdot s^{-1}$

Figures 5.7 and 5.8, show values for the media and the adventitia layers, respectively. As with the graph of the intima values (Figure 5.6) the increments shown are linear even with the same values for the three layers. Therefore the displacement for the complete aorta is linear

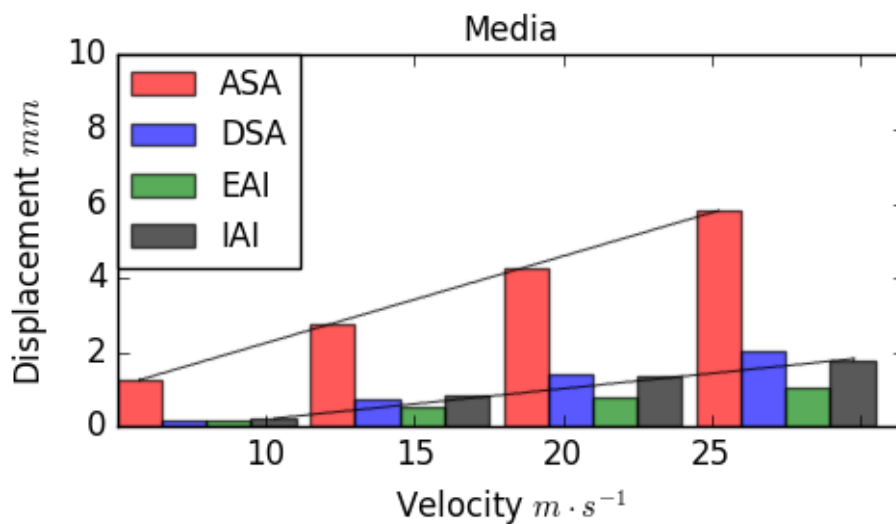


Figure 5.7: Displacement at media layer, selected zones / velocity range 10 – 25 $m \cdot s^{-1}$

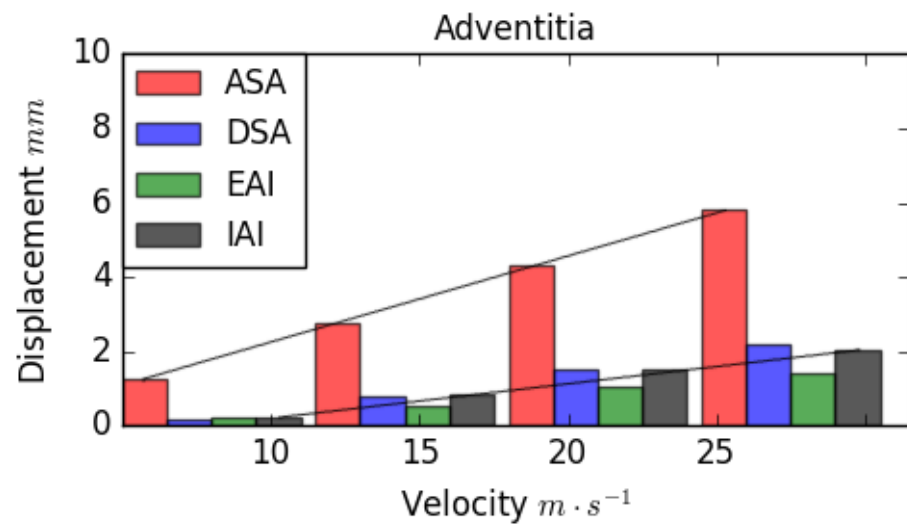


Figure 5.8: Displacement at adventitia layer, selected zones / velocity range 10 – 25 $m \cdot s^{-1}$

The second value selected to analyse is the pressure that the different layers are subjected during the test (shown in Figures 5.9, 5.10, 5.11), showing which parts of the aortic wall are subjected to compression or to tension.

Figure 5.9 shows the values of pressure that the Intima layer is subjected during the impact. At $10 \text{ m} \cdot \text{s}^{-1}$ the median of the values is closer to zero even with the standard deviation of the IAI zone that shows the higher increment compared to the other zones.

From 15 to $25 \text{ m} \cdot \text{s}^{-1}$, the values of pressure are showing an inclination to being in tension for the ASA and for the other zones it tend to show compression.

Higher concentration of pressure is observed at the IAI zone, it can be seen from the velocities of $20 - 25 \text{ m} \cdot \text{s}^{-1}$.

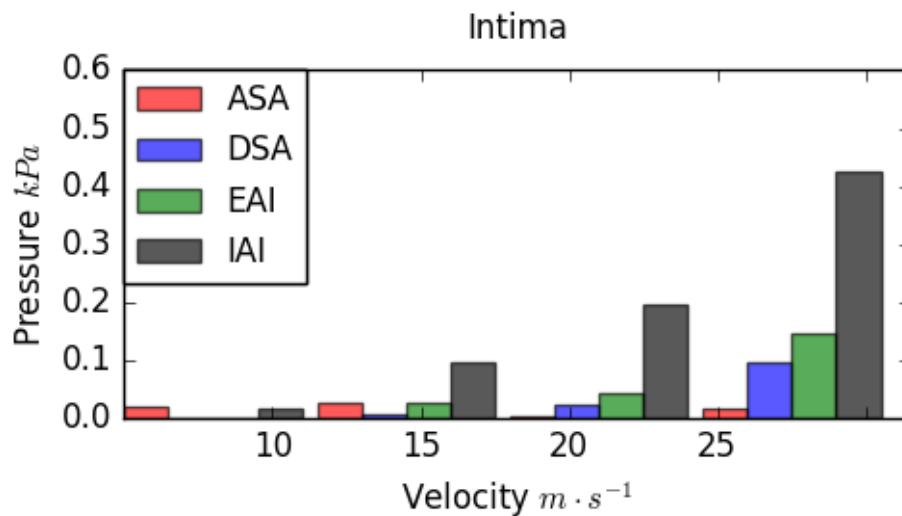


Figure 5.9: Pressure intima, selected zones / velocity range $10 - 25 \text{ m} \cdot \text{s}^{-1}$

Figures 5.10 and 5.11, shows the media and adventitia layer respectively, at 10 and $15 \text{ m} \cdot \text{s}^{-1}$ the values are similar for the three layers, the behaviour for these two layers it is really close, even for the last velocity.

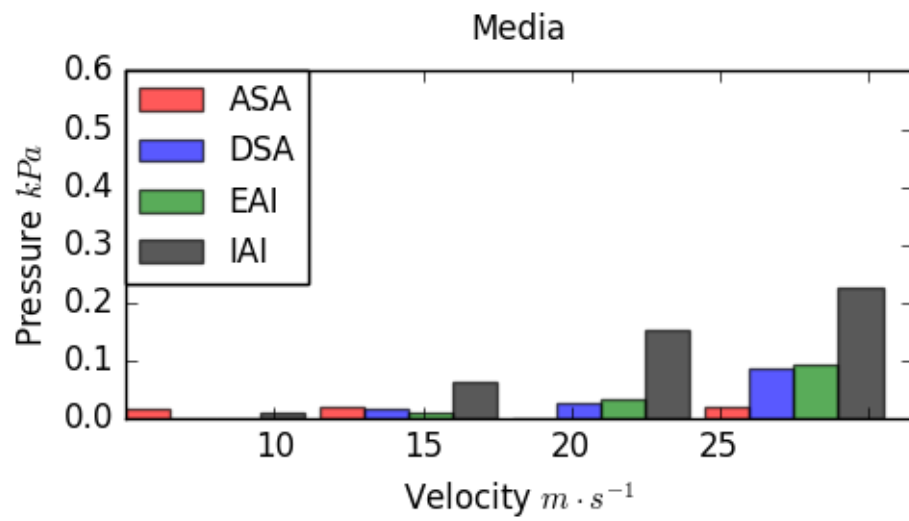


Figure 5.10: Pressure media, selected zones / velocity range 10 – 25 $m \cdot s^{-1}$

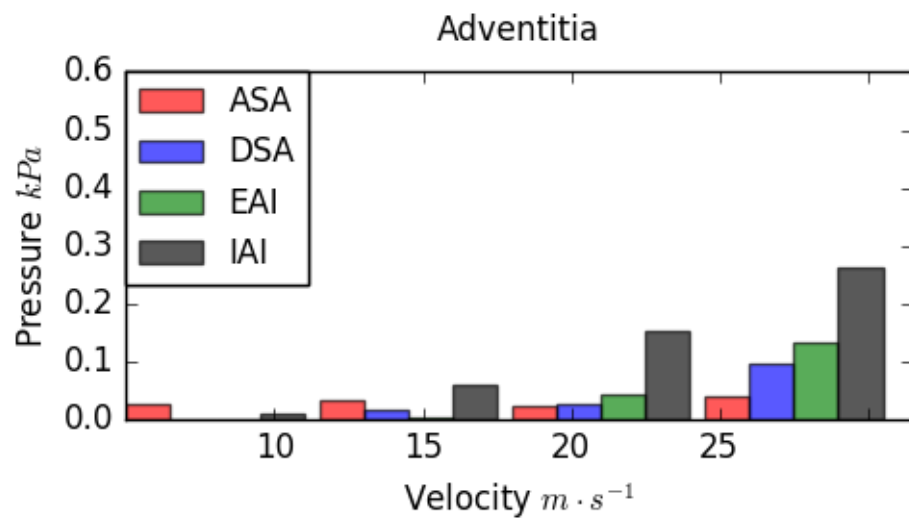


Figure 5.11: Pressure adventitia, selected zones / velocity range 10 – 25 $m \cdot s^{-1}$

The final value to be compared is Von-Mises strain (defined in chapter 2), also this value is measured at the aortic wall for the different selected zones. Shown in Figures 5.12, 5.13 and 5.14.

Figure 5.12 shows the values of strain for the intima layer, it can be seen that the values for the ASA zone increase close to linear, meanwhile the velocity increases, not only increasing the median values but the range for the standard deviation increases as well.

It is clear for the velocity of $15 \text{ m} \cdot \text{s}^{-1}$ that the values of strain for the DSA, in comparison with the ASA, the increments of the DSA zone are higher. And if the velocity increases the values for strain gets even higher, even in velocities of 20 to $25 \text{ m} \cdot \text{s}^{-1}$ values of DSA are higher than for ASA.

The values at the isthmus zone are important because the increment of the EAI and the ASA zones are similar. The IAI zone values increases as the velocity is increasing. This statement will be explained in detail with Figure 5.16 with all the steps of the test for $20 \text{ m} \cdot \text{s}^{-1}$ where the stress and strain are plotted.

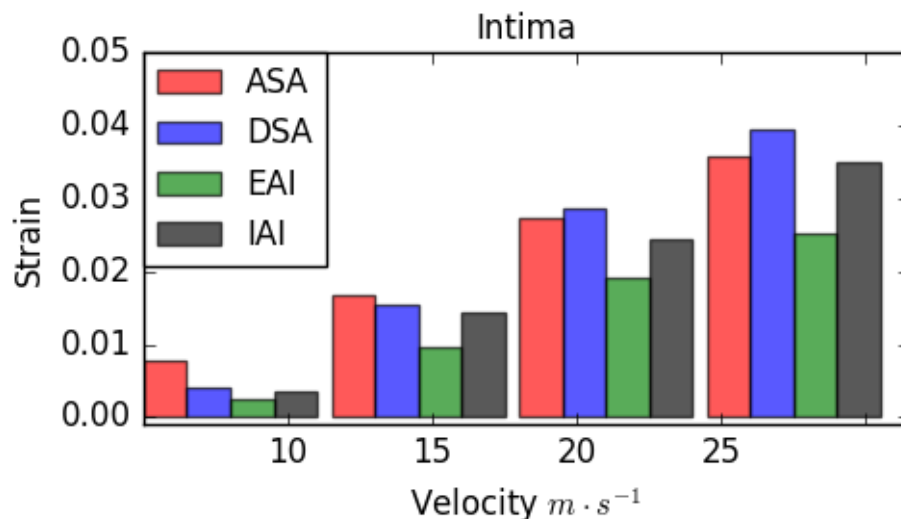


Figure 5.12: Strain intima, selected zones / velocity range 10 – $25 \text{ m} \cdot \text{s}^{-1}$

Figure 5.13 shows the reaction for the media layer and it is closer to the intima layer, but the values are not as higher as for the intima layer. But in the media values the DSA or IAI never exceeds the values of the ASA.

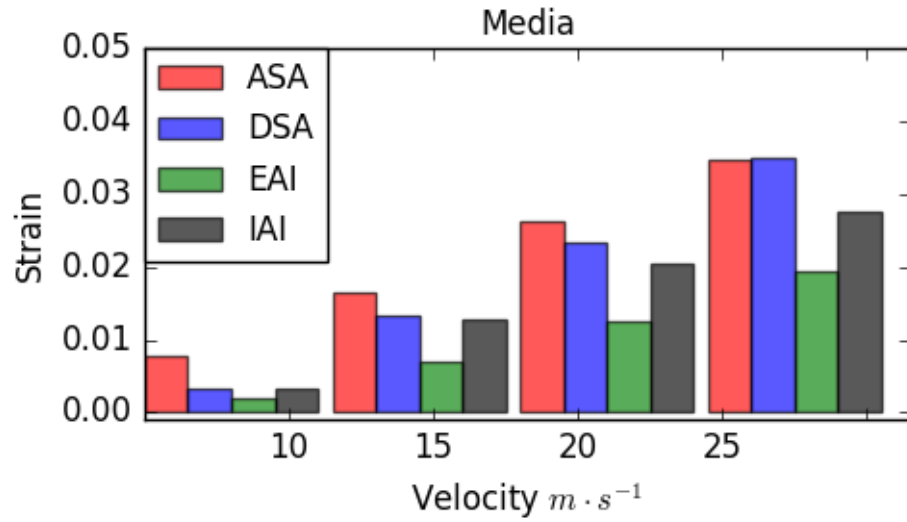


Figure 5.13: Strain media, selected zones / velocity range 10 – 25 $m \cdot s^{-1}$

Figure 5.14 shows the reaction of the adventitia layer, for 10 and 15 $m \cdot s^{-1}$ the increments of strain shown a close to linear growth. For 20 and 25 $m \cdot s^{-1}$ the media values of DSA and IAI never exceed values for ASA.

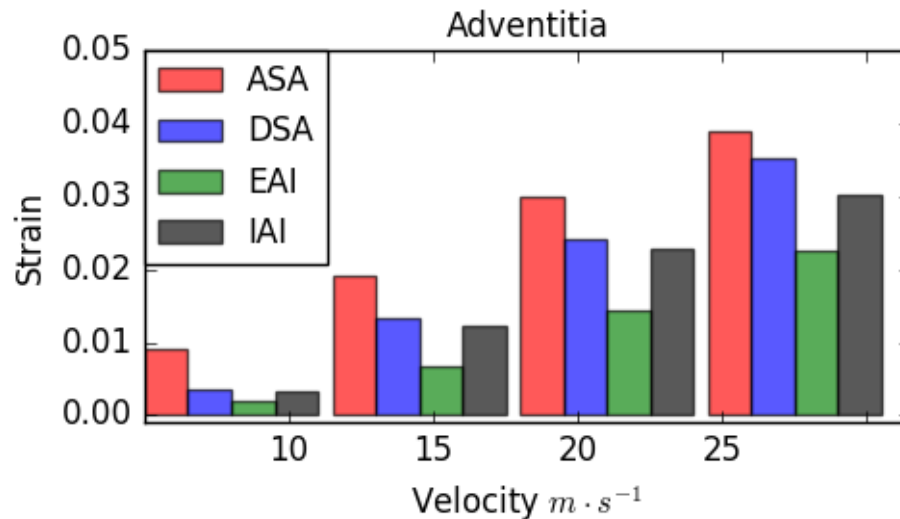


Figure 5.14: Strain adventitia, selected zones / velocity range 10 - 25 $m \cdot s^{-1}$

The first part of the results shows, critical values of pressure are located at the intima layer at the IAI zone, achieving higher pressure values at 20 $m \cdot s^{-1}$ and at 25 $m \cdot s^{-1}$. Also the ASA zone is the one which shows a close to linear displacement during impact loading.

Therefore on the next part of the analysis of the results these zones are compared, with the addition of the EAI as a control measurement of the Isthmus zone.

This second part of the results, three figures are evaluated, showing results of displacement, pressure and strain of the intima layer of the aortic wall; against 20 steps of time, each 0.1 ms , at $20 \text{ m} \cdot \text{s}^{-1}$. This velocity is chosen because it is where the most critical values were found.

Figure 5.15, shows the displacement of two zones of the aorta, ascending aorta and isthmus, having the ASA zone as the maximum displacement of the vessel, and the comparison between the internal and external part of the isthmus, in this case it is important to say that none of the selected zones pass over the ASA zone. But it is clear that the internal part of the isthmus moves more than the external part, thus the EAI could be used as a control measure of the isthmus.

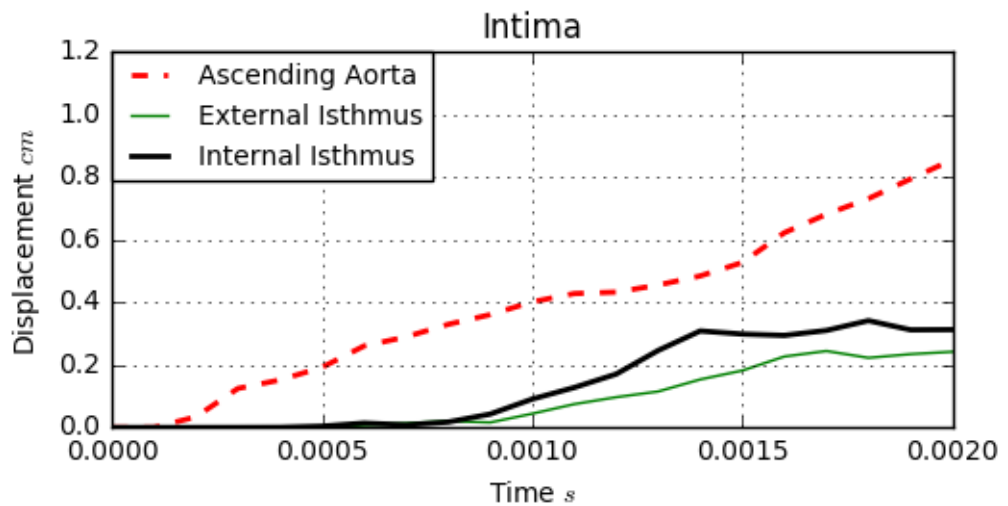


Figure 5.15: Comparison of ascending aorta, external isthmus and internal isthmus of displacement of the intima layer at $20 \text{ m} \cdot \text{s}^{-1}$

In Figure 5.16, the comparison of pressure for the intima layer of the aortic wall is analysed, the ASA zone is showing higher values at the beginning of the simulation, because is the zone which receives the first impact. During slower simulations analysed, ASA shows the highest values.

Figure 5.16 also shows an impact wave reaction, at the ASA, starting as a reaction of the aorta, which starts with the contact of the sternum with the heart, following to the aorta, this wave is lowering until the middle of the test when it starts again, this restart could be explained as a reactive wave reaction.

At the beginning of the test the pressure values show an inclination for the tension of the wall, at the middle of the test the tension behaviour is reduced and the wall starts to go down to the compression zone but between a range from ± 0.4 *MPa*.

The EAI behaviour does not exceeds the magnitude of the wave shown by the ASA zone. Both zones the EAI and ASA shows an instability of the wave between $0.5 - 1.5$ *ms* then both zones show a similar wave.

The highest pressure values are achieved by the IAI zone, with values higher than 600 *kPa*. The first peak of pressure at this zone is followed by an instability until the end of the test.

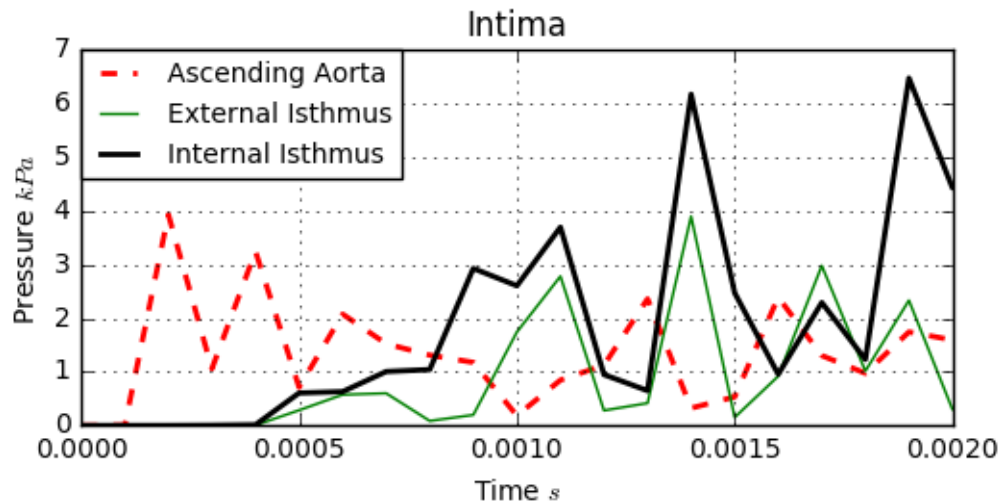


Figure 5.16: Comparison of ascending aorta, external isthmus and internal isthmus of pressure of the intima layer at $20 m \cdot s^{-1}$

Figure 5.17 and Figure 5.18, show the strain and stress reaction respectively of the intima layer for the three selected zones, i.e. ASA, EAI and IAI; including a graphical representation of the magnitude and direction of the displacement at critical steps, related to a side cut of the aorta which is subjected to the impact load.

The critical zone for this test is the IAI zone, it marks a deep slope until it achieves the highest concentration of stress and strain for the test at a time of $1.2 ms$ with values in strain of 6.6% and $2.6 MPa$ of stress; and the highest concentration at the IAI zone is at $1.3 ms$ with values in strain of 6.7% and $2.7 MPa$ of stress.

In contrast with the pressure graph (Figure 5.16) at $1.2 ms$ it is the tension at this side of the inner wall and the next step $1.3 ms$ it start to going down to the compression zone, but in the stress-strain graph increases concentration.

For the ASA zone which receives the highest displacement of this layer of the aorta (Figure 5.15) for the concentration of stress and strain it is clear in Figure 5.18 that the highest concentration at this zone is for $1.5ms$ with a strain value of 5.7% and $2.7 MPa$ for stress, followed by $0.2ms$ with a strain value of 4.5% and $2.2 MPa$, but these values not being the top values of the test.

In comparison with the IAI, the EAI does not shows considerable increments, or concentration of stress or strain, showing a stable behaviour.

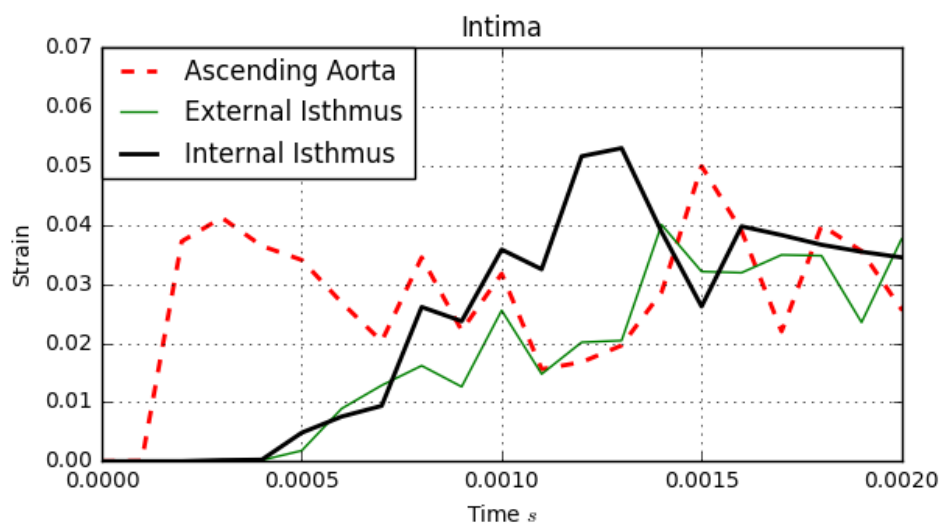


Figure 5.17: Comparison of ascending aorta, external isthmus and internal isthmus of strain for the Intima layer at $20 m \cdot s^{-1}$

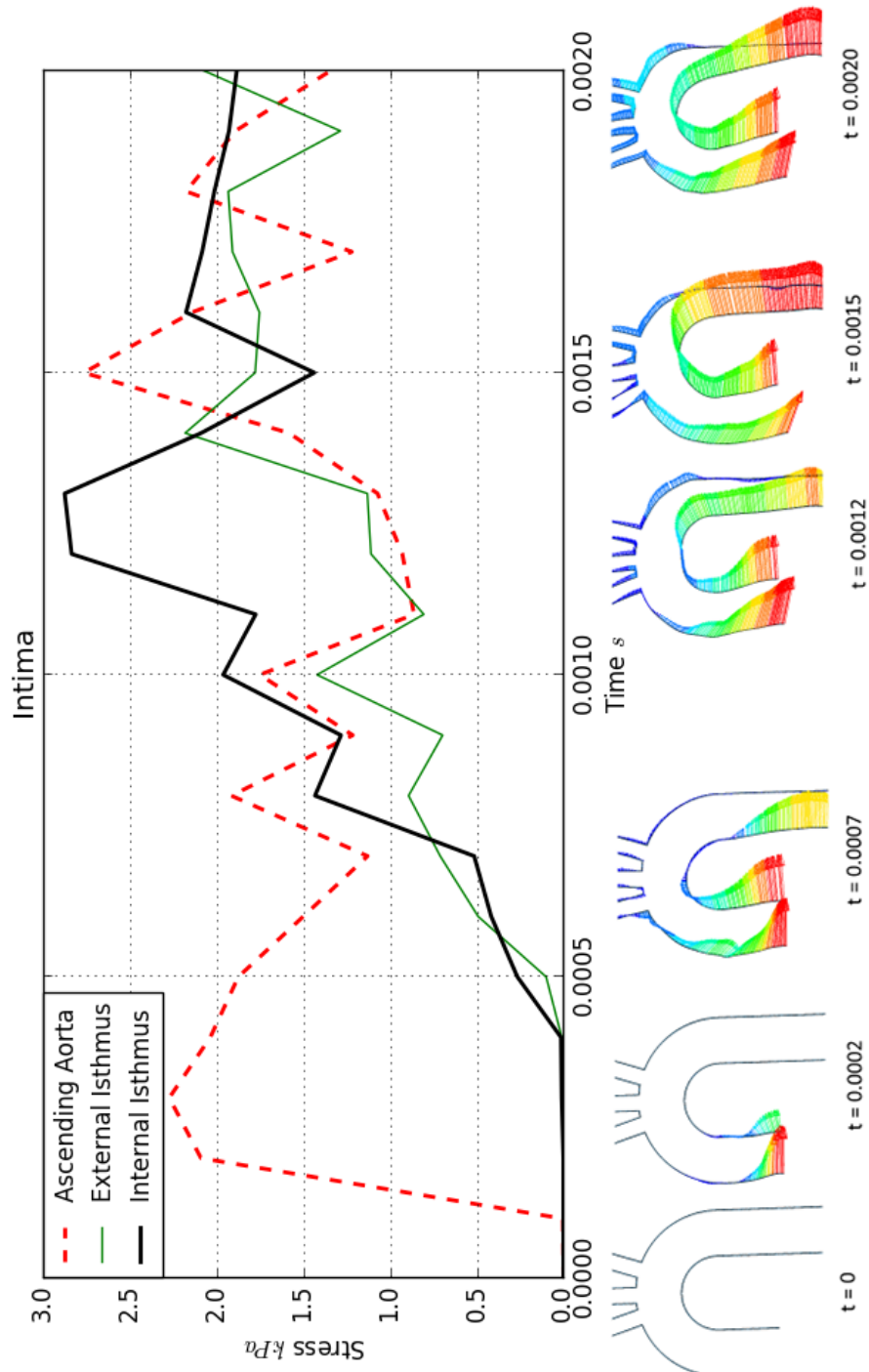


Figure 5.18: Comparison of ascending aorta, external isthmus and internal isthmus of stress for the Intima layer at $20 \text{ m} \cdot \text{s}^{-1}$

5.5 Discussion

In this chapter, the FEM is used to explain the mechanism of the Blunt Thoracic Trauma followed by Aortic Rupture (BTAR), with the use of two of the main hypotheses that has been used to understand it. The first hypothesis is to see the aorta as a beam in cantilever resting in a column; and the second hypothesis is about the deficiency of space that organs have inside the chest.

After the result analysis it is observed that the water hammer hypothesis should be included in the mechanism of the aorta when is subjected to BTAR. Because of the reaction in Figure 5.16, that is explained as an impact wave reaction, this reaction could be consider as a water hammer effect on the aortic wall.

Figure 5.19 shows different stages of the $20 \text{ m} \cdot \text{s}^{-1}$ test with vectors which show the displacement of the different zones of the aorta, showing how the vessel reacts when it is subjected to an impact load.

The restrictions of the DSA zone with the spine prevents movement at the DSA, IAI and EAI. Therefore the ASA zone has higher displacement shown in Figures 5.6 - 5.8.

It is shown that the IAI zone is behaving against the blood flow, therefore the bubble inflation analysis of the different zones of the aorta done by Pearson [Pearson et al., 2008], has to be done loading the intima layer, instead of the adventitia layer, due that in has been demonstrated with the above simulation that in BTAR the forces goes against the blood flow, instead against to the outside of the vessel.

Figures 5.9 - 5.11, show how the ASA is working mainly in tension and the IAI is working in compression, these are observed for all the layers at 10 and 15 $\text{m} \cdot \text{s}^{-1}$, and for the next tests 20 and 25 $\text{m} \cdot \text{s}^{-1}$ the values of compression for DSA, EAI and IAI are higher and the values for IAI are totally in the compression zone.

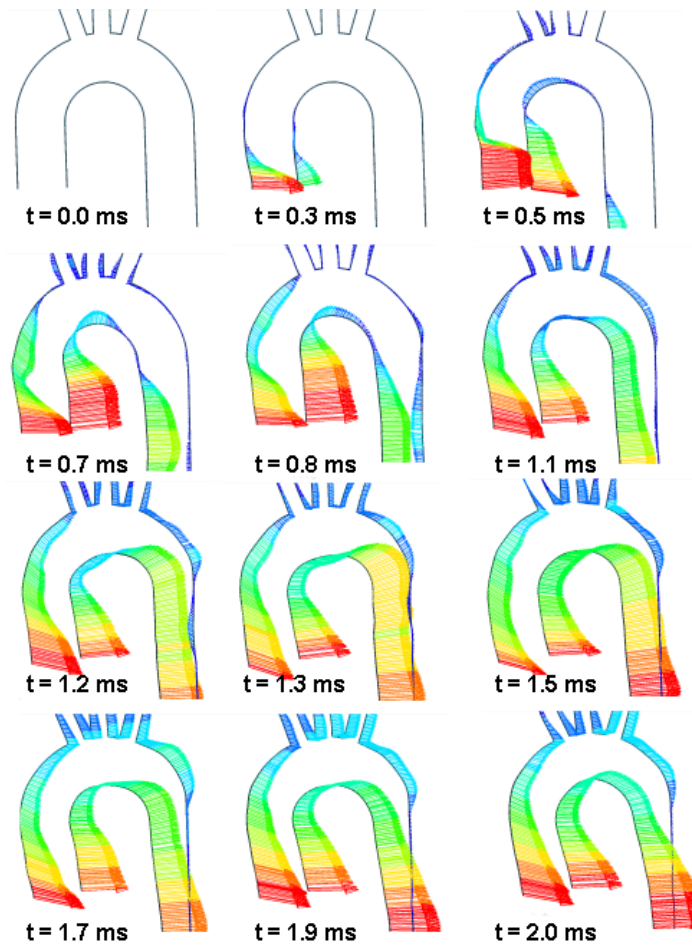


Figure 5.19: Displacement vectors for the Intima layer of selected steps in a $20 \text{ m} \cdot \text{s}^{-1}$ chest impact simulation

In general the highest values are located in the Intima layer, being the thinnest of the vessel. Therefore the second section of the results the innermost layer is evaluated for $20 \text{ m} \cdot \text{s}^{-1}$ because at this speed the evaluated values are going into an instability after 0.8 ms .

Values for rupture pressure (270 kPa) are surpassed by the IAI zone, in four steps 0.8 , 1.1 , 1.4 , 1.9 , 2.0 ms , being the highest pressure of -600 kPa at 1.4 ms , shown in Figure 5.15, this Figure also shows that the ASA zone achieves a pressure of 400 kPa , but this energy is dissipated by the wave reaction, the following measures shows a decreasing of pressure,

in comparison with the IAI that the movement is restricted the pressure increases until the end of the test. Figure 5.15 shows the Displacement of the ASA zone is higher than the IAI and the EAI, being the EAI with lowest displacement.

A normal behaviour of the aorta is to allow the generation of waves, caused by the heart beat, this pulse could stretch the artery. If the artery is full of blood, then at the systole of the heart, the aortic valve will open and increase the blood flow, to a full aorta. These will generate an arterial wave, known as Korotkoff sound, produced by the impact of new blood flow from the heart, against the column of fluid of the artery, stretching the aortic wall [Erlanger, 1921].

Taking the Korotoff sound in account for the incidence of BTAR: Figure 5.16 shows that the first impact of the chest to the heart, after this first impact, the values of pressure fluctuate between compression and tension, this fluctuation is explain as a wave reaction, therefore the impact load initiates a wave, starting at the aortic valve, propagating through the ascending aorta, then the aortic arch, passing through the aortic isthmus and next through the descending aorta, when it achieves the descending aorta a reflected wave reaction is initiated, due to the closure of the diaphragm.

The wave reaction is transmitted through the aortic wall, these waves will coincide at the first change of direction of the descending aorta, which is at the internal zone of the aortic isthmus. In that event, the wave reaction could be linked with the water hammer effect.

Figure 5.16 shows a concentration of stress and strain at the IAI of the Intima layer. This is linked with the water hammer effect, if the blood flow inside of the aorta is closed by compression of the diaphragm (in this simulation the heart closes the DSA), in consequence the blood at the descending aorta generates a way back pressure, the systole of the heart opens the aortic valve pouring out more blood trough the vessel,

because of the first impact at the heart, the aortic wall is affected by the wave reaction, colliding the waves presumably at the inner zone of the aortic isthmus, increase the BP from the descending aorta at the isthmus at 1.4 ms , increasing the pressure at the aortic wall at IAI.

Showing the different reactions on the aorta at different velocities, gave a safety range of Occupant injury velocities, when the arrangement of the internal organs of the chest can disperse the energy that the impact load generate and avoid extensive damage of the aorta.

The structure of the rib cage also can disperse the energy generated by the impact, in these simulations this structure is not included. Therefore the velocity consider is not from an external impact, it has to be the velocity that the sternum needs to achieve.

It is also important that these simulations are applied in a geometric approximated model of the chest. The complementary simulation of the complete chest, using a segmented model as object of study has to be performed, in order to get results more attached to reality.

5.6 Conclusion

For this chapter two of the most important hypothesis, which search for an explanation of the mechanism of BTAR, were observed. The aim of this chapter was to combine these two hypotheses (i.e. Archimedes lever and Osseous Pinch), into a Multivariate hypothesis, which can be employ to prove that the mechanism of this trauma is not based on only one factor. After the simulations and analysis of the results the hypothesis of a water hammer effect is also included, due to the ability of the vessel to propagate waves through the wall.

In conclusion, if the sternum reaches a velocity of $20 \text{ m} \cdot \text{s}^{-1}$ ($72 \text{ km} \cdot \text{h}^{-1}$) a wave is generated at the aortic valve zone, and due to the closure of the diaphragm a reflected wave is also generated, therefore the collide of this two waves at the aortic isthmus a concentration of stress (exceeding ultimate tensile stress showed on Figure 2.6) will lead to a tear in the inside wall of the vessel, which due to the over pressure of the vessel will break the other layers and break all the circumference of the vessel, continuing with an internal bleeding.

Chapter 6

Conclusions and future work

6.1 General discussion

This research is focus on the specific case of a rapid deceleration of Blunt Thoracic Trauma followed by Aortic Rupture (BTAR), precisely described as an abrupt non-penetrating trauma located on the chest, which leads to a compression of it, followed by a compression of the internal organs.

The importance for its study is summarised as:

- BTAR is the second most common cause of death in a car crash. In the United Kingdom, 21% of car occupant death is caused by BTAR. In the United States of America and Canada, each year around 7500 - 8000 occupants die due to this trauma;
- 80% of the times that BTAR takes place at the aortic arch in the inner aspect of the Isthmus. The rupture of the aortic wall starts at the inner most layer and develops outwards the following layers;
- BTAR can occur at low severity crashes, and the use of contemporary seat belt or air bags does not eliminate the risk of BTAR.

The main aim of this research is to explain the mechanism which leads to BTAR, knowing that is a complex trauma, the mechanism which will be used as an explanation, is the combination of different simple mechanisms:

- **SCAR AT THE ISTHMUS** A scar in the tissue, caused by the closure of the Ductus Arteriosus, will locate a concentration of stress in the border of the discontinuity of the wall.
- **ARCHIMEDES LEVER** The aorta is fulfilled with blood, this will lead taking it as a solid beam. The geometry of the aorta suggest that it could be explained as a cantilever beam supported in a column. The beam consisting of the ascending aorta and the aortic arch, and the column the descending aorta. The initial load will be at the open end (aortic valve), of the beam, forcing the open end move to the support.
- **OSSEOUS PINCH** The descending aorta is fixed to the spine, preventing the aorta to move up or down, hence, the force at the aortic valve will deflect the aortic arch concentrating forces at the inner part of the isthmus. The compression of the chest will force everything to pack, tensing the aortic arch, and twisting the descending aorta. The tension of the aortic arch and the torsion forces of the descending aorta, will force the aortic wall to move to the inside of the vessel.
- **WATER HAMMER** In a stage of hypertension, caused by an stressful situation or/and by the closure of the aortic valve, and the blockage of the blood flow at the descending aorta, due to a compression by the diaphragm. The reaction of the wall could be by two waves, first generated by the initial impact at the aortic valve, and the second by the impact of the heart at the descending aorta. The aortic wall conduct any movement of the heart along the vessel, being the im-

pact force higher than the usual systole and diastole of the heart, the vibration of the aortic wall caused by these waves will start a water hammer effect, leading to the collapse of the tissue caused by surpassing the natural vibration frequency.

Every chapter of this thesis uses the Finite Element Method technique, to simulate tests that are willing to prove each simple mechanism proposed:

- Chapter 02 - **SCAR AT THE ISTHMUS**

Mechanical properties and material model were validated against experimental and analytical studies. Good agreement for the deformation up to rupture was achieved in a bubble inflation experiment.

In relation to the specific location of the injury (the Isthmus), a scar at this place could generate a concentration of stress when the internal pressure increases.

The healing process of the cardiovascular tissue could generate a scar of arbitrary dimensions and mechanical properties. The scar is due to the closure of a small vessel (*Ductus arteriosus*) which connects the aortic arch to the pulmonary artery. When the *Ductus arteriosus* closes, the *ligamentum arteriosus* is generated.

A scar in the aortic tissue at the Isthmus affects the strength of the wall. Therefore, this chapter recreates a scar in the tissue by the inclusion of a patch in a aortic tissue specimen, that simulates the closure of the *ductus arteriosus*. This is contrary with the study of Pearson et al. [Pearson et al., 2008] in which it is determined that the wall thickness is not determining for the weakness at the Isthmus.

A rise of 40% of an intensity factor is observed when a 1 mm patch is introduced to the specimen in a bubble inflation test. These will affect the strength of the tissue, generating a concentration of stress and strain at the border of the change of material.

- Chapter 03 - **ARCHITECTURAL TEST**

A study of the most accurate methodology to generate a geometry and to develop a numerical simulations are analysed in chapter 03. The generation of geometries for the use in FEM could be done by CAD software or segmentation of 3D medical images - The aim of this chapter was to compare the these two ways of generate a geometry.

During these simulations, pros and cons were founded comparing these two ways of geometric generation:

1. The segmented model took more than 180 times longer to produce, than the geometric model simulation.
2. The generation of a segmented model, requires a higher level of knowledge in imaging, and also knowledge in exporting files from the image generation software to a solid FEM model. Meanwhile to generate a geometric approximated model, requires the knowledge of CAD, but the exportation of files, to FEM is straight forward.

This simulation determines the path that the subsequent studies should follow. As a way to test the different conditions for a complex model, for example: boundary conditions, contact conditions, material model, mechanical properties, among others.

A geometric approximated model gives the possibility to generate closer results to the segmented model, because in these studies the error between geometries decreases when the segmented model changes its cross section to one closer to the geometric approximated model.

Also these simulations, shows that the outermost layer (adventitia) is the most affected of all the layers, when the tissue is subjected to an increment of blood pressure, the smaller vessels generate a concentration of stress at its root where in contact with the main vessel.

- Chapter 04 - **ARCHIMEDES LEVER AND WATER HAMMER**

The mechanism tested in this chapter simulates the weaker parts of the thoracic aorta when is subjected to the different stages of hypertension.

The aorta has to be fulfilled of blood to start the Archimedes lever mechanism and the water hammer effect, this will lead taking the aorta as a solid beam, and a shock wave could be transfer across the wall.

The architecture of the aorta is influenced by a stage of hypertension, caused by a stressful situation or/and by the closure of the aortic valve, and the blockage of the blood flow at the descending aorta, due to a compression by the diaphragm.

Hypertension values affects the internal part of the aortic arch, changing the cross section of the vessel. Hypertension defined by an increment of systolic blood pressure which surpass $140mmHg \approx 18.7kPa$, after this pressure, the aortic arch starts to move against the blood flow, generating a tension of the Intima layer.

As a way to recreate if the aorta changes its shape due to an over pressure, a simulation of a geometric tube with a “U” shape is subjected to the same increment of internal pressure. The results shows that after $18.7kPa \approx 140mmHg$ the internal part of the aortic arch start being tensed from Adventitia to Intima layer.

Simulations on this chapter proves that a geometric model can accurately show zones of concentration of stress and strain, in the comparison with the segmented model. The second chapter proves that the error between a segmented model and a geometric approximated model decreases when are subjected to higher values of pressure.

Therefore in the next chapter a geometric model is used to recreate an impact to the chest, moving the sternum which will compress the internal organs. Since it is compulsory to start with the aorta full of blood and with a cross section closer to a circle, the inner zone of the aortic arch moves against the blood flow.

- Chapter 05 - **SCAR AT THE ISTHMUS, ARCHIMEDES LEVER, WATER HAMMER AND OSSEOUS PINCH**

At $20m \cdot s^{-1}$ and $25m \cdot s^{-1}$ at the inner part of the aortic isthmus at the Intima layer, values of stress higher than $1819.2kPa$ (experimental minimum ultimate stress [Pearson et al., 2008]) are located. A scar in this zone will rise the possibility of aortic rupture. This supports the rationale of a combination of simple mechanisms.

Starting with an aorta fulfilled of blood with the aortic valve closed. The initial load will be an impact to the sternum, that reacts to the aortic valve (open end of the Archimedes lever), this force will compress all the organs (osseous pinch), tensing the aortic arch and twisting the descending aorta, the aortic valve will move against the descending aorta (column of the Archimedes lever), also the Isthmus will be twisting as the descending aorta (osseous pinch). The tension of the aortic arch, the increment of blood pressure and the torsion forces of the descending aorta and the isthmus, will force the aortic wall to move to the inside of the vessel. A scar in the aortic wall at this zone will act as a stress concentration (scar at the isthmus).

Two shock waves will start on each end of the aorta, at the ascending aorta by the initial load, and at the descending aorta by the closure of the diaphragm (in this simulation, the heart is starting the second shock wave), the vibration of the wall caused by these waves will start a water hammer effect, leading to the collapse of the tissue caused by surpassing the natural vibration frequency.

6.2 Limitations

This section shows deficiencies of the different simulations shown in this thesis.

In the bubble inflation test, as simulated in chapter two, the pressure loading is on the intima layer whereas simulations elsewhere in the thesis demonstrated that the pressure should be applied to the adventitia layer. This simulation was used as a validation of an experimental study, therefore the input data should be representative of the conditions which apply to the experimental study.

For the architectural comparison showed on the third chapter, the geometric approximated model clearly differs from the segmented model. A closer approximated model should be created. The initial idea in this analysis was to compare the two ways to generate geometries, on one side the easiest (a simple CAD geometry) and on the other side the harder way (a segmented model). The main question was that, if these two models will have less error between them, the closer the approximated model to the segmented will be less error.

The thoracic aorta model used for the fourth chapter was obtained from one specimen, and no other comparison was performed. This study could be expanded using different aortas, use the medical images of different patients and see if the reaction of the isthmus is the same as predicted.

The final simulation uses a simplified geometry, where the heart is in line with the descending aorta. In an anatomically correct model, the aortic arch makes a complicated tri-dimensional path, it arches superiorly, posteriorly and left, then inferiorly.

In an anatomically corrected model, the torsion on the descending aorta and the tension of the arch will show higher values. Due to the misalignment of the heart with the descending aorta, and the constrictions of the descending aorta with the spine.

Also at these simulations there blood was static, even though that the blood flow happens in seconds and the time of the simulation is performed in mili-seconds. If the blood moves, it could give more importance to a water hammer effect generating a back pressure at the descending aorta generated by the blockage of the diaphragm with the aorta.

The simulations shows the closure of the ductus arteriosus as a scar on the aortic isthmus. The closure of the ductus arteriosus generate the Ligamentus arteriosus, which is an attachment of the Isthmus with the pulmonary artery. The importance of the use of this attachment is that it will restrict the aortic arch to move superiorly, therefore the use of another attachment of the arch will give importance to the osseous pinch mechanism.

In the last simulation the crash pulse was simplified, by applying the impact load to the sternum. Therefore, the speed that was used is not the speed that a car could have which to leads to BTAR. This analysis removes the reaction of the rib cage, which acts as a shell to the internal organs of the chest. The rib cage will help to dissipate the kinetic energy, generated by the impact load, so an impact located at the thorax could handle higher speed, due to the protection of the rib cage. It is important to add that the simulations shown in this thesis work do not replicate loading from the seat belt or an airbag.

6.3 Future work

After showing the limitations of the simulations of this thesis, the next step is to suggest the steps beyond that will make fully verified the mechanism to explain BTAR.

As a way to test experimentally different scar sizes, where it is suggested, to generate specimens with a controlled design crack, varying diameters or even geometries. Subject these specimens to a bubble inflation test and analyse the crack growth, these cracks generate a discontinuity of the tissue, so a concentrator of stress and strain will be located at the tips of the crack.

Another bubble inflation test is suggested, to a aortic isthmus specimen, applying the load to the adventitia layer. This test will subject the Intima layer to higher stress, due to the direction of the load and the disposition of the layers. Therefore this study will subject the aortic wall to a closer BTAR load, where the aortic wall is loaded from outside to inside.

Simulations using different models obtained by medical images from different patients, and subject them to an increment of inner pressure, if the results shows that the aortic isthmus is subjected to a concentration of stress after 140mmHg these will reinforce the idea of the fourth chapter, where is suggested that if the aorta changes its cross section with hypertension values, the aortic isthmus will get weaker.

From the last chapter, the immediate action is to generate a segmented model of the complete chest, which includes sternum, rib cage, cartilage, lungs, stomach, liver, heart, three layered aorta and blood flow.

For this model, material properties and material model for each one of the components should be validated, with the methodology shown in this thesis. It is suggest to model the stomach and the liver as a air bag, LS-DYNA has material model for lungs and heart to simulate them.

Different ranges of blood pressure should be simulated, using the Smooth-Particle Hydrodynamics (SPH) method, to formulate the blood flow, these ranges will support the rationale that hypertension values change the reaction of the aorta to BTAR. The actual chest compression and velocity values can be obtained from chest test dummies, cadaver test and human body models.

For the delimit of the velocity of injury to the passenger, shorter steps on the speed range should be analysed. To define impact speed first a strain rate analysis, for define the impact load; together with a Delta-V analysis to assess crash severity.

To determine the strength of the aortic tissue to a shock wave. A vibration analysis of the aortic wall, should be performed. This analysis will describe the stress wave propagation and the reactive wave. Including a natural frequency analysis for the aortic wall.

This thesis analyses only frontal impact to the chest. A variation of angles of impact related to real car collisions, should be performed to test the reaction of the architecture of the chest at different locations.

To understand the mechanical mechanism of an aortic rupture that depending on severity it injure one or all the layers. Also it should be included a tribology analysis for dynamic loads, applied to the aortic wall, to see the reaction of the contact between layers of the aortic wall.

These research would sustain the speculation that if the aorta is at its maximum filling of blood, at the end of the systole of the heart achieving $140mmHg$, the cross section of the vessel would change to a circular shape, leading to a concentration of stress and strain located at the isthmus zone, thus during a compression of the chest the inner part of the isthmus is overloaded.

An anti-lock brake system should be designed for the seat belt, this will allow the heart to go to the diastole phase, release pressure at the aorta and dissipate kinetic energy of the impact.

6.4 General conclusion

Blunt thoracic trauma followed by aortic rupture (BTAR) is a serious injury, killing 7500 - 8000 people a year in the United States of America and Canada. BTAR shows a site of predilection, at the inner part of the aortic arch starting a tear at the innermost layer of the aortic tissue. BTAR can occur at a low velocity crashes and the use of a contemporary seat belt or air bag does not eliminate the risk.

Simulations which recreate the conditions of the human body when it is subjected to impact loads were developed in this thesis, by the use of Finite Element Method (FEM), these simulations were validated in a three way analysis, i.e. experimental, analytical and numerical. Proving the numerical methods as an accurate non-destructive technique, for the use in cardiovascular biomechanics.

It is supported the segmentation of 3-dimensional medical images, to generate complex geometries, for the use in the FEM. A methodology for simplifying the generation of complex simulations has been developed in this thesis, and could be applied to any other biomechanical simulation study.

Throughout the path of this research, it is a new approach which proves the complex mechanism which leads to BTAR as a combination of simpler mechanisms including, the insertion of a scar to the aortic wall, a new explanation of the Archimedes lever mechanism, a proper explanation of the water hammer effect, the osseous pinch mechanism and also including hypertension as a physical condition which increases the possibility of BTAR takes place.

The Aortic Isthmus is where the tear starts due to this reasons:

- The mechanism proposed with the insertion of a scar, which simulates the closure of the Ductus Arteriosus, weakens the tissue at the isthmus zone and leads to a concentration of stress and strain at the border of the tissue and the scar.
- Adding that when the vessel is subjected to hypertension values of pressure, the cross section of the vessel changes the shape to a circle, the change of shape also influences the strength of the tissue at the aortic isthmus, applying the load from outside to inside, subjecting the Intima layer to tension.
- An instability of the aortic wall starts and a shock wave is observed when the sternum compress at a speed of $20m \cdot s^{-1}$, showing a pressure concentration at the isthmus zone.

Acronyms

BTAR Blunt thoracic trauma followed by aortic rupture.

FEM Finite element method.

AIS Abbreviated injury scale.

GM Geometric approximated model.

SM Segmented model.

BP Blood pressure.

ASA Ascending aorta.

EAI External aortic isthmus.

IAI Internal aortic isthmus.

DSA Descending aorta.

JNC7 Joint national comitee on prevention, detection, evaluation and treatment of high blood pressure.

CVD Cardiovascular disease.

ALE Arbitrary lagrangian - eulerian formulation.

SPH Smoothed - particle hydrodynamics meshless formulation.

OIV Occupant injury velocity.

Glossary

Aorta Main artery of the human body, output of blood from the left side of the heart.

Trauma A body wound or shock produced by a physical injury.

Numerical simulation A representation of a physical system which implements mathematical models, solved numerically. Using a computer program.

Mechanical properties Characteristics of a material that indicates the behaviour of it under loads.

Material model Specific equation that describes the relation between stress and strain, for a specific material.

Stress Measurement of the internal forces of a body when is subjected to external forces

Strain Measurement of the deformation of a body when is subjected to external forces

Mediastinal The partition which separates the right and left thoracic cavities, formed by the two inner pleural walls, and contains all the soft organs of the thorax except the lungs.

Haematoma A collection of blood outside of a blood vessel, caused by an injury to wall of a blood vessel.

Mediastinal haematoma It is an injury may caused by mediastial vascular injury such as aortic injury, and by fractures of the sternum and vertebral column.

Contusion The injured region of a tissue or skin in which blood capillaries have been rupted.

Laceration A tear in the flesh by a blunt object producing a wound with irregualr edges.

Haemorrhage The scape of blood from a ruptured blood vessel, externally or internally. Arterial blood is bright red and emerges in spurts, venous blood is dark red and flows steadily, while damage to minor vessels may produce only a oozing. Rupture of a major blood vessel such as the femoral artery can lead to the loss of several liters of blood in a few minutes, resulting in shock, collapse and death, if untreated.

Ventricular Related to the ventricle of the heart, a chamber of the heart which recieves blood from a corresponding atrium and from which blood is forced into the arteries.

Mediastinum The space in the thorax (chest cavity) between the two pleural sacs. The mediastinum contains the heart, aorta, trachea, oesophagus and thymus gland, and is divided into anterior, middle, posterior, and superior regions.

Interventricular septum Is the stout wall separating of the lower chambers of the heart from one another.

Interatrial septum Is the wall of the tissue that separates the right and left atria of the heart

Intracardiac Situated within, occurring within, introduced into, or involving entry into the heart.

Laryngeal-tracheal Of or common to the larynx and trachea

Flail chest Fracture of two or more ribs in two or more places, resulting from trauma. It produces unstable 'flail' segment and is often associated with underlying lung trauma or pneumothorax. It leads to asphyxia unless corrected promptly.

Haemothorax Blood in the pleural cavity, usually due to injury. If the blood is not drained dense fibrous adhesions occur between the pleural surfaces, which can impair the normal movement of the lung. The blood may also become infected.

Pneumothorax Air in the pleural cavity. Any breach of the lung surface or chest wall allows air to enter the plural cavity, causing the lung to collapse. The leak can occur without apparent cause, in otherwise healthy people (spontaneous pneumothorax), or result from injuries to the chest (traumatic pneumothorax). In tension pneumothorax a breach in the lung surface acts as a valve, admitting air into the pleural cavity when the patient breathes in but preventing this escape when he breathes out. This air must be let out by surgical incision.

A former treatment for pulmonary tuberculosis - artificial pneumothorax - was the deliberate injection of air into the pleural cavity to collapse the lung and allow the tuberculous areas to heal.

Haemomediastinum An effusion of blood into the mediastinum

Pneumomediastinum The abnormal presence of air or gas in the mediastinum, which may interfere with respiration and circulation, and may lead to such conditions as pneumothorax or pneumopericardium. It may occur spontaneously or as a result of trauma or a pathologic process, or it may be induced deliberately as a diagnostic procedure.

Thymus gland Located in front of the heart, organ of the immune system.

Lumen The space within a tubular or sac-like part, such as a blood vessel, the intestine, or the stomach.

Systole The period of the cardiac cycle during which the heart contracts. The term usually refers to ventricular systole, which lasts about 0.3 seconds. Atrial systole lasts about 0.1 seconds.

Diastole The period between two contractions of the heart, when the muscle of the heart relaxes and allows the chambers to fill with blood. The term usually refers to ventricular diastole, which lasts about 0.5 seconds in a normal heart rate of about 70/minute. During exertion this period shortens, so allowing the heart rate to increase.

References

- (2009). Human Anatomy Charts.
- Aidinian, G., Karnaze, M., Russo, E. P., and Mukherjee, D. (2006). Endograft Repair of Traumatic Aortic Transection in a 10-Year-Old: A Case Report. *Vascular and Endovascular Surgery*, 40(3):239–242.
- Apostolakis, E. E., Baikoussis, N. G., Kalogeropoulou, C., Koletsis, E., Koniari, I., Karnabatidis, D., and Karanikolas, M. (2010). Remnant of a non-patent ductus arteriosus mimicking traumatic thoracic aorta transection: a case report. *Journal of cardiothoracic surgery*, 5:24.
- Benjamin, M. M. and Roberts, W. C. (2012). Fatal aortic rupture from nonpenetrating chest trauma. *Proceedings (Baylor University. Medical Center)*, 25(2):121–3.
- Bower, A. F. (2009). *Applied mechanics of solids*. CRC press.
- Bronzino, J. D. (1999). *Biomedical engineering handbook*, volume 2. CRC press.
- Brown, R. (1994). *Biomaterials, medical devices and tissue engineering: An integrated approach*: Frederick H. Silver. 300 pages, 34 figures. Chapman and Hall, London, 1994. ISBN 0-412-41260-8. Price{£} 49.50.
- Candell, J., Valle, V., Payá, J., Cortadellas, J., Esplugas, E., and Rius, J. (1979). Post-traumatic coronary occlusion and early left ventricular aneurysm. *American heart journal*, 97(4):509–512.

- Carew, T. E., Vaishnav, R. N., and Patel, D. J. (1968). Compressibility of the Arterial Wall. *Circulation Research*, 23(1):61–68.
- Caro, C. G. (2012). *The mechanics of the circulation*. Cambridge University Press.
- Charalambides, M., Wanigasooriya, L., Williams, G., and Chakrabarti, S. (2002). Biaxial deformation of dough using the bubble inflation technique. I. Experimental. *Rheologica Acta*, 41(6):532–540.
- Chobanian, A. V., Bakris, G. L., Black, H. R., Cushman, W. C., Green, L. a., Izzo, J. L., Jones, D. W., Materson, B. J., Oparil, S., Wright, J. T., and Roccella, E. J. (2003). Seventh report of the Joint National Committee on Prevention, Detection, Evaluation, and Treatment of High Blood Pressure. *Hypertension*, 42(6):1206–52.
- Cohen, A. M., Crass, J. R., Thomas, H. A., Fisher, R. G., and Jacobs, D. G. (1992). CT evidence for the "osseous pinch" mechanism of traumatic aortic injury. *AJR. American journal of roentgenology*, 159(2):271–4.
- Dobrin, P. B. (1978). Mechanical Properties of Arteries. *Physiological Reviews*, 58(2).
- Drake, R., Vogl, A. W., and Mitchell, A. W. M. (2014). *Gray's anatomy for students*. Elsevier Health Sciences.
- Erlanger, J. (1921). The movements in the artery under compression during blood pressure determination. *American Journal of Physiology*, 55(1):84 – 155.
- Estrera, A. L., Miller, C. C., Guajardo-Salinas, G., Coogan, S., Charlton-Ouw, K., Safi, H. J., and Azzizadeh, A. (2013). Update on blunt thoracic aortic injury: Fifteen-year single-institution experience. *Journal of Thoracic and Cardiovascular Surgery*, 145(3 SUPPL.):S154–S158.
- Fildes, B. N., Lane, J. C., Lenard, J., and Vulcan, A. P. (1991). Passenger cars and occupant injury. (March).

- Fung, Y.-C. (1993). *Biomechanics Mechanical Properties of Living Tissues*. Springer-Verlag, New York, second edition.
- Fung, Y.-c. (2013). *Biomechanics: circulation*. Springer Science & Business Media.
- Gabauer, D. J. and Gabler, H. C. (2008). Comparison of roadside crash injury metrics using event data recorders. *Accident Analysis & Prevention*, 40(2):548–558.
- Gadd, C. W. and Patrick, L. M. (1968). System versus laboratory impact tests for estimating injury hazard. Technical report, SAE Technical Paper.
- Golden, P. A. (2000). Thoracic Trauma. *Orthopaedic Nursing*, 19(5):37–48.
- Hachmann, P. and Meissner, J. (2003). Rheometer for equibiaxial and planar elongations of polymer melts. *Journal of Rheology*, 47:989 – 1010.
- Haddadin, S., Albu-sch, A., Albu-Schäffer, A., and Hirzinger, G. (2007). Dummy crash-tests for the evaluation of rigid human-robot impacts. In *International Workshop on Technical Challenges for dependable robots in Human Environments*. Citeseer.
- Hallquist, J. O. and Others (2006). LS-DYNA theory manual. *Livermore software Technology corporation*, 3:25–31.
- Hallquist, J. O. and Others (2013a). *KEYWORD USER ' S MANUAL*, volume I. Livermore Software Technology Corporation.
- Hallquist, J. O. and Others (2013b). *KEYWORD USER ' S MANUAL VOLUME II*, volume II. Livermore Software Technology Corporation.
- Hammer, M. M., Raptis, D. A., Cummings, K. W., Mellnick, V. M., Bhalla, S., Schuerer, D. J., and Raptis, C. A. (2016). Imaging in blunt cardiac injury: Computed tomographic findings in cardiac contusion and associated injuries. *Injury*, 47(5):1025–1030.

- Hemmasizadeh, A., Autieri, M., and Darvish, K. (2012). Multilayer material properties of aorta determined from nanoindentation tests. *Journal of the Mechanical Behavior of Biomedical Materials*, 15:199–207.
- Hemmasizadeh, a., Cheheltani, R., Assari, S., Pleshko, N., and Darvish, K. (2013a). Spatial Variation in Aorta Composition and Correlation with Mechanical Properties. *2013 39th Annual Northeast Bioengineering Conference*, pages 94–95.
- Hemmasizadeh, A., Darvish, K., and Autieri, M. (2013b). Characterization of Changes to the Mechanical Properties of Arteries due to Cold Storage using Nanoindentation Tests. *Annals of Biomedical Engineering*, 40(7):1434–1442.
- Holzapfel, G. A., Gasser, T. C., and Ogden, R. W. (2000a). A new constitutive framework for arterial wall mechanics and a comparative study of material models. *Journal of elasticity and the physical science of solids*, 61(8):1–48.
- Holzapfel, G. A., Gasser, T. C., and Ogden, R. W. (2000b). A new constitutive Framework for arterial wall mechanics and a comparative study of material models. *Journal of Elasticity*, 61:1–48.
- Holzapfel, G. A. and Ogden, R. W. (2003). Biomechanics of soft tissue in cardiovascular systems.
- Holzapfel, G. A., Sommer, G., Gasser, C. T., Regitnig, P., and Gerhard, A. (2005). Determination of layer-specific mechanical properties of human coronary arteries with nonatherosclerotic intimal thickening and related constitutive modeling. *American Journal of Physiology-Heart and Circulatory Physiology*, 289:2048–2058.

- Iadicola, M. A., Creuziger, A. A., and Foecke, T. (2014). Advanced biaxial cruciform testing at the NIST Center for Automotive lightweighting. In *Residual Stress, Thermomechanics & Infrared Imaging, Hybrid Techniques and Inverse Problems, Volume 8*, pages 277–285. Springer.
- Ismailov, R. M. (2006). Arch vessel injury: geometrical considerations. Implications for the mechanism of traumatic myocardial infarction II. *World journal of emergency surgery : WJES*, 1:28.
- Jackson, K. E. and Fuchs, Y. T. (2010). Comparison of ALE and SPH Simulations of Vertical Drop Tests of a Composite Fuselage Section into Water. *10th International LS-DYNA® Users Conference*, pages 1–20.
- Johannknecht, R. and Jerrams, S. (1999). The need for equi-biaxial testing to determine elastomeric material properties. *Constitutive Models for Rubber, Editors Dorfman A, Muhr A*, pages 73–76.
- Joye, D. D. (1972). A Bubble Inflation Technique for the Measurement of Viscoelastic Properties in Equal Biaxial Extensional Flow. *Journal of Rheology*, 16(3):421.
- Kerut, E. K., Kelley, G., Falco, V. C., Ovella, T., Diethelm, L., and Helmcke, F. (2005). Traumatic deceleration injury of the thoracic aorta. *Echocardiography (Mount Kisco, N.Y.)*, 22(8):697–704.
- Le Tallec, P. (2001). Fluid structure interaction with large structural displacements. *Computer Methods in Applied Mechanics and Engineering*, 190(24-25):3039–3067.
- Lee, S.-h. and Kent, R. (2007). Blood Flow and Fluid-Structure Interactions in the Human Aorta during Traumatic Rupture Conditions. *Stapp Car Crash Journal*, 51(October):1–23.
- Levick, J. R. (2013). *An introduction to cardiovascular physiology*. Butterworth-Heinemann.

- Li, N., Fang, H., Zhang, C., Gutowski, M., Palta, E., and Wang, Q. (2015). Advances in Engineering Software A numerical study of occupant responses and injuries in vehicular crashes into roadside barriers based on finite element simulations. *Advances in Engineering Software*, 90:22–40.
- Liu, F., Lai, Y., Huang, X., and Chan, C. T. (2011). Dirac cones at $k=0$ in phononic crystals. *Physical Review B*, 84(22):224113.
- Liu, G.-R. and Quek, S. S. (2013). *The finite element method: a practical course*. Butterworth-Heinemann.
- Macaulay, M. (2012). *Introduction to impact engineering*. Springer Science & Business Media.
- Mancia, G., Fagard, R., Narkiewicz, K., Redon, J., Zanchetti, A., Böhm, M., and Others (2013). 2013 ESH/ESC guidelines for the management of arterial hypertension: the Task Force for the Management of Arterial Hypertension of the European Society of Hypertension (ESH) and of the European Society of Cardiology (ESC). *European heart journal*, 34(28):2159–219.
- Meyers, M. A., Chen, P.-y., Lin, A. Y.-m., and Seki, Y. (2008). Biological materials : Structure and mechanical properties. *Progress in Material Science*, 53:1–206.
- Mohan, D. H. and Melvin, J. W. (1982). FAILURE PROPERTIES OF PASSIVE HUMAN AORTIC TISSUE I - UNIAXIAL TENSION TESTS. *Journal of Biomechanics*, 15(11):887–902.
- Moller, J. H. and Hoffman, J. I. (2012). *Pediatric Cardiovascular Medicine*. Wiley-Blackwell, second edi edition.
- Motors, G., Arbor, A., Viano, D. C., King, A. I., Melvin, J. W., and Weber, K. (1989). Injury biomechanics research: an essential element in the prevention of trauma. *Journal of Biomechanics*, 22(5):403–417.

- Nano, G., Mazzaccaro, D., Malacrida, G., Occhiuto, M. T., Stegher, S., and Tealdi, D. G. (2011). Delayed endovascular treatment of descending aorta stent graft collapse in a patient treated for post- traumatic aortic rupture: a case report. *Journal of cardiothoracic surgery*, 6:76.
- Ndiaye, A., Chambost, M., and Chiron, M. (2009). The fatal injuries of car drivers. 184:21–27.
- Nsiampa, N. N., Robbe, C., and Papy, A. (2011). Development of a thorax finite element model for thoracic injury assessment. In *Proceedings of the 8th European Ls-Dyna Users Conference, Strasbourg*, number May.
- Okubo, K. (2009). Anatomography Body Parts 3D.
- Pavlidis, A. N., Tsoukas, A., Zissimopoulos, I., Hesketh, G., Patestos, D., and Manolis, A. J. (2011). Aortic arch rupture following blunt chest trauma. *Echocardiography (Mount Kisco, N.Y.)*, 28(2):E42–3.
- Payne, A. R. (2017). Vehicle Crashworthiness Accelerations , Forces and Energies in Collisions and Impacts. Technical report, Horiba-MIRA.
- Pearson, R., Philips, N., Hancock, R., Hashim, S., Field, M., Richens, D., and McNally, D. (2008). Regional wall mechanics and blunt traumatic aortic rupture at the isthmus. *European journal of cardio-thoracic surgery : official journal of the European Association for Cardio-thoracic Surgery*, 34(3):616–22.
- Rao, S. S. (2010). *The finite element method in engineering*. Elsevier.
- Rastgar-Agah, M. and Darvish, K. (2013). Theoretical Study of Dynamic Viscoelastic Behaviour of Aorta under Impulsive Internal Pressure. *2013 39th Annual Northeast Bioengineering Conference*, pages 61–62.
- Reid, C., Livesey, S. a., and Egleston, C. V. (1999). Aortic rupture as a result of low velocity crush. *Emergency Medicine Journal*, 16(4):299–300.
- Resourse, M. (2014). MVP Resourse.

- Reuge, M., Schimdt, F. M., Le Maout, Y., Rachik, M., and Abbe, F. (2001). Elastomer biaxial characterization using bubble inflation technique. I: experimental investigations. *Polymer Engineering and Science*, 41(3):522–541.
- Richens, D., Field, M., Hashim, S., Neale, M., and Oakley, C. (2004). A finite element model of blunt traumatic aortic rupture. *European journal of cardio-thoracic surgery : official journal of the European Association for Cardio-thoracic Surgery*, 25(6):1039–47.
- Richens, D., Field, M., Neale, M., and Oakley, C. (2002). The mechanism of injury in blunt traumatic rupture of the aorta. *European journal of cardio-thoracic surgery : official journal of the European Association for Cardio-thoracic Surgery*, 21:288–293.
- Richens, D., Kotidis, K., Neale, M., Oakley, C., and Fails, A. (2003). Rupture of the aorta following road traffic accidents in the United Kingdom 1992 to 1999. The results of the co-operative crash injury study. *European journal of cardio-thoracic surgery : official journal of the European Association for Cardio-thoracic Surgery*, 23:143–148.
- Robinson, S. (1994). *Successful simulation: a practical approach to simulation projects*. McGraw-Hill Companies.
- Scali, S. T., Neal, D., Sollanek, V., Martin, T., Sablik, J., Huber, T. S., and Beck, A. W. (2015). Outcomes of surgeon-modified fenestrated-branched endograft repair for acute aortic pathology. *Journal of Vascular Surgery*, 62(5):1148–1159.
- Schmoker, J. D., Lee, C. H., Taylor, R. G., Chung, A., Trombley, L., Hardin, N., Russell, S. R., and Howard, A. (2008). A novel model of blunt thoracic aortic injury: a mechanism confirmed? *Journal of Trauma and Acute Care Surgery*, 64(4):923–931.

- Sevitt, S. (1977). The mechanisms of traumatic rupture of the thoracic aorta. *British Journal of Surgery*, 64:166–173.
- Shigley, J. E. (1961). *Theory of machines*. McGraw Hill.
- Siegel, J. H., Belwadi, A., Smith, J. A., Shah, C., and Yang, K. (2010). Analysis of the mechanism of lateral impact aortic isthmus disruption in real-life motor vehicle crashes using a computer-based finite element numeric model: with simulation of prevention strategies. *Journal of Trauma and Acute Care Surgery*, 68(6):1375–1395.
- Siegel, J. H., Yang, K. H., Smith, J. A., Siddiqi, S. Q., Shah, C., Maddali, M., and Hardy, W. (2006). Computer simulation and validation of the Archimedes Lever hypothesis as a mechanism for aortic isthmus disruption in a case of lateral impact motor vehicle crash: a Crash Injury Research Engineering Network (CIREN) study. *Journal of Trauma and Acute Care Surgery*, 60(2):1–11.
- Sommer, G., Gasser, T. C., Regitnig, P., Auer, M., and Holzapfel, G. a. (2008). Dissection properties of the human aortic media: an experimental study. *Journal of biomechanical engineering*, 130(2):021007.
- Souli, M., Ouahsine, A., and Lewin, L. (2000). ALE formulation for fluid-structure interaction problems. *Computer Methods in Applied Mechanics and Engineering*, 190(5-7):659–675.
- Souli, M. and Zolesio, J. P. (2001). Arbitrary Lagrangian–Eulerian and free surface methods in fluid mechanics. *Computer Methods in Applied Mechanics and Engineering*, 191(3):451–466.
- Spirka, T. a., Erdemir, A., Ewers Spaulding, S., Yamane, A., Telfer, S., and Cavanagh, P. R. (2014). Simple finite element models for use in the design of therapeutic footwear. *Journal of Biomechanics*, 47:1–8.

- Spitzer, V., Ackerman, M. J., Scherzinger, a. L., and Whitlock, D. (1996). The visible Human Male: A Technical Report. *Journal of the American Medical Informatics Association*, 3(2):118–130.
- Stapp, J. P. (1970). Voluntary human tolerance levels. *Impact injury and crash protection*, pages 308–349.
- Stein, E., De Borst, R., and Hughes, T. J. R. (2004). *Encyclopedia of computational mechanics*. Wiley.
- Strassmann, G. (1947). Traumatic rupture of the aorta. *American heart journal*, 33(4):508–515.
- van Vonderen, J. J., te Pas, A. B., Kolster-Bijdevaate, C., van Lith, J. M., Blom, N. a., Hooper, S. B., and Roest, A. a. W. (2014). Non-invasive measurements of ductus arteriosus flow directly after birth. *Archives of disease in childhood. Fetal and neonatal edition*, 99(5):F408–12.
- Yousef, R. and Carr, J. A. (2014). Blunt cardiac trauma: a review of the current knowledge and management. *The Annals of thoracic surgery*, 98(3):1134–1140.
- Zhao, A. R., Field, M. L., Digges, K., and Richens, D. (2008). Blunt trauma and acute aortic syndrome: a three-layer finite-element model of the aortic wall. *European journal of cardio-thoracic surgery : official journal of the European Association for Cardio-thoracic Surgery*, 34(3):623–9.